AD-A067 214 MASSACHUSETTS INST OF TECH CAMBRIDGE RESEARCH LAB OF--ETC F/G 20/14
SHORT PULSE PROPAGATION IN THE SUBMILLIMETER REGION.(U)
JAN 79 H A HAUS DAAG29-77-C-0043

UNCLASSIFIED ARO-15323.1-P NL

1 OF 2
AD A067 214

SHORT PULSE PROPAGATION IN THE SUBMILLIMETER REGION

H. A. Haus

Unclassified

SECURITY CLASSIFICATION OF THIS PAGE (When Data Entered)

REPORT DOCUMENTATION PAGE		READ INSTRUCTIONS BEFORE COMPLETING FORM
1. REPORT NUMBER	2. GOVT ACCESSION NO.	3. RECIPIENT'S CATALOG NUMBER
4. TITLE (and Subtitle) SHORT PULSE PROPAGATION IN THE SUBMILLIMETER REGION		5. TYPE OF REPORT & PERIOD COVERED Final Sep. 1,1977 - Nov. 30, 1978 6. PERFORMING ORG. REPORT NUMBER
7. AUTHOR(s) H. A. Haus		8. CONTRACT OR GRANT NUMBER(s) DAAG29-77-C-0043
9. PERFORMING ORGANIZATION NAME AND ADDRESS Research Laboratory of Electronics Massachusetts Institute of Technology Cambridge, Massachusetts 02139		10. PROGRAM ELEMENT, PROJECT, TASK AREA & WORK UNIT NUMBERS P-15323-P
11. CONTROLLING OFFICE NAME AND ADDRESS U. S. Army Research Office P. O. Box 12211 Research Triangle Park, NC 27709		12. REPORT DATE January 31, 1979 13. NUMBER OF PAGES 190
14. MONITORING AGENCY NAME & ADDRESS(if different from Controlling Office)		15. SECURITY CLASS. (of this report) Unclassified 15a. DECLASSIFICATION/DOWNGRADING SCHEDULE

16. DISTRIBUTION STATEMENT (of this Report)

Approved for public release; distribution unlimited.

17. DISTRIBUTION STATEMENT (of the abstract entered in Block 20, if different from Report)

ACCESSION for	
NTIS	White Section [X]
DDC	Buff Section [ ]
UNANNOUNCED	[ ]
JUSTIFICATION	
BY	
DISTRIBUTION/AVAILABILITY CODES	
Dist.	AVAIL. and/or SPECIAL
A	

18. SUPPLEMENTARY NOTES

The view, opinions, and/or findings contained in this report are those of the author(s) and should not be construed as an official Department of the Army position, policy, or decision, unless so designated by other documentation.

19. KEY WORDS (Continue on reverse side if necessary and identify by block number)

Zero-pi pulse
Atmospheric propagation
Nonlinear propagation

20. ABSTRACT (Continue on reverse side if necessary and identify by block number)

The potential of high intensity pulses, in particular socalled zero-pi pulses, is investigated for transmission of submillimeter waves through the atmosphere. In the theoretical part of the paper the inverse scattering method is applied. A numerical investigation of pulse propagation in the presence of loss is made. The report contains many computer plots which aid in the physical understanding of nonlinear propagation.

DD FORM 1 JAN 73 1473 EDITION OF 1 NOV 65 IS OBSOLETE

Unclassified

SECURITY CLASSIFICATION OF THIS PAGE (When Data Entered)

FINAL REPORT

1. ARO PROPOSAL NUMBER: _____

2. PERIOD COVERED BY REPORT: 1 September 1977 - 30 November 1978

3. TITLE OF PROPOSAL: Short Pulse Propagation in the Submillimeter Region

4. CONTRACT OR GRANT NUMBER: DAAG29-77-C-0043

5. NAME OF INSTITUTION: Massachusetts Institute of Technology

6. AUTHOR(S) OF REPORT: H. A. Haus

7. LIST OF MANUSCRIPTS SUBMITTED OR PUBLISHED UNDER ARO SPONSORSHIP DURING THIS PERIOD, INCLUDING JOURNAL REFERENCES:

H. A. Haus, Physical Interpretation of Inverse Scattering Formalism Applied to S.I.T. (Rev. Modern Phys.) (accepted for publication)

8. SCIENTIFIC PERSONNEL SUPPORTED BY THIS PROJECT AND DEGREES AWARDED DURING THIS REPORTING PERIOD:

H. A. Haus (Principal Investigator)
F. A. Jones (Research Assistant)
P. L. Kelley (unpaid consultant)
P. L. Hagelstein (Hertz Fellow)

15323-P

Dr. Hermann A. Haus
Massachusetts Institute of Technology
Department of Electrical Engineering
and Computer Science
Cambridge, MA 02139

Table of Contents

Short Pulse Propagation in the Submillimeter Region

Abstract:

The potential of high intensity pulses, in particular socalled zero-pi pulses, is investigated for transmission of submillimeter waves through the atmosphere. The water vapor lines cause absorption which can be partly reduced via saturation effects.

In the theoretical part of the paper, the inverse scattering method as applied to selfinduced transparency of a lossless medium is reconsidered, physical interpretations of the mathematical steps are introduced, and some errors that appeared in the literature are corrected. It is found that the zero pi pulse "soliton" solution of a lossless medium (no collisions) exists only for pulses with the spectrum centered at the medium line center, and that pulses with phase reversal, like the zero-pi pulse, but with the spectrum put off line center, break-up.

A numerical investigation of pulse propagation in the presence of loss is made. The analysis is carried out in two stages. First, we look at short pulse propagation with a carrier

frequency at, or near, the 6.1 cm^{-1} absorption line of H_2O with $T_1 = T_2 = 183$ psec. The line was chosen because it lies in the low absorption part of the spectrum and permits propagation over the order of 100 km permitting a test of the stability of the computer program for long distance propagation. This part of the analysis shows that for the carrier frequency centered at the absorption line the loss experienced by a pulse with phase reversal may be reduced initially to 55% of the loss that would be experienced by a small signal pulse of the same spectrum. For a pulse spectrum detuned so that one of the maxima coincides with the peak of the absorption line, the reduction is greater, to 25% of the linear loss. As soon as an appreciable portion of the energy is depleted, the linear limit of absorption is reached. Typical intensities for this nonlinear effect to happen are 8 MW/cm^2 for a pulsewidth of 100 psec.

Contrary to some statements in the literature, the zero-pi pulse does not possess a small signal limit because it calls for full inversion during part of its evolution. For this reason, an optical beam of finite cross section that initially behaves like a zero-pi pulse across its cross section is subject to diffraction effects not unlike the 2π-pulse.

In the second stage of the numerical analysis the two H_2O lines adjacent to the methyl fluoride (CH_3F) laser line (496 μ) and D_2O laser line (385 μ) are investigated. The level

degeneracy is taken into account. The dipole moments are of the same order as that of the 6.1 cm^{-1} line and therefore the intensity levels are comparable. The degeneracy counteracts somewhat the nonlinear loss reduction, but not greatly.

Linear propagation of the CH_3F line and D_2O line achieves greater propagation distances (0.57 km and 1.13 km respectively for the 1/e decay) than nonlinear propagation at, or near, the respective absorption lines.

The report contains many computer plots which aid in the physical understanding of nonlinear propagation.

Short Pulse Propagation in the Submillimeter Region

Introduction

The use of laser radar as opposed to microwave radar in tactical weaponry has the advantage of greater resolution. Ten micrometer CO_2 laser systems are under development for radar applications. This wavelength does not lend itself to all weather operation and can be countermeasured by dispersing aerosols. Submillimeter waves would not be so susceptible to fogs and aerosols but would still afford higher resolution than microwaves. In the submillimeter region molecular absorption becomes a severe problem, particularly absorption by pure rotational transitions in water. Fig. 1 gives a sea level 1 km transmission spectrum in this wavelength region.

It is known that intense pulses much shorter than T_2 may propagate through a resonantly absorbing medium without experiencing loss. This phenomenon is called self-induced transparency. A pulse with an electric field of "area"

$$\frac{\mu}{\hbar}\int_{-\infty}^{\infty} E\,dt \equiv \theta = 2\pi \qquad (1)$$

where μ is the dipole moment and $\hbar$ is Planck's constant, can propagate through a inhomogeneously broadened medium without

attenuation. The pulse is so intense that it inverts the two level system, initially in the ground state, and then returns it to the ground state so that no net absorption occurs.

If one intends to utilize this phenomenon for long distance propagation of intense pulses, one quickly finds that the natural spreading of the beam diameter via diffraction changes the "area" of the electric field assigned to different points in the beam cross section from its value of 2π. When the beam spreads the decrease in intensity causes a decrease of the field amplitude, and hence a decrease of the "area" to less than 2π. When this happens, an appreciable portion of the population of the two level system is left in the upper level thus causing loss and a rapid absorption of the optical pulse.

Socalled zero-π pulses (Lamb, 1974) have a phase reversal so that θ of Eq. (1) integrates to zero. Offhand one might expect that zero-π pulses would be affected less by diffraction effects than 2π pulses. The question then arises whether the potential for low-loss propagation of zero-π pulses may be utilized for transmission of millimeter-wave pulses through the atmosphere, decreasing the effect of water vapor absorption.

Also, computer solutions have shown that zero-pi pulses evaluated for nondegenerate two level systems propagate with little loss in a level degenerate system (Lamb, 1974). Therefore, particular attention has been devoted to the study of

propagation of the zero-pi pulse.

To date, only the zero-pi pulse with carrier frequency tuned to the center of a symmetric line of an inhomogeneously broadened system has been treated in the literature. Let us briefly review the principal findings and explain their importance for the study of low loss propagation.

The zero-pi pulse changes phase by 180° in its "life-time". The individual positive areas and negative areas of the electric field as defined by the integral over time (1) are of the order of 2π however, i.e. the E-field never becomes small in the strict sense of the word. Contrary to popular belief (Lamb, 1974) a small signal analysis is never applicable because the medium experiences full inversion and returns to the ground state within the lifetime of a pulse. (Remember, this is a discussion for the collision free case. The field has a longer time to act if the amplitude is reduced.) Therefore, a zero-pi pulse of a given duration ceases to be a zero-pi pulse when reduced in amplitude, i.e. it will not leave the medium in the ground state, just like a pulse scaled down in amplitude from a 2π pulse. Yet, the situation is not as bad for the zero-pi pulse. Because of its phase reversal, part of the "damage" done in one part of the pulse is undone during the phase reversal part, less population is left in the upper state after passage of a "reduced zero-pi pulse" than after the passage of a "reduced 2π pulse". One confirmation of this fact are computations (Lamb, 1974) on a system with

a degenerate level in which the differences of dipole moment cause different time evolutions of the individual systems. A degenerate system causes less loss to a zero-pi pulse than to a 2π pulse. For this reason, the effect of diffraction is to be expected to be less on the zero-pi pulse.

The present work is an analysis of propagation of the zero-pi pulse, with carrier frequency on line center and off line center, in the presence of collisions. It consists of an analytic part and a computational part. The analytic part is concerned with an application of the Inverse Scattering Method (ISM) to the evaluation of the zero-pi pulse. Previous work in the literature (Lamb, 1973, 1974) has not made mention of a zero-pi pulse solution in the offresonant case (carrier frequency detuned from the center of a symmetric line). Offhand, one would expect that in a medium with multiple lines lower loss is achieved when the carrier frequency of the pulse is placed between the lines. Therefore, it was necessary to apply the analytic theory of zero-pi pulses to this case.

A reader of the literature on ISM, who is not a professional mathematician, tends to be dazed by the seeming complexity of the subject. This was the case with the author of this report. We perceived it, therefore, to be our first task to cast the terminology developed in the ISM into language familiar to the physicist and electrical engineer. This topic is covered in detail in Appendix I. Suffice it to state here that we succeeded in simplifying greatly the derivation of the zero-pi pulse.

The computational part studies propagation of pulses of zero area in the presence of collisional deexcitation. The loss of a zero-pi pulse is compared with the loss that would be experienced by an equivalent low intensity pulse. By this we mean, a pulse with the same spectrum and frequency dependent loss matching the linear transmission characteristic of the medium. The investigation is divided into two parts. First we ignore the orientational degeneracy and study nonlinear propagation in a medium with loss. The parameters of the medium are picked so as to model the water absorption line near 6.1 cm^{-1} where the loss is relatively small and long distance propagation can occur. This is one test on the stability of the computer program. This part of the study gave a great deal of insight into the possibility of loss reduction by nonlinear effects. It was found that the loss of a pulse of 100 psec duration of 8MW/cm peak power could be reduced to about 20% of the loss experienced by a linear medium. Of course this reduction lasts only for a few 1/e attenuation lengths after which the loss is that of a linear medium. It was also found "empirically" in this investigation that zero-pi like pulses tuned off-resonance tend to break up under lossless propagation. This prompted the analytic study to look for a general proof that detuned zero-pi pulses do not exist which is reproduced in the appendix.

The second part of the study is concerned with a realistic

modeling of the propagation of pulses at resonance with the absorption lines adjacent to the 495 μ line of the CH_3F and the 385 μ line of the D_2O laser. Here we took the orientational degeneracy into account finding that it changes the propagation characteristics only very little. The penetration depths at these frequencies are discouragingly low however. Greater propagation distances are achieved by small signal propagation of the CH_3F and D_2O lines proper, because they lie relatively close to local absorption minima.

Part I

Analytic Treatment

I. The Inverse Scattering Method

A large amount of literature has evolved in recent years (see References) on the Inverse Scattering Method (ISM) which yields exact solutions to a class of nonlinear partial differential equations in two dimensions (time and one space variable). The equations of self-induced transparency (S.I.T.) are a member of this class, and the zero-pi pulse is a solution of these equations that has been derived by means of the method (Lamb, 1974).

It seemed appropriate, therefore, to devote some effort to the exploration of the method. It became soon apparent that the research on the I.S.M. had been conducted exclusively by mathematicians and had not been assimilated by physicists and engineers, like circuit theory had been adapted in the thirties after its original development by mathematicians. For this reason we set out to develop an understanding of the I.S.M. Appendix I is the outcome of this study. Here we summarize the principal issues. The flow chart of Fig. 2 will help the reader in following the development.

The I.S.M. associates with the original nonlinear differential equation a linear (quantum mechanical) scattering problem, the solution of which provides the general solution of the nonlinear differential equation. This association is done ad hoc, no general methods exist to find the linear scattering problem. In the S.I.T. problem Lamb (1973) found the linear scattering equations, the socalled Zakharov Shabat equations, after a series of ingenious transformations of the Bloch equations. Because S.I.T. is a quantum mechanical problem (so far as the medium description is concerned) one would expect that the linear scattering problem is naturally imbedded in the inverse scattering method applied to S.I.T., in other words, is part of the defining equations. This has not been generally recognized and only McLaughlin and Corones (1974) have made the connection, but not explicitly. We showed that the linear scattering equations of S.I.T. are the equations of the two-level system before they have been cast into the Bloch equation form.

Next we study the solutions of the Zakharov-Shabat equations. Here we establish the analogy of these equations with those of the parametric oscillator-- a well known problem in Optical Electronics (Yariv). This analogy is helpful in locating the poles in the complex plane of the eigenfunctions of the Zakharov-Shabat equations that give the "soliton" solutions of S.I.T. These poles must be invariants of the S.I.T. equations if the inverse scattering method is to be applicable. We give a proof

of the invariance following a method of Ablowitz et al. (1974a). The invariance leads to a set of equations that are shown to be identical with Hilbert Transforms of the Bloch Equations. The invariance may be utilized to obtain the spatial evolution of the pulse determined at one value of the spatial coordinate; the entire spatial dependence is contained in the residues of the poles, the location of the poles is invariant. Because the residues may be shown to be independent of the time variable τ evaluation may occur in the limit $\tau \to -\infty$ which leads to great simplification.

In this manner we obtain the 2π-pulse and zero-pi pulse. We can also show that no soliton solution with zero area exists off resonance (carrier not centered with absorption line). In this connection one should emphasize the shape of the spectrum of a zero-pi pulse (or a zero degree, the terminology used by Grieneisen et al., 1972, 1973, who considered small signal properties of pulses with phase reversal). The spectrum of a zero-pi pulse has a zero at the carrier frequency. This accounts for the low loss observed with zero-degree pulses (Grieneisen et al., 1972) when propagating through a medium whose absorption line was centered with the carrier frequency.

II. The Zero-Pi Pulse

The zero-pi pulse with a carrier frequency centered with the symmetric line of a two level system distribution has been derived by Lamb (1974) from the Inverse Scattering Method. It is rederived in the appendix and has the following form in the notation of the appendix:

$$\mathcal{E} = 8\beta \frac{\cosh 2\beta(\tau - \tau_o)\cos 2\alpha(\tau - \tau_1) - \frac{\beta}{\alpha}\sinh 2\beta(\tau - \tau_o)\sin 2\alpha(\tau - \tau_1)}{\cosh^2 2\beta(\tau - \tau_o) + \frac{\beta^2}{\alpha^2}\sin^2 2\alpha(\tau - \tau_1)} \tag{2.1}$$

α and β are adjustable constants. $\mathcal{E}$ is the normalized E field

$$\mathcal{E} = \frac{2\bar{p}_{12} \cdot \bar{E}}{i\hbar\Omega} \tag{2.2}$$

where $\bar{p}_{12}$ is the dipole moment, $\hbar$ is Planck's constant, and

$$\Omega^2 \equiv \frac{\omega N |p_{12}|^2}{2\hbar\varepsilon} \tag{2.3}$$

where

ω - carrier frequency

N - particle density

$\hbar$ - Planck's constant

ε - dielectric constant of (nonresonant part of) medium

Further, τ is the normalized space-time variable which refers to a frame translated along the x-axis at the speed of light

$$\tau \equiv \Omega\left(t - \frac{x}{c}\right) . \tag{2.4}$$

The normalized spatial variable is

$$z = \Omega x/c \tag{2.5}$$

in terms of which one may write

$$\beta\tau_o = \frac{1}{4} z \left\langle \frac{\beta}{(\xi - \alpha)^2 + \beta^2} \right\rangle \tag{2.6}$$

$$\alpha\tau_1 = \frac{1}{4} z \left\langle \frac{\xi - \alpha}{(\xi - \alpha)^2 + \beta^2} \right\rangle . \tag{2.7}$$

The pointed brackets indicate an average over all two level systems

of different transition frequency (inhomogeneous broadening). In the limit of no inhomogeneous broadening, ξ can be set equal to zero in the above equations and the pointed brackets can be omitted. This is the limit of particular interest, because the lines of water vapor in the centimeter and millimeter region in the atmosphere are homogeneously broadened.

In this limit one finds that the zero-pi pulse consists of an envelope traveling at less than the speed of light, and a substructure with a phase velocity greater than the speed of light. The inverse speeds are disposed symmetrically around $1/c$.

Some features of the zero-pi pulse are apparent from (2.1) and also follow from its derivation via the Inverse Scattering Method. The zero-pi pulse may be considered to be constructed by a limit of two 2π-pulses that propagate at the same speed, are in antiphase and are made to overlap. This, of course, is a construction in the "indirect space" of the linear scattering problem, not in the "direct" space of the nonlinear differential equation, in which superposition does not hold. An indication of this "superposition" is the fact that the sech^2 of the two-pi pulse has the same scale parameter β, which also appears in the amplitude of the pulse in front of expression (2.1). This means that the individual "areas" of the zero-pi pulse are of the order of 2π and not <u>small</u>. Therefore, the

zero-pi pulse shares with the 2π pulse the property that, strictly, a small signal limit does not exist. In both cases, appreciable inversion occurs during the time evolution of the pulse. Therefore, the zero-pi pulse is susceptible to diffraction effects just like the 2π pulse. In other words, spreading via diffraction that changes the field intensity while not changing the time evolution will change the positive and negative portions of the pulse in different parts of the beam and make it become different from the ideal zero-pi pulse. It is important therefore to study propagation of intense pulses other than zero-pi pulses by computer in order to ascertain the potential of intense pulse propagation through the atmosphere.

In the appendix, an investigation is made of the existence of zero-pi pulses with a carrier detuned from line center. The requirement that the contributions of the two poles propagate at the same speed imposes a constraint which is shown to be equivalent to constraining the spectrum to be centered with the material line.

Part II

Computation

III. The Starting Equations for Computation

For the computation of pulse propagation with loss, it is necessary to use the Bloch equations, or density matrix equations. The loss is introduced phenomenologically in terms of the "longitudinal" and "transverse" relaxation times T_1 and T_2. In the slowly varying envelope approximation of an electric field, $E(x, t) \exp - i(\omega t - kx)$, these are (Kryukov, Letokhov, 1970) (compare (1.10), (1.15) and (1.16) of the appendix)

$$\left(\frac{\partial}{\partial x} + \frac{1}{c}\frac{\partial}{\partial t}\right) E(x, t) = i2\pi \frac{\omega}{c} P(x, t) \tag{3.1}$$

$$\left(\frac{\partial}{\partial t} + \frac{1}{T_2} - i\Delta\omega\right) P(x, t) = \frac{i|\bar{\mu}|^2}{\hbar} N(x, t)\, E(x, t) \tag{3.2}$$

$$\frac{\partial}{\partial t} N(x, t) + \frac{N(x, t) - N_o}{T_1} = \frac{i}{\hbar}\left[\frac{E^*(x, t)\, P(x, t) - E(x, t)\, P^*(x, t)}{2}\right] \tag{3.3}$$

with

$$\Delta\omega = \omega - \omega_o \tag{3.4}$$

where ω_o is the resonance frequency of the two-level system. We use here cgs units. $N(x, t)$ is the difference of the population densities in the lower and upper levels, $N(x, t) = N(\rho_{11} - \rho_{22})$ of the appendix; $P(x, t)$ is the polarization density, $\bar{\mu}$ ($= \bar{p}_{12}$ of the appendix) is the matrix element, T_2 is the dephasing time, T_1 is the energy changing collision time; N_o is the equilibrium population density difference.

In the case of more than one line we have

$$\left(\frac{\partial}{\partial x} + \frac{1}{c}\frac{\partial}{\partial t}\right) E(x, t) = \sum_j i2\pi \frac{\omega}{c} P_j(x, t) \tag{3.5}$$

$$\left(\frac{\partial}{\partial t} + \frac{1}{T_{2j}} - i\Delta\omega_j\right) P_j(x, t) = \frac{i|\bar{\mu}_j|^2}{\hbar} N_j(x, t)\, E(x, t) \tag{3.6}$$

$$\frac{\partial}{\partial t} N_j(x, t) + \frac{N_j(x, t) - N_{oj}}{T_{1j}} = \frac{i}{\hbar}\left[\frac{E^*(x, t)\, P_j(x, t) - E(x, t)\, P_j^*(x, t)}{2}\right] \tag{3.7}$$

In the case of one single line, we normalize as follows:

t in units of t_o

x in units of ct_o

E in units of E_o

P in units of P_o

N in units of N_o

where

t_o is arbitrary

$$E_o = \frac{i\hbar}{\mu t_o}$$

$$P_o = \mu N_o.$$

With this normalization, (3.1)-(3.3) become

$$\left(\frac{\partial}{\partial x} + \frac{\partial}{\partial t}\right) E(x, t) = - \alpha P(x, t) \tag{3.8}$$

$$\left(\frac{\partial}{\partial t} + \frac{1}{T_2} - i\Delta\omega\right) P(x, t) = - N(x, t)\, E(x, t) \tag{3.9}$$

$$\frac{\partial}{\partial t} N(x, t) + \frac{N(x, t) - 1}{T_1} = \frac{E^*(x, t)\, P(x, t) + E(x, t)\, P^*(x, t)}{2} \tag{3.10}$$

where

$$\alpha = \frac{2\pi\omega\ t_o^2 N_o |\bar{\mu}|^2}{\hbar} . \tag{3.11}$$

In the case of many lines, the normalization is slightly different. If we define

$$\mu_o = \sum_j |\mu_j| \tag{3.13}$$

and express μ_j in units of μ_o, then we recover the following normalized equations

$$\left(\frac{\partial}{\partial x} + \frac{\partial}{\partial t}\right) E(x, t) = - \sum_j \alpha_j P_j(x, t) \tag{3.14}$$

$$\left(\frac{\partial}{\partial t} + \frac{1}{T_{2j}} - i\Delta\omega_j\right) P_j(x, t) = - \mu_j N_j(x, t)\ E(x, t) \tag{3.15}$$

$$\frac{\partial}{\partial t} N_j(x, t) + \frac{N_j(x, t) - 1}{T_{1j}} = \mu_j \left[\frac{E^*(x, t)\ P_j(x, t) + E(x, t)\ P_j^*(x, t)}{2}\right] \tag{3.16}$$

where

$$\alpha_j = \frac{2\pi\omega t_o^2 \mu_o \mu_j\ N_{oj}}{\hbar} \tag{3.17}$$

and

$E(x, t)$ in units of $E_o = \frac{i\hbar}{\mu_o t_o}$

$P_j(x, t)$ in units of $P_o = \mu_j N_{oj}$

$N_j(x, t)$ in units of N_{oj}.

Numerical values are

$$|E_o| = \frac{\hbar}{\mu_o t_o} = 6.5821 \times 10^{-8} (t_o \mu_o)^{-1} \frac{\text{Volts}}{\text{cm}} \tag{3.18}$$

$$\alpha = \frac{2\pi\omega t_o^2 N_o |\mu_o|^2}{\hbar} = 2.59 \times 10^4 \frac{t_o^2 N_o |\mu_o|^2}{\lambda} \tag{3.19}$$

$$|\bar{S}| = \left[\frac{c}{4\pi} \bar{E} \times \bar{H}\right] = 2.65 \times 10^{-3} E_o^2 \text{ Watts/cm}^2 \tag{3.20}$$

where

μ_o is in $e\mathring{A}$ (1eA = 4.80 Debye)

t_o is in sec

N_o is in cm^{-3}

λ is in cm

E_o is in Volts/cm.

IV. Differencing the S.I.T. Equations

In this section we develop the differencing scheme that has been used in the computer program to evaluate the pulse propagation. The S.I.T. equations in normalized units are given by (3.14) through (3.16). If the polarization is now split into real and imaginary parts,

$$P_j(x, t) = P_{Rj}(x, t) + iP_{Ij}(x, t). \tag{4.1}$$

then (3.15) and (3.16), separated into real and imaginary parts, can be written in matrix form

$$\frac{\partial}{\partial t}\begin{pmatrix} N_j \\ P_{Rj} \\ P_{Ij} \end{pmatrix} = \begin{pmatrix} -\frac{1}{T_{ij}} & \mu_j E_R & \mu_j E_I \\ -\mu_j E_R & -\frac{1}{T_{2j}} & -\Delta\omega \\ -\mu_j E_I & \Delta\omega & -\frac{1}{T_{2j}} \end{pmatrix}\begin{pmatrix} N_j \\ P_{Rj} \\ P_{Ij} \end{pmatrix} + \begin{pmatrix} \frac{1}{T_{ij}} \\ 0 \\ 0 \end{pmatrix} \tag{4.2}$$

If we define

$$\bar{Y}_j = \begin{pmatrix} N_j \\ P_{Rj} \\ P_{Ij} \end{pmatrix} \tag{4.3}$$

$$\bar{\bar{A}}_j = \begin{pmatrix} -\frac{1}{T_{1j}} & \mu_j E_R & \mu_j E_I \\ -\mu_j E_R & -\frac{1}{T_{2j}} & -\Delta\omega \\ -\mu_j E_I & \Delta\omega & -\frac{1}{T_{1j}} \end{pmatrix} \tag{4.4}$$

$$\bar{b}_j = \begin{pmatrix} 1/T_{1j} \\ 0 \\ 0 \end{pmatrix} \tag{4.5}$$

Then

$$\frac{\partial}{\partial t}\bar{y} = \bar{\bar{A}} \cdot \bar{y} + \bar{b} \tag{4.6}$$

where the j subscripts are omitted.

The strategy is to solve the polarization and population equations at a given point in space for all time, and then increment the space point and again solve for the populations in time. The time difference equations are

$$\bar{y}_o = \begin{pmatrix} 1 \\ 0 \\ 0 \end{pmatrix} \tag{4.7}$$

$$\bar{y}_1 = \left(\bar{\bar{I}} - \frac{\Delta t}{2}\bar{\bar{A}}_1\right)^{-1}\left(\bar{y}_o + \frac{\Delta t}{2}\bar{\bar{A}}_o \cdot \bar{y}_o + \Delta t\bar{b}\right)$$

$$\bar{y}_{n+1} = \left(\bar{\bar{I}} - \frac{\Delta t}{2}\bar{\bar{A}}_{n+1}\right)^{-1}\left(\bar{y}_{n-1} + \frac{\Delta t}{2}(\bar{\bar{A}}_{n-1}\cdot\bar{y}_{n-1} + 2\bar{\bar{A}}_n\cdot\bar{y}_n) + 2\Delta t\bar{b}\right) \qquad (n \geq 1)$$

where $\bar{y}_n$ and $\bar{\bar{A}}_n$ denote the values at the n-th time step.

The electric field is solved for in the moving frame. If we define

$$\tau \equiv t - x \qquad \text{and} \qquad z = x \qquad (4.8)$$

as the new variables, then (compare Section 1 of Appendix) the derivative $\partial/\partial t$ becomes $\partial/\partial\tau$ and the "convective" derivative of E becomes $\partial/\partial z$ at constant τ.

$$\frac{\partial}{\partial z}E(z, t) = \sum_j \alpha_j P_j(z, t). \qquad (4.9)$$

This equation can be solved numerically using a predictor-corrector scheme, where the predictor is

$$\bar{E}^{i+1} = \bar{E}^i + \Delta\eta \sum_j \alpha_j \bar{P}_j{}^i \qquad (4.10)$$

and the corrector is

$$\bar{E}^{i+1} = \bar{E}^{i-1} + \frac{\Delta\eta}{2}\left[\sum_j \alpha_j(\bar{P}_j^{i-1} + 2\bar{P}_j{}^i + \bar{P}_j^{i+1})\right]. \qquad (4.11)$$

The algorithm works as follows: first the field E_{n+1}^{i+1} is predicted according to

$$E_{n+1}^{i+1} = E_{n+1}^{i} + \Delta\eta\left(\sum_j \alpha_j (P_j)_{n+1}^{i}\right). \tag{4.12}$$

The polarization and population is then computed by

$$\bar{y}_{n+1}^{i+1} = \left(\bar{\bar{I}} - \frac{\Delta t}{2}\bar{\bar{A}}_{n+1}^{i+1}\right)^{-1} \cdot \left(\bar{y}_{n-1}^{i+1} + \frac{\Delta t}{2}\left(\bar{\bar{A}}_{n-1}^{i+1} \cdot \bar{y}_{n-1}^{i+1} + 2\,\bar{\bar{A}}_{n}^{i+1} \cdot \bar{y}_{n}^{i+1}\right) + 2\Delta t\bar{b}_o\right). \tag{4.13}$$

This is done for all the transitions yielding values for the polarization. With the new polarization values, the field can be updated according to

$$E_{n+1}^{i+1} = E_{n+1}^{i-1} + \frac{\Delta\eta}{2}\left(\sum_j \alpha_j\left((P_j)_{n+1}^{i-1} + 2(P_j)_{n+1}^{i} + (P_j)_{n+1}^{i+1}\right)\right). \tag{4.14}$$

From the corrected value of the field, the populations and polarizations are recomputed.

The code was originally intended to use a quadrature of the form

$$\bar{y}_{n+1} = \bar{y}_n + \frac{\Delta t}{3}\left(\bar{\bar{A}}_{n-1} \cdot \bar{y}_{n-1} + 4\,\bar{\bar{A}}_n \cdot \bar{y}_n + \bar{\bar{A}}_{n+1} \cdot \bar{y}_{n+1}\right)$$

However, this scheme when applied to the field and populations was found to be unstable.

V. Absorption Coefficients

In this section we give the definition of the absorption coefficient and relations which will be relevant in the next sections. The normalized wave equation is (3.14)

$$\left(\frac{\partial}{\partial x} + \frac{\partial}{\partial t}\right) E(x, t) = -\sum_j \alpha_j P_j(x, t). \tag{3.14}$$

The normalized absorption nonlinear coefficient κ is the loss of energy per unit normalized length

$$\kappa = \frac{-\frac{\partial}{\partial x}\int_{-\infty}^{\infty} |E|^2 dt}{\int_{-\infty}^{\infty} |E|^2 dt} = \frac{\sum_j \alpha_j \int_{-\infty}^{\infty} (E^* P_j + E P^*) dt}{\int_{-\infty}^{\infty} |E|^2 dt}. \tag{5.1}$$

One can define a linear absorption coefficient by solving for the linear polarization assuming that the normalized population keeps its small signal value, and then computing κ according to (5.1). The ratio of the nonlinear absorption coefficient to the linear absorption coefficient is a measure of the nonlinearity of the medium response. In order to get from normalized to absolute absorption coefficients, one divides by (ct_o).

VI. Fourier Transform

The Fourier transform of a function $f(t)$ *is*

$$\mathfrak{F}(\omega) = \int_{-\infty}^{\infty} e^{-i\omega t} f(t)\, dt \tag{6.1}$$

and the inverse transform is

$$f(t) = \frac{1}{2\pi} \int_{-\infty}^{\infty} e^{i\omega t} \mathfrak{F}(\omega)\, d\omega. \tag{6.2}$$

We give results for the transform of the field in the following sections.

VII. Results - One Line, Resonant Case

We shall attack the numerical solution in stages. We study first 2π pulse propagation with no loss and check the computer solution against the analytic solution. In this part of the problem, the choice of numerical values for the parameters is not crucial. Indeed, the matrix element μ and the number density N_o jointly establish distance and time scales. A change in the values of μ and N_o is accomodated fully by a change of the numerical values of distance and time on a computer printout made for a particular initial choice of μ and N_o.

When collisions are introduced, they introduce a rate constant that must be normalized. A change of μ and/or N_o calls for a change of normalized rate constant, a new independent parameter has been introduced.

The same statements hold for the lossless $0\text{-}\pi$ pulse and $0\text{-}\pi$ pulse propagation in the presence of collisions (loss). Hence one must be careful to use appropriate numerical values for the physical problem to be solved. All this is rather obvious, but there is additional complication. H_2O is an asymmetric rotor molecule and all levels of interest are orientationally degenerate; i.e. for a given angular momentum J, there are $2J + 1$ possible M eigenvalues ("projection of

angular momentum" into the spatial axis around which the angular momentum has been quantized). Each value of M gives a different dipole moment. Thus, a given pair of energy levels interacting nonlinearly with an electric field must be treated as $2J + 1$ level pairs where J is the quantum number of the lower level. Each level interacts with the E-field with its own value of μ and thus ideal 2π-pulses or $0\text{-}\pi$ pulses do not exist.

In order to break down the problem into stages of increasing difficulty, we consider first the case of no M-degeneracy. We shall first pick values for the line strengths and widths from the computer print-out of S. A. Clough based on work by L. S Rothman and R. A. McClathey (Applied Optics, 15, 2616, 1976) in the low absorption regime around 6 cm^{-1} to test how the program would handle long distance propagation. These computations will be useful in isolating the problems inherent in $2\text{-}\pi$ and $0\text{-}\pi$ pulse propagation in the presence of loss and also ascertain the capability of the program to handle long distance propagation. Then we shall pick the more realistic cases of nonlinear propagation near the two submillimeter lasers, methyl fluoride at 496 μ and D_2O at 385 μ, using H_2O line parameters for the two absorption lines nearest the pertinent laser line. Here, the full M-degeneracy of the lines will be taken into account.

Table 7.1 gives the line parameters used for the $6.1\ cm^{-1}$ propagation.

Table 7.1 Data for $6.1\ cm^{-1}$ line of H_2O.

frequency $\omega = 1.2 \times 10^{12}\ sec^{-1}$

relaxation times $T_1 = T_2 = 0.094\ cm^{-1}$ or 185 psec

matrix element $\mu = 0.2204$ debye $= 4.58 \times 10^{-2}$ eÅ

energy of lower level $131.2\ cm^{-1}$

quantum numbers J, K_{-1}, K_{+1}

lower level	3	1	3
upper level	2	2	0

linear absorption $1.135 \times 10^{-6}\ cm^{-1}$

number density in lower level 2.77×10^{11}

$\alpha = 9.18 \times 10^{-7}$

$E_o = 1.44 \times 10^{4}$ V/cm

$P_o = 5.50 \times 10^{5}$ watts/cm^2

Run 1: Lossless 2π pulse propagation.

In the first run we consider propagation of a 2π pulse on resonance, comparing the analytical results with the numerical results as a check on the computer program. In this problem we take the following parameter values:

$$\begin{aligned} t_o &= 100 \text{ psec} & \lambda^{-1} &= 6.1 \text{ cm}^{-1} \\ N_o &= 2.77 \times 10^{11} \text{ cm}^{-3} & \Delta\omega &= 0 \\ \mu &= 4.58 \times 10^{-2} \text{ e}\mathring{\text{A}} & T_1 &= T_2 = 10^{50} \text{ sec} \end{aligned} \tag{7.1}$$

and for time and space steps we have

$$\begin{aligned} x_{min} &= 0 & t_{min} &= -1 \text{ nsec} \\ x_{max} &= 3 \times 10^7 \text{cm} & t_{max} &= 1 \text{ nsec} \\ \Delta x &= 3 \times 10^5 \text{ cm} & \Delta t &= 6.67 \text{ psec} \\ nx &= 100 \text{ steps} & nt &= 300 \text{ steps} \end{aligned} \tag{7.2}$$

The input field is $2 \operatorname{sech} t$ in normalized units. The time axis was shifted on each space step such that the average

$$\langle t \rangle = \frac{\sum_i t_i ((\text{Re } E)_i^2 + (\text{Im } E)_i^2)\Delta t}{\sum_i ((\text{Re } E)_i^2 + (\text{Im } E)_i^2)\Delta t} \tag{7.3}$$

was kept between the centermost two time bins. The column marked R1 in Table 7.2 gives the distance in cm at which the remaining quantities defined below are evaluated.

$$\text{AREAR} = \sum_i (\text{Re } E)_i \, \Delta t \tag{7.4}$$

$$\text{ENERGY} = \sum_i (E^*E)_i \, \Delta t \tag{7.3}$$

$$\text{VELOCITYC} = 1 - (\partial \langle t \rangle / \partial x)^{-1} \tag{7.6}$$

$$\text{KAPPA1} = \frac{\sum_j \alpha_j \sum_i (E^*P_j + EP_j^*)_i \, \Delta t}{\sum (E^*E)_i \, \Delta t} \tag{7.9}$$

The summation over j in KAPPA1 is over the different transitions, in this case there is only one considered. AREAR is the trapezoidal rule integration for the real area of the electric field and should be equal to 2π for the entire problem. The error is seen to be of order 0.1% or less. The pulse energy rises slowly, with an error of 0.28%. The pulse velocity is the speed of light to within about one part in 10^6, the computed value of VELOCITYC is accurate to about 0.7%, rendering the absolute velocity accurate to 7 parts in 10^9. The absorption coefficient analytically is exactly zero, the error is such that the growth in energy is of the order of one part in

Table 7.2

Run 1. The 2π-pulse, error check.

BLOCH R = [illegible]E+07 NCYCLE = 101

VARIABLES IN SPACE

	ANEAR	ENERGY	VELOCITYC	KAPPA1
	0	0	0	0

	R1				
1	9.00E+05	6.000451E+00	7.977513E+00	9.218753E-07	-2.674499E-14
2	2.10E+06	6.000419E+00	7.977514E+00	9.218692E-07	-2.660431E-14
3	3.30E+06	6.000390E+00	7.977514E+00	9.218661E-07	-1.550319E-14
4	4.50E+06	6.000361E+00	7.977513E+00	9.218640E-07	8.151560E-15
5	5.70E+06	6.000187E+00	7.977512E+00	9.218637E-07	-2.759370E-14
6	6.90E+06	6.000744E+00	7.977512E+00	9.218642E-07	-4.245370E-14
7	8.10E+06	6.000807E+00	7.977513E+00	9.218639E-07	-4.265259E-14
8	9.30E+06	6.000863E+00	7.977514E+00	9.218645E-07	-4.294529E-14
9	1.05E+07	6.000920E+00	7.977514E+00	9.218649E-07	-3.344156E-14
10	1.17E+07	6.000978E+00	7.977515E+00	9.218647E-07	-2.459672E-14
11	1.29E+07	6.001040E+00	7.977515E+00	9.218649E-07	-2.786428E-14
12	1.41E+07	6.001105E+00	7.977515E+00	9.218647E-07	-3.640600E-14
13	1.53E+07	6.001168E+00	7.977515E+00	9.218647E-07	-4.103808E-14
14	1.65E+07	6.001232E+00	7.977515E+00	9.218644E-07	-4.108993E-14
15	1.77E+07	6.001293E+00	7.977515E+00	9.218647E-07	-4.075503E-14
16	1.89E+07	6.001354E+00	7.977516E+00	9.218644E-07	-3.663616E-14
17	2.01E+07	6.001421E+00	7.977515E+00	9.218651E-07	-3.237336E-14
18	2.13E+07	6.001485E+00	7.977517E+00	9.218652E-07	-3.109623E-14
19	2.25E+07	6.001546E+00	7.977517E+00	9.218661E-07	-3.466797E-14
20	2.37E+07	6.001603E+00	7.977518E+00	9.218663E-07	-3.913333E-14
21	2.49E+07	6.001655E+00	7.977518E+00	9.218674E-07	-4.029814E-14
22	2.61E+07	6.001682E+00	7.977518E+00	9.218678E-07	-4.023484E-14
23	2.73E+07	6.001740E+00	7.977519E+00	9.218697E-07	-3.980705E-14
24	2.85E+07	6.001800E+00	7.977519E+00	9.218701E-07	-3.683766E-14
25	2.97E+07	6.001801E+00	7.977520E+00	9.218719E-07	-3.397246E-14

10^6 over 3×10^7 cm propagation.

Basically, the numerical errors introduced are of order 10^{-3} to 10^{-2}, which are acceptably small for the calculation. That is to say, the numerical accuracy is of order 99.0% to 99.9%.

Run 2: Lossless 0π Pulse Propagation

In this run we use the same parameters as given in (6.1) and (6.2), however, the input field is now

$$E(0, t) = \frac{4}{t_e} \frac{\cos(t/t_f)\cosh(t/t_e) - \frac{t_f}{t_e}\sin(t/t_f)\sinh(t/t_e)}{\cosh^2\frac{t}{t_e} + (t_f/t_e)^2 \sin^2(t/t_f)\sinh^2(t/t_e)} \tag{7.8}$$

in normalized units. Values of t_e and t_f are

$$t_e = 10^{-10} \text{ sec}$$
$$t_f = 10^{-10} \text{ sec.} \tag{7.9}$$

In Table 7.3 we give the same values of the parameters as listed in Table 7.2, now for the case of 0-π pulse. The pulse energy is within 0.2% of its analytical value. The velocity is correct to within 1% in terms of its deviation from c, and the absorption coefficient is of order $\pm 5 \pm 10^{-14}$ cm^{-1} which is close to the analytical result 0.

Table 7.3. Run 2, Zero-π Pulse Error Check

BLOCH R = 1.011E+07 NCYCLE = 101

VARIABLES IN SPACE

	R1	AREAR 0	ENERGY 0	VELOCITYC 0	KAPPA1 0
1	9.00E+05	1.412776E-02	1.596934E+01	4.552030E-07	1.45[illegible]E-13
2	2.10E+06	1.262059E-02	1.597074E+01	4.[illegible]E-07	2.03[illegible]E-13
3	3.30E+06	4.819920E-03	1.597209E+01	4.5[illegible]E-07	2.40[illegible]E-14
4	4.50E+06	-1.171548E-03	1.597281E+01	4.5[illegible]E-07	2.10[illegible]E-13
5	5.70E+06	-4.392617E-03	1.597303E+01	4.5[illegible]E-07	1.43[illegible]E-13
6	6.90E+06	-6.274506E-03	1.597217E+01	4.[illegible]E-07	2.72[illegible]E-14
7	8.10E+06	-8.102992E-03	1.597056E+01	4.5[illegible]E-07	7.57[illegible]E-15
8	9.30E+06	-9.000454E-03	1.596845E+01	4.5[illegible]E-07	5.63[illegible]E-15
9	1.05E+07	-1.030551E-02	1.596695E+01	4.5[illegible]E-07	4.07[illegible]E-14
10	1.17E+07	-1.068030E-02	1.596620E+01	4.5[illegible]E-07	5.02[illegible]E-14
11	1.29E+07	-8.679084E-03	1.597137E+01	4.55[illegible]E-07	1.78[illegible]E-14
12	1.41E+07	-5.372670E-03	1.597247E+01	4.5[illegible]E-07	-5.8[illegible]E-16
13	1.53E+07	-1.109944E-03	1.597283E+01	4.557[illegible]E-07	1.0[illegible]E-14
14	1.65E+07	3.470508E-03	1.597251E+01	4.556[illegible]E-07	2.5[illegible]E-14
15	1.77E+07	7.923043E-03	1.597160E+01	4.55[illegible]E-07	1.47[illegible]E-14
16	1.89E+07	1.141643E-02	1.597019E+01	4.5[illegible]E-07	-2.5[illegible]E-14
17	2.01E+07	1.315833E-02	1.[illegible]E+01	4.5[illegible]E-07	-1.8[illegible]E-14
18	2.13E+07	1.266452E-02	1.596926E+01	4.5[illegible]E-07	5.12[illegible]E-14
19	2.25E+07	1.036675E-02	1.597051E+01	4.55[illegible]E-07	4.27[illegible]E-14
20	2.37E+07	6.207010E-03	1.597191E+01	4.55[illegible]E-07	-1.1[illegible]E-15
21	2.49E+07	1.893693E-03	1.597272E+01	4.55[illegible]E-07	3.59[illegible]E-15
22	2.61E+07	-2.370777E-03	1.597264E+01	4.557[illegible]E-07	3.30[illegible]E-14
23	2.73E+07	-6.221853E-03	1.597209E+01	4.5[illegible]E-07	4.13[illegible]E-14
24	2.85E+07	-9.434073E-03	1.597103E+01	4.55[illegible]E-07	-4.61[illegible]E-15
25	2.97E+07	-1.162734E-02	1.596959E+01	4.552[illegible]E-07	-5.35[illegible]E-14

In Figures 3a-d we show, as a function of time, the pulse field, polarization, population and power for the 0π pulse considered. The frame is 2 nsec wide in time and shifts from one space point to the next to keep the pulse center in the center of the frame. The points in space cover up to 2.67×10^7 cm (267 kilometers) propagation. Of note is that the pulse experiences a bit more than one period in its cycle by the end of the distance propagated. In Fig. 3e we show the magnitude squared of the Fourier transform of the normalized electric field. The frequency is measured in cm^{-1}. One observes that the transform is periodic in space, "breathing" as it were while propagating.

In 4a-d we show "three dimensional" displays of the normalized field, polarization, population and power for lossless 10 psec 0π propagation, in time (T) and space (R).

Run 3: Lossy 0π pulse propagation.

In this run we use the following parameters for the case of lossy propagation of a 0π pulse:

$$\begin{aligned} t_o &= 100 \text{ psec} & \lambda^{-1} &= 6.1 \text{ cm}^{-1} \\ N_o &= 2.77 \times 10^{11} \text{ cm}^{-3} & \Delta\omega &= 0 \\ \mu &= 4.58 \times 10^{-2} \text{ e}\mathring{A} & T_1 &= T_2 = 185 \text{ psec} \\ t_e &= t_f = 100 \text{ psec} \end{aligned} \tag{7.10}$$

and for time and space steps we use the values in (7.2).

The primary results are shown in Figs. 5a-d. Note that the computer graphics omitted the very first values of the function plotted. The pulse area is initially close to zero and increases to slightly more than unity by 5×10^6 cm propagation. This is due to the absorption of the second lobe of the electric field which has negative phase. As the pulse continues through its cycle the area decreases and becomes negative by 1.5×10^7 cm. The pulse energy is initially at the $0\text{-}\pi$ value of 16 in normalized units, and decreases to about 5% of that value by the end of the run. In Fig. 5c the linear (upper curve) and nonlinear (lower curve) absorption coefficients are shown. The linear absorption coefficient is determined by solving first

$$\left(\frac{\partial}{\partial t} + \frac{1}{T_{2j}} - i\Delta\omega_j\right) P_j(x, t) = - \mu_j E(x, t) \qquad (7.11)$$

for the polarization (this is the linear limit of the equation in (2.4)) and then computing the absorption coefficient through (4.2) and dividing by (ct_o) to get the result in absolute units. Basically the nonlinear absorption coefficient is initially about 0.6 the value of the linear equivalent, and the ratio increases towards unity as the pulse energy decreases. The medium response becomes increasingly linear as the pulse is attenuated. The ratio of the absorption coefficients is shown in Fig. 5d.

In Figs. 6a-d we show plots versus time, at different spatial positions, of the field, population, power and the magnitude squared of the Fourier transform. The electric field is seen to decay, although it manages to cycle through more than a period as in the nonlinear case. In 6b the populations are shown, demonstrating that as the pulse propagates, the saturation decreases markedly. The pulse power is attenuated as shown in 6c, and in 6d one can get a glimpse of what the attenuation means in transform space, namely that the medium is chewing out the center of the spectrum.

Run 4: Lossy short 0π-pulse propagation.

We now consider propagation of a much shorter 0π pulse in the resonant absorption case. We assume the following parametric values

$$\begin{aligned} t_o &= 10 \text{ psec} & \lambda^{-1} &= 6.1 \text{ cm}^{-1} \\ N_o &= 2.77 \times 10^{11} \text{ cm}^{-3} & \Delta\omega &= 0 \\ \mu &= 4.58 \times 10^{-2} \text{ e}\mathring{\text{A}} & T_1 &= T_2 = 185 \text{ psec} \\ t_e &= t_f = 10 \text{ psec} \end{aligned} \tag{7.12}$$

and for time and space steps we use

$$\begin{aligned} x_{min} &= 0 & t_{min} &= -130 \text{ psec} \\ x_{max} &= 3 \times 10^8 \text{ cm} & t_{max} &= 130 \text{ psec} \\ \Delta x &= 3 \times 10^6 \text{ cm} & \Delta t &= 0.52 \text{ psec} \\ nx &= 100 \text{ steps} & nt &= 500 \text{ steps.} \end{aligned} \tag{7.13}$$

In Figs. 7a-d the primary results are summarized. Fig. 7a shows the pulse area which makes excursions between 0.04 and -0.05. Since the pulse is shorter now than in the previous runs, the loss plays a smaller role and the pulse area stays much closer to zero. The pulse energy is shown in Fig. 7b, illustrating near linear decay from 16 to about 9 in normalized units during 3×10^8 cm propagation. The linear (upper curve)

and nonlinear (lower curve) absorption coefficients are shown in 7c, illustrating a "ringing" in the linear absorption coefficient. This result is due to the fact that the Fourier spectrum "breathes" as it propagates, and the different parts of the cycle see different absorption coefficients. The ratio of the nonlinear to the linear absorption coefficient is shown in 7d. In Fig. 8a-d we give the field, population, power and square of the transform for the run, as function of time, at different spatial positions.

Run 5: Lossy long 0π-pulse propagation.

In this run we example lossy long pulse propagation, using the following parameters

$$\begin{aligned} t_o &= 1 \text{ nsec} & \lambda^{-1} &= 6.1 \text{ cm}^{-1} \\ N_o &= 2.77 \times 10^{11} \text{ cm}^{-3} & \Delta\omega &= 0 \\ \mu &= 4.58 \times 10^{-2} \text{ eÅ} & T_1 &= T_2 = 185 \text{ psec} \\ t_e &= t_f = 1 \text{ nsec} \end{aligned} \tag{7.14}$$

and for time and space steps we use

$$\begin{aligned} x_{min} &= 0 & t_{min} &= -13 \text{ nsec} \\ x_{max} &= 3 \times 10^6 \text{ cm} & t_{max} &= 13 \text{ nsec} \\ \Delta x &= 3 \times 10^4 \text{ cm} & \Delta t &= 52 \text{ psec} \\ nx &= 100 \text{ steps} & nt &= 500 \text{ steps.} \end{aligned} \tag{7.15}$$

The results are shown in Fig. 9a-d in which plots of the pulse area, energy, absorption coefficients and ratio of absorption coefficients are found.

VIII. Results: One Line, Off Resonant Case

Run 1: Lossless 2π pulse propagation.

In the first run we consider propagation of a 2π pulse off resonance, comparing analytical results with the numerical results. In this problem we take the following parameter values

$$\begin{aligned} t_o &= 100 \text{ psec} & \lambda^{-1} &= 6.1 \text{ cm}^{-1} \\ N_o &= 2.77 \times 10^{11} \text{ cm}^{-3} & \Delta\omega &= -0.05 \text{ cm}^{-1} \\ \mu &= 4.58 \times 10^{-2} \text{ eÅ} & T_1 &= T_2 = 10^{50} \text{ sec} \end{aligned} \tag{8.1}$$

and for time and space steps

$$\begin{aligned} x_{min} &= 0 & t_{min} &= -1 \text{ nsec} \\ x_{max} &= 3 \times 10^7 \text{ cm} & t_{max} &= 1 \text{ nsec} \\ \Delta x &= 3 \times 10^5 \text{ cm} & \Delta t &= 6.67 \text{ psec} \\ nx &= 100 \text{ steps} & nt &= 300 \text{ steps.} \end{aligned} \tag{8.2}$$

The input field was $2\operatorname{sech} t$ in normalized units. The results are given in Table 8.1. The real pulse area oscillates sinusoidally, the pulse energy is within 0.3% of the analytic value. The pulse velocity is probably accurate to within 1% in the difference between it and c. The absorption coefficient

Table 8.1

BLOCH R = 1.011E+07 NCYCLE = 101

VARIABLES IN SPACE

	AREAR	ENERGY	VELOCITYC	KAPPAI
	0	0	0	0

	R1				
2	2.10E+06	5.961888E+00	7.977261E+00	4.833019E-07	6.289094E-14
3	3.30E+06	5.509465E+00	7.977259E+00	4.833023E-07	4.067003E-14
4	4.50E+06	4.875769E+00	7.977256E+00	4.833014E-07	5.480655E-14
5	5.70E+06	4.080944E+00	7.977255E+00	4.833010E-07	3.436070E-14
6	6.90E+06	3.150494E+00	7.977254E+00	4.833013E-07	4.410132E-14
7	8.10E+06	2.114616E+00	7.977253E+00	4.833005E-07	6.193655E-14
8	9.30E+06	1.007266E+00	7.977251E+00	4.833005E-07	5.422004E-14
9	1.05E+07	-1.350010E-01	7.977250E+00	4.833006E-07	4.454500E-14
10	1.17E+07	-1.274145E+00	7.977249E+00	4.833001E-07	5.191272E-14
11	1.29E+07	-2.372004E+00	7.977248E+00	4.832997E-07	6.046662E-14
12	1.41E+07	-3.391639E+00	7.977247E+00	4.832997E-07	5.470850E-14
13	1.53E+07	-4.298672E+00	7.977247E+00	4.833001E-07	4.266604E-14
14	1.65E+07	-5.062542E+00	7.977246E+00	4.833001E-07	3.020252E-14
15	1.77E+07	-5.657596E+00	7.977246E+00	4.833000E-07	4.074611E-14
16	1.89E+07	-6.063974E+00	7.977246E+00	4.832999E-07	4.962900E-14
17	2.01E+07	-6.268262E+00	7.977245E+00	4.833001E-07	3.456227E-14
18	2.13E+07	-6.263063E+00	7.977245E+00	4.833003E-07	2.087634E-14
19	2.25E+07	-6.051231E+00	7.977245E+00	4.833005E-07	2.730579E-14
20	2.37E+07	-5.637773E+00	7.977245E+00	4.833002E-07	2.817435E-14
21	2.49E+07	-5.037567E+00	7.977245E+00	4.833003E-07	2.883990E-14
22	2.61E+07	-4.270845E+00	7.977246E+00	4.833005E-07	2.624766E-14
23	2.73E+07	-3.363276E+00	7.977246E+00	4.833005E-07	2.490846E-14
24	2.85E+07	-2.345005E+00	7.977246E+00	4.833006E-07	2.612571E-14
25	2.97E+07	-1.250029E+00	7.977246E+00	4.833005E-07	3.85214[illegible]

is less than 10^{-13} cm^{-1}. The accuracy of the calculation is sufficient for the purposes of the analysis.

Off-Resonant Propagation of "Zero-pi Pulse"

As explained in the appendix, there is no zero-pi pulse like solution for propagation in a collision free medium, i.e. a pulse with its spectrum not centered at the material line. Computer runs made with a zero-pi pulse with a spectrum computed at resonance and then simply shifted off resonance show break-up of the pulse into two separate pulses.

When loss is introduced, the pulse does not necessarily break before linear propagation is reached due to the loss. In this set of runs we consider the case of lossy propagation at several values of the detuning $\Delta\omega$. In 10a-d we show the Fourier transform magnitude squared of the normalized field in space (cm) and frequency (cm^{-1}), at $\Delta\omega = 0$, .05 cm^{-1}, .10 cm^{-1} and .20 cm^{-1}. Basically, when the pulse is chirped, one of the lobes (this one which has more overlap with the lossy line) is eaten away faster than the other.

In Fig. 11a-d are shown the normalized field, polarization, population and absolute power for a chirped 0π pulse defined to $\Delta\omega = 0.05$ cm^{-1}. Of note is that the pulse does not break up-- a result which follows simply from the fact that breaking up is a nonlinear effect, and the pulse does not remain nonlinear

long enough to break up ($t_e = t_f = 100$ psec). In Fig. 12a-d are presented the normalized electric field versus T and R at $\Delta\omega = 0$, .10 cm^{-1}, .20 cm^{-1}, 0.60 cm^{-1}. One can see that the nonlinear gyrations of the field are slower in the case of detuned propagation; when the line is detuned, the effect of the line on the pulse becomes less.

In 13a-c are displayed the normalized real polarizations (Imaginary polarizations are not shown). The effect of the field on the medium is less off resonance. In Fig. 14 are shown the populations (normalized) at $\Delta\omega = 0$, 0.1 and 0.2 cm^{-1}. The saturation is much less off resonance, and the "rippling" which is a nonlinear effect is virtually absent off resonance.

Fig. 15 shows the pulse power at $\Delta\omega = 0$, .10 cm^{-1} and .20 cm^{-1}. One observes simply that the rippling is less at resonance. The message is that as one gets further off-resonance, the 0-π-like nonlinear effect (i.e. rippling) is weaker. The difference between the linear absorption and nonlinear absorption is primarily a saturation effect rather than due to any other special 0π property.

Figs. 16, 17 and 18 give plots versus distance respectively at $\Delta\omega = 0$, 0.05, and 0.10, for $t_e = t_f = 100$ psec.

(a) pulse area (real and imaginary)

(b) normalized pulse energy

(c) the deviation of the pulse velocity u from the speed of light in terms of $1 - u/c$

(d) the loss coefficients for linear and nonlinear absorption

(e) the ratio of nonlinear to linear loss.

IX. H_2O Lines Adjacent to CH_3F and D_2O Laser Lines

The Methyl Fluoride (CH_3F) laser at 496 μ and the D_2O laser at 385 μ are two available submillimeter sources whose radiations fall between main absorption lines of H_2O. For this reason we study specifically the two radiations and represent the water vapor absorption by the nearest adjacent lines.

Water is an "asymmetric-top" molecule (Townes-Schawlow, 1955). The energy levels of such a molecule are described in terms of three numbers, J, K_{-1} and K_1 respectively. J is the total angular momentum and is a "good" quantum number. K_{-1} and K_1 are not "good" quantum numbers in that they do not represent the angular momentum around one of the three principal axes of the molecule. In general, there is no level degeneracy for a particular set of values of J, K_{-1}, K_1. There is, however, an orientational degeneracy.

We obtained line strengths from the computer printouts of S. A. Clough. These line strengths contain information on the dipole moment $\langle|\mu|^2\rangle$ averaged over all orientations of the molecules. One may start with the two level system equations, (1.15) and (1.16) of the Appendix, in the small signal limit in which $\rho_{11} - \rho_{22}$ can be treated as constant. Then, one

solves for ρ_{12} on line center and puts the result into (1.10) of the Appendix. The spatial rate of change of E may be equated to the amplitude decay coefficient (α in the notation of Marcuse, 1970, p. 286, not to be confused with the α used here earlier). One finds, in agreement with Marcuse,

$$\alpha = \frac{\omega|\mu|^2 T_2}{2\varepsilon ch} N(\rho_{22} - \rho_{11}). \tag{9.1}$$

An orientational degeneracy forces one to take averages over all M so that the average α, $\langle\alpha\rangle$, contains the average of $|\mu|^2$, $\langle|\mu|^2\rangle$.

The line strengths s, as used by Clough, are the $\langle\alpha\rangle$ integrated over the line width function

$$g(\nu) = \frac{1}{1 + \left(\frac{\nu - \nu_o}{\Delta\nu}\right)^2} \tag{9.2}$$

where $2\pi\Delta\nu = 1/T_2$, and expressed in inverse centimeters. The conversion factor is

$$1 \text{ sec}^{-1} = 3.34 \times 10^{-11} \text{ cm}^{-1}. \tag{9.3}$$

Combining all this one finds

$$\mu_D \equiv \sqrt{\langle|\mu|^2\rangle} = \left[\frac{s\lambda}{\frac{N_{abs}}{N_{H_2O}}\ 7.85 \times 10^{-15}}\right]^{1/2} \text{ debye} \qquad (9.4)$$

with $N_{abs}/N_{H_2O} \equiv \rho_{22} - \rho_{11}$ defining the ratio of the population density difference participating in the transition to the total population density of water molecules.

Further,

$$N_{abs}/N_{H_2O} = \frac{g(2J+1)}{2} \exp -\left(\frac{h\nu_\ell}{kT}\right)\left[1 - \exp -\frac{h\nu_u - h\nu_\ell}{kT}\right] . \qquad (9.5)$$

Any molecule of angular momentum J can have $2J + 1$ orientations with respect to a fixed spatial axis (say the applied electric field direction). These orientations are described by the "good" quantum number M where Z is the partition function. For H_2O at $T = 296°K$, $Z = 174.83$ (S. A. Clough, private communication).

The constant g is the statistical weight of the lower level (Townes-Schawlow, Table 4-7)

$g = 1$ for symmetric level

$g = 3$ for antisymmetric level.

The symmetry or antisymmetry is determined from K_{-1} and K_1, depending upon whether $K_{-1} + K_1$ is even or odd. Further, $h\nu_o = h\nu_u - h\nu_\ell$, where $h\nu_u$ is the energy of the upper level, $h\nu_\ell$ that of the lower level. Now, $\langle|\mu|^2\rangle$ gives the average matrix element for absorption of a field, with fixed orientation with respect to a spatial axis, say the z-axis. The z-component of μ has two different dependences upon M, one for a transition, $J \to J' = J + 1$, the other for $J \to J' = J$. In the Fourier case (Townes-Schawlow, 1-73)

$$|\mu_z|^2 \propto (J + 1)^2 - M^2; \qquad J' = J + 1 \tag{9.6}$$

In the latter case,

$$|\mu_z|^2 \propto M^2; \qquad J' = J. \tag{9.7}$$

We find by simple recursion

$$\sum_{-J}^{J} M^2 = \frac{1}{3} J(2J + 1)(J + 1). \tag{9.8}$$

The initial population difference for nonlinear interaction with any one of the transitions of given M is

$$N_{H_2O} \frac{g(2J + 1)}{Z} \exp - \left(\frac{h\nu_\ell}{kT}\right)\left[1 - \exp - \left(\frac{h\nu_u - h\nu_\ell}{kT}\right) \quad \frac{g_\ell}{g_u}\right]$$

where

$$g_\ell/g_u = 1 \qquad \text{for} \quad \Delta J = 0$$

$$g_\ell/g_u = \frac{2J + 1}{2J + 3} \qquad \text{for} \quad \Delta J = 1.$$

The reason for this is that, in the absence of collisions, a transition $J \to J + 1$, $M \to M$, reaches only the $M' = M$ states, and not the final ones $M' = \pm (2J + 3)$. These states are unaffected by the radiation and get filled only after M-changing collisions have occurred. Such collisions cannot be dipole-dipole collisions, and thus they occur at a much lower rate than $1/T_2$. We shall ignore these collisions and hence ignore the $M' = \pm (2J + 3)$ states of the upper level in our propagation studies.

The parameters used in the computations are summarized in Tables 9.1 and 9.2. We studied resonant excitation of the four lines at 18.577, 20.704, 25.080 and 30.560 cm^{-1}, that lie near the CH_3F and D_2O laser lines. The new feature is that these lines are degenerate and therefore the different M-levels are excited differently. There is no zero-pi pulse solution in the loss-free case, strictly speaking. We picked a pulse that would be a zero-pi pulse in a nondegenerate system

Table 9.1

Summary of H_2O Data on 4 Lines

Line cm^{-1}	$(JK_{-1}K_1)_{lower}$	$(JK_{-1}K_1)_{upper}$	g	F_ℓ cm^{-1}	F_u cm^{-1}	N_L $\times 10^{15}$	$(1 - e^{-\frac{E}{kT}})$ $\times 10^{-2}$	N_{abs} $\times 10^{14}$
18.577	110	101	3	23.794	42.371	9.04	8.62	7.79
20.704	532	441	3	488.1	508.1	3.48	9.56	3.33
25.080	211	202	1	70.091	95.171	4.01	11.5	4.61
30.560	422	331	1	285.219	315.779	2.54	13.8	3.51

Population density of lower level:

$$N_L = \frac{g_N(2J + 1)\, e^{-E/kT}}{Z}; \qquad Z = 174.83$$

Population difference:

$$N_{abs} = N_L(1 - e^{-\Delta E/kT})$$

Line cm^{-1}	s per molecule × cm	N_{abs}/N_{H_2O} $\times 10^{-3}$	μ debye $\times 10^{-2}$	$S(N_{abs})$ per molecule × cm $\times 10^{-17}$
18.577	5.00×10^{-20}	3.95	2.95	1.27
20.704	5.65×10^{-22}	1.69	0.454	0.0334
25.080	3.47×10^{-20}	2.34	2.74	1.48
30.560	1.43×10^{-21}	1.78	0.579	0.0803

The relaxation time:

$$T_2(\text{sec}) = \frac{3.34 \times 10^{-11}}{2\Delta\nu} \qquad \Delta\nu \text{ in } cm^{-1}.$$

Table 9.2

Summary of Input Data for Individual Levels

Case 1: J = 1, J' = 1.

Line	μ	N_{abs} × density	T_2
cm^{-1}	debye × 10^{-1}	$cm^{-3} \times 10^{14}$	sec × 10^{-12}
18.577	2.95	7.79	155
|M| = 1	4.43	5.19	

Case 2: J = 5, J' = 4

Line	μ	N_{abs} × density	T_2
cm^{-1}	debye × 10^{-2}	$cm^{-3} \times 10^{13}$	sec × 10^{-12}
20.704	4.54	33.3	230
|M| = 3	3.96	7.40	
|M| = 2	5.20	7.40	
|M| = 1	5.94	7.40	
|M| = 0	6.19	3.70	

Table 9.2 (continued)

Case 3: J = 2, J' = 2.

Line cm^{-1}	μ debye $\times 10^{-1}$	$N_{abs} \times$ density $cm^{-3} \times 10^{14}$	T_2 sec $\times 10^{-12}$
25.080	2.74	4.61	164
|M| = 2	5.48	1.84	
|M| = 1	1.37	1.84	

Case 4: J = 4, J' = 3.

Line cm^{-1}	μ debye $\times 10^{-2}$	N_{abs} density $cm^{-3} \times 10^{14}$	T_2 sec $\times 10^{-12}$
30.560	5.79	3.51	199
|M| = 2	5.79	1.00	
|M| = 1	7.24	1.00	
|M| = 0	7.72	0.500	

with the same value of $\sqrt{<|\mu|^2>}$. Note that the power in such a pulse scales like $1/<|\mu|^2>t_e^2$. Because the $<|\mu|^2>$ values of the lines are not greatly different, we are dealing in all cases with pulses of peak power of the order of 10 Mw/cm^2 for 100 psec pulse-length-- comparable to the pulse power of the 6.1 cm^{-1} line analyzed earlier.

The 18.577 line does not represent much novelty. It behaves like a nondegenerate line because only the levels $M = 1$ interact with the radiation and they have the same dipole moment. The only feature worth noting is that the penetration dipole is very short. The distance scale terminates at 10 m-- the absorption line is indeed very strong. Saturation has reduced the loss to 55% of its nonlinear value, but after about 6 m propagation the loss has approached the linear loss to within 85%-- the penetration has been improved, but very little.

Figure 21 plotted for the 20.704 cm^{-1} line is on a scale of 1.4 km-- a much weaker absorption. We note that the different M-levels are acted upon differently by the radiation, and the loss in each is reduced by different amounts due to nonlinear effects. The transition is one with $\Delta J = 1$ so that the strongest dipole moment is for $M = 0$. Figure 21d shows that indeed the largest reduction in loss occurs for $M = 0$,

to about 45% of the linear value. For the $M = 0$ line the equivalent "average" zero pi pulse used for the computation has more energy than a true zero-π-pulse would have for this level of strongest dipole moment, hence the large reduction in loss. Yet, after roughly a 1/e decay length the loss reduction has disappeared for all practical purposes.

Figure 22 is for a line with $\Delta J = 0$. The strongest dipole moment is for $|M| = 2$. From Fig. 22c we gather that indeed this level has the larger loss reduction, to about 60% of its linear value. Note that the penetration depth is of the order of 5 m, again this is a very strong absorption line.

Figure 23 is for a $\Delta J = 1$ transition and qualitatively duplicates the behavior of the $\Delta J = 1$ transition at 20.704 cm^{-1}, Figure 21. It is a weaker absorption line, the horizontal scale extends to 450 m.

X. Propagation of CH_3F Laser Radiation

In the preceding section we studied propagation of radiation in resonance with the degenerate lines adjacent to the CH_3F and D_2O lines at 495 μ and 385 μ respectively. The propagation characteristics were not greatly different from those in resonance with a nondegenerate line. As a final test, we study the propagation of 495 μ radiation as it is affected by absorption via the strongest adjacent line , the 18.577 cm^{-1} line. Figs. 24a,b show the propagation of a 10 psec pulse. The shape of the pulse is taken as that of a zero-pi pulse on resonance with the line, detuned to 495 μ = 20.2 cm^{-1}. Curve A of Fig. 24a has the energy appropriate for a zero pi pulse, the others are of higher energy. The 1/e decay is roughly 500 m. Fig. 24b shows several interesting features. Curve A is for a small signal pulse. It shows a dramatic decrease of κ-- the attenuation constant, as a function of propagation. This is due to the fact that the portion of the spectrum that lies on the high absorption side of the line gets "eaten-up" initially. The remaining part of the spectrum has smaller loss as it continues its propagation.

Curve B of Fig. 24b corresponds to curve A of Fig. 24a. The initial saturation effect is very noticeable reducing κ to about 30% of its small signal value. As the pulse propagates,

the absorption coefficient exceeds the small signal value because the most "favored" part of the spectrum, nearest to the line center of the absorption line, has a weaker saturation effect after attenuation has occurred.

Conclusions

The zero-pi pulse as published by Lamb (1974) is a special case of a self induced transparency solution obtained when the spectral line of the medium is symmetric and the carrier frequency of the pulse is centered with respect to the line. Following "small signal" reasoning, we were interested in detuning pulses from line center so that the loss is avoided at least partially when the "center of gravity" of the spectrum lies outside the absorption line. Generalized solutions have not been published although the formalism of inverse scattering theory can be applied to that case. Lamb, in another paper (1973), gave a general formula which is wrong (his equation 16). For this reason the analysis was redone to provide the starting point for the computations presented in this report.

We have, therefore, applied the Inverse Scattering Theory to obtain an expression for the generalized zero-pi pulse. In the course of this work we found it necessary to cast the formalism developed by mathematicians into language and models understandable to the physicist and engineer. A paper on the first version of this work will appear in Reviews of Modern Physics. The appendix of this report is a further simplification which avoids entirely the use of the Marchenko equation of Fourier transform space and thus gives more rapidly results

useful to the evaluation of the zero-pi pulse. One important outcome of the analysis is that there exists no zero-pi pulse detuned from line center. Any pulse of the "breather type" (such as the zero-pi pulse is called because it changes shape as it propagates) breaks up when its spectrum is not centered with the line of the medium. Therefore, we used in the computer analysis in the off-resonant case an electric field envelope evaluated from the on-resonant case, and shifted off resonance. Such pulses are found not to break up when sufficient loss is introduced so that the intensity of the pulse is decreased to a sufficiently low level before the break-up had a chance to occur.

The numerical studies proceeded in two stages. First, we looked at 2π and $0\text{-}\pi$ pulse propagation in the absence and presence of loss at and near the $6.1\ cm^{-1}$ line of H_2O, without including the degeneracy of the level so that ideal 2π pulse and $0\text{-}\pi$ pulse propagation in the absence of loss was possible. This numerical study showed certain features of zero-pi pulse propagation in the presence of loss in the simplest possible context. The analysis also enabled one to test the program for its potential of predicting long distance propagation (up to 3×10^7 cm), in this case of low absorption. The following specific findings are of interest, but note that level degeneracy had not been taken into account-- thus the beneficial effects of saturation are exaggerated.

(a) The attenuation of the 6.1 cm^{-1} H_2O line is reduced to .6 of its linear value for a zero-pi pulse over a distance within which the energy has not been greatly depleted. After that the pulse propagates in essentially a linear manner. For a 100 psec pulse, the required peak intensity is 8 MW/cm^2. Typical propagation distances are 20 km.

(b) The off-resonant "zero-pi pulse" can lead to a further reduction of loss to .25 of its linear value, if one peak of the double-peaked spectrum of the zero-pi pulse is made to coincide with the absorption line. This is an indication of a saturation-bleaching effect, the bleaching is more effective when the spectrum has greater net intensity within the spectral response width of the medium.

(c) Further detuning of the "zero-pi" pulse spectrum from the absorption line gives less loss reduction.

(d) As a pulse is detuned from line center, the loss is reduced as one would expect from a linear analysis because less of the spectrum coincides with the absorption line. In fact, a "zero pi" pulse of 8 MW/cm^2 intensity as defined for on resonance propagation, when detuned by more than a linewidth, interacts with the medium in an

almost linear fashion. This is because a relatively small portion of the spectrum interacts with the medium.

(e) The zero-pi pulse has no small signal limit. Accordingly, diffraction effects will have an effect on zero-pi pulse propagation within a beam of finite cross section similar to that of 2π pulses.

(f) The CH_3F and D_2O laser lines lie in the wings of very strong water vapor absorption lines. These lines connect degenerate levels and hence S.I.T. solutions do not exist in the lossless (collision-free) case (except for the 18.577 line). Using on resonant propagation at any one of the four lines of "equivalent" zero-pi pulses with (+ -) areas chosen to correspond to the average matrix element of the transition, one observes reductions of absorption due to saturation very similar to those of the nondegenerate case, of the order of 55% of the linear loss. The penetration depths are now much shorter; of the order of 5 m for the two strong lines, 500 m for the two weak lines.

(g) The peak power of the equivalent zero-π pulse scales like $1/|\mu|^2 t_e^2$. Hence the peak power one needs to experience nonlinear loss reduction is of the order of 10 Mw/cm^2 for all the lines-- their dipole moments being all of order 0.5 debye.

(h) The CH_3F and D_2O laser lines lie in a regime of relatively weak absorption. Fig. 1 shows that the linear loss exponent $2\alpha\ell_o$ within 1 km is 9.5 and 16 respectively, corresponding to 1/e decay distances of 105 m and 62 m respectively.

(i) On-resonant propagation on the 20.704 cm^{-1} line produces 1/e decay distances of the order of 360 m which is much greater than the 105 m distance of linear propagation read off the graph. The discrepancy is due to the fact that the wing of the strong adjacent line at 18.577 influences the linear loss at the 20.02 cm^{-1} line of the CH_3F laser reducing the 1/e decay distance appreciably.

(j) Off-resonant propagation, at the frequency of the CH_3F line, of a zero-pi-like pulse of 10 psec duration shows the following characteristics: In the small signal limit, the spectral component of the pulse on the high side of the absorption line gets eaten up and the attenuation coefficient decreases with further propagation. An intense pulse achieves appreciable initial reduction of attenuation (to 30% of small signal limit) until the absorption has reduced its intensity.

(k) In the case when the pulse energy is several times the on-resonant zero-pi-pulse energy, the pulse breaks up into a series of pulses traveling at different speeds.

(l) The zero-degree pulse propagation with low loss as observed by Grieneisen et al. was a linear phenomenon, associated with the peculiar spectral distribution characteristic of a zero degree, small signal pulse (which is also characteristic of the zero-pi large signal pulse). The spectrum has zero intensity at the carrier frequency. Hence a zero-degree pulse with the carrier centered at the line experiences reduced absorption because the "bulk" of the spectrum lies outside the absorption line. There are other subtle effects in the limit of inhomogeneous broadening, that were discussed by Grieneisen et al., but do not concern us here because H_2O is homogeneously broadened at atmospheric pressure.

(m) The overall conclusion is that lower loss can be achieved in the linear regime when the spectrum is moved away from the frequencies of maximum absorption. The use of carrier frequencies that are far from the peak of the absorption lines are equally or more effective. The zero-degree pulse would be useful only in those cases in which the use of a laser frequency coincident with an atmospheric absorption line were required, e.g. when a CO_2 laser

is used and absorption by atmospheric CO_2 is to be reduced.

Acknowledgements

Fred Jones, the graduate student supported by this contract did much of the literature search and assimilation, and developed a computer program. The computer plots were supplied by Peter Hagelstein at Lawrence Livermore Laboratory, whose help was invaluable when the deadline of the contract approached. Dr. Paul Kelley of Lincoln Laboratory advised us on the water vapor absorption physics. Professor M. W. P. Strandberg was also very helpful in explaining to us some of the fine points of the quantum mechanics of the asymmetric top.

Appendix I

Derivation of Two-pi-pulse and Zero-pi-pulse by the Inverse Scattering Method

Abstract:

The Inverse Scattering Method (ISM) as applied to Self-Induced Transparency (SIT) is reviewed. It is shown that the (Zakharov-Shabat) scattering equations follow directly from the two level system equations. The analytic continuation of the Zakharov Shabat equations into the complex plane is interpreted by an analog: the excitation of a parametric oscillator by sources growing exponentially in time. This model gives a "physical feel" for the behavior of the eigenfunctions of the scattering problem. The spatial invariance of the eigenvalues is proven following a method outlined by Ablamovitz et al. (1974). The 2π pulse and zero-pi pulse follow immediately and concisely from the preceding analysis. It is shown that no zero-pi-like solution exists with a spectrum centered off the material line.

Introduction

The inverse scattering method (I.S.M.) is one of the very few general methods of solution of a class of nonlinear differential equations in one spatial dimension and time (Gardner et al., 1967; Zakharov and Shabat, 1972; Whitham, 1974; Ablowitz et al., 1974a; Lamb, 1973). In the application of the I.S.M. a linear scattering problem of quantum-mechanical nature is associated with the nonlinear differential equation (Whitham, 1974). The sought-for solution of the nonlinear differential equation at the initial time $t = 0$ plays the role of the scattering potential or "well" of the linear scattering problem. The initial conditions of the problem to be solved prescribe the transmission and reflection coefficients of the linear scattering problem from which the scattering "well" may be determined by standard techniques of (inverse) scattering theory. The evolution in time of the scattering problem, which may take several forms (Ablowitz et al., 1974a,b), then prescribes the evolution in time of the solution of the nonlinear equation-- or alternately-- the form of the nonlinear differential equation associated with this particular scattering problem (see Fig. 2).

In 1973 Lamb showed (Lamb, 1973) how one may associate with the equations of self-induced transparency (S.I.T.) one of the standard equations of the I.S.M., the Zakharov-Shabat equations (Zakharov and Shabat, 1972). He proceeded through a set of variable transformations with no apparent physical interpretation. In fact, one of the intriguing unsolved problems of the I.S.M. is the development of a

procedure to find the scattering problem associated with a particular differential equation.

In many cases the scattering problem of quantum-mechanical character will have no physical interpretation. It is to be expected, however, that in those cases in which the physics underlying the nonlinear differential equation is based on quantum mechanics the associated scattering problem must have a direct physical meaning. In the case of the Josephson transmission line and S.I.T., this has been pointed out by McLaughlin and Corones (McLaughlin and Corones, 1974). The physical interpretation of the scattering problem obtained after Lamb had reduced the S.I.T. problem to one amenable to the inverse scattering method is but one example of various developments presented by different authors in the course of time. The present author attempted to gain an understanding of the I.S.M. by uncovering physical interpretations for the mathematical steps. Even though most of the specifics have appeared in the literature (Gardner et al., 1967; Zakharov and Shabat, 1972; Whitham, 1974; Ablowitz et al., 1974a,b; Lamb, 1973; McLaughlin and Corones, 1974; Ablowitz et al. 1973; Faddeyev, 1962), this paper may serve as a guide for the physically inclined to an important mathematical method.

The Zakharov-Shabat equations written as differential equations in normalized time τ with the electric field $\mathcal{E}(\tau, z)$ as the scattering "well" define the linear scattering problem associated with S.I.T. The spatial variable z plays the role of a parameter. In Section I we show the direct connection between the Zakharov-Shabat equations and the equations of the two-level system inter-

acting with the electric field in S.I.T.

The nature of the solutions to the Zakharov-Shabat equations may be anticipated by recognizing their similarity with a well known physical problem: the parametric interaction of two waves via a nonlinear medium excited by a pump wave (Yariv, 1976). This is done in Section II. In particular, it is known that "unstable" solutions growing in time are encountered in parametric interactions. This fact may be used to predict the location of the eigenvalues of the Zakharov Shabat equations in the complex plane.

The exploration in Section III of the behavior of the Zakharov-Shabat equation in the complex plane leads directly to an equation for those solutions of the Zakharov-Shabat equations that correspond to a reflection-free well, and the shape of the well.

In Section IV we show that the assumption of independence of z of the eigenvalues of the Zakharov-Shabat equations leads to a form of the Maxwell-Bloch equations of S.I.T. In Section V we obtain the 2π-pulse and zero-π pulse solutions.

I. The Zakharov-Shabat Equations as the Equations of the Two-Level Systems

The Zakharov-Shabat equations are central to the inverse scattering method applied to self induced transparency. In this section we review briefly the equations of a two level system excited by an E-field and show that the resulting equations are equivalent to the Zakharov-Shabat equations (Zakharov and Shabat, 1972) arrived at by Lamb (Lamb, 1973).

In the slow envelope approximation, the wave equation for the electric field envelope $\bar{E}(x, t)$ of a plane wave propagating in the x-direction is in mks units (compare (Lamb, 1973))

$$\frac{\partial \bar{E}}{\partial x} + \frac{1}{c}\frac{\partial \bar{E}}{\partial t} = \frac{i}{2}\frac{\omega}{c\varepsilon}\bar{P} \tag{1.1}$$

where ω is the "carrier" frequency, c the speed of light, ε the dielectric constant, and $\bar{P}$ the polarization in the medium. $\bar{P}$ and $\bar{E}$ are parallel to each other and transverse to the x-direction. The polarization of the medium is obtained from the analysis of two level systems with a distribution of energy-level spacings. Denote the amplitude of the wave function of the upper level (1) by a_1, that of the lower level (2) by a_2. One may write down two differential equations for the amplitudes a_1 and a_2 as coupled by the $\bar{E}$-field (Vuylsteke, 1960). Factoring out the natural time dependences and retaining only the slowly time varying portions of the variables, one has

$$\dot{a}_1 = \frac{i}{\hbar} \bar{E} \cdot \bar{p}_{12} \, e^{i\delta t} \, a_2 \tag{1.2}$$

$$\dot{a}_2 = \frac{i}{\hbar} \bar{E}^* \cdot \bar{p}^*_{12} \, e^{-i\delta t} \, a_1 \tag{1.3}$$

where $\delta = \omega - \omega_{12}$, and $\bar{p}_{12}$ is the matrix element between the two levels. If we define

$$a_1 \, e^{-\frac{i\delta}{2} t} \equiv v_1 \tag{1.4}$$

$$a_2 \, e^{+\frac{i\delta}{2} t} \equiv v_2 \tag{1.5}$$

we obtain

$$\frac{dv_1}{dt} + i \frac{\delta}{2} v_1 = i \frac{\bar{E} \cdot \bar{p}_{12}}{\hbar} v_2 \tag{1.6}$$

$$\frac{dv_2}{dt} - i \frac{\delta}{2} v_2 = i \frac{\bar{E}^* \cdot \bar{p}^*_{12}}{\hbar} v_1. \tag{1.7}$$

These are already the Zakharov-Shabat equations, except for a normalization. The density matrix ρ is the statistical average of the products of the amplitudes a_1, a_2 or v_1, v_2 and their

complex conjugates. Since we are dealing here with a pure state (no collisions) no statistical average need be performed.

$$\rho_{ij} = v_i \, v_j^* . \tag{1.8}$$

The positive frequency portion of the polarization $\bar{P}$ is given by

$$\bar{P} = \langle N \bar{p}_{21} \, \rho_{12} \rangle = N \, \bar{p}_{21} \langle v_1 v_2^* \rangle \tag{1.9}$$

where N is the particle density and the brackets indicate an average over all two level systems. One obtains from (1.1) and (1.11) by dot-multiplication of both sides by $\bar{p}_{12}/i\hbar$

$$\frac{c}{\Omega^2} \frac{\partial}{\partial x} \left(\frac{\bar{p}_{12} \cdot \bar{E}}{i\hbar} \right) + \frac{\partial}{\Omega^2 \partial t} \left(\frac{\bar{p}_{12} \cdot \bar{E}}{i\hbar} \right) = \langle v_1 v_2^* \rangle \tag{1.10}$$

where

$$\Omega^2 \equiv \frac{\omega N |\bar{p}_{12}|^2}{2 \hbar \varepsilon} . \tag{1.11}$$

The equation for the electric field (1.10) completes the system of equations; the solution of the Zakharov-Shabat equations

appears directly as a drive in the equation of the field. The system of equations is nonlinear in that the drive is nonlinear in v_1, v_2^*.

Through the use of the normalized variables

$$\mathcal{E} \equiv \frac{2\bar{p}_{12} \cdot \bar{E}}{i\hbar\Omega} \qquad 2\zeta \equiv \delta/\Omega$$

$$\tau = \Omega\left(t - \frac{x}{c}\right) \qquad z = \Omega x/c,$$

the equations (1.6), (1.7) and (1.10) assume the form

$$\frac{\partial \mathcal{E}}{\partial z} = \langle 2v_1 v_2^* \rangle \tag{1.12}$$

$$\frac{\partial v_1}{\partial \tau} + i\zeta\, v_1 = \frac{1}{2}\mathcal{E}\, v_2 \tag{1.13}$$

$$\frac{\partial v_2}{\partial \tau} - i\zeta\, v_2 = -\frac{1}{2}\mathcal{E}^*\, v_1. \tag{1.14}$$

These equations are already in one of the standard forms of inverse scattering theory. McLaughlin and Corones (1974) have pointed out the relation between the linear (Zakharov-Shabat) problem and the quantum mechanical equations of the Josephson

junction. They also touched on the problem of S.I.T. without making the connection of the v's with the wave function amplitudes.

For later reference, and to make connection with the Bloch equations, we also list the differential equations for the density matrix elements (1.8). They follow directly from (1.6) and (1.7)

$$\frac{d\rho_{12}}{dt} + i\delta\rho_{12} = \frac{\bar{E} \cdot \bar{p}_{12}}{i\hbar} (\rho_{11} - \rho_{22}) \tag{1.15}$$

$$\frac{d}{dt} (\rho_{11} - \rho_{22}) = - 2 \left\{ \frac{\bar{E} \cdot \bar{p}_{12}}{i\hbar} \rho_{21} - \frac{\bar{E}^* \cdot \bar{p}^*_{12}}{i\hbar} \rho_{12} \right\}. \tag{1.16}$$

After introduction of the variable τ and the definitions

$$\lambda \equiv 2\rho_{12} = 2v_1 v_2^*$$

$$N \equiv \rho_{11} - \rho_{22}$$

one obtains the normalized Bloch equations:

$$\frac{\partial \lambda}{\partial \tau} + 2i\zeta\lambda = \xi N \tag{1.17}$$

$$\frac{\partial N}{\partial \tau} = - \frac{1}{2} (\xi^* \lambda + \xi \lambda^*). \tag{1.18}$$

Lamb (1973) used the Bloch equations, and the field equation

$$\frac{\partial \mathcal{E}}{\partial z} = \langle \lambda \rangle \qquad (1.19)$$

as the defining equation of S.I.T. Lamb had to go through a series of transformations to derive the Zakharov-Shabat equations. Our way of deriving the equations shows, much more simply, that the Bloch equations are implied by the Zakharov-Shabat equations.

II. The Scattering Problem

We have shown that the nonlinear selfinduced transparency equation is cast naturally in terms of a set of linear differential equations for the amplitudes of the wave functions of the upper and lower levels coupled by the electric field. These were the equations of Zakharov and Shabat (1972) central to their formulation of the inverse scattering problem for the nonlinear Schroedinger equation and derived by Lamb (1973) from the density matrix equations of the two level system by a set of variable transformations. In this section we shall elaborate on the significance of the Zakharov-Shabat equations.

We consider them to be a set of equations of mode coupling in space, treating τ as if it were the distance coordinate, ζ the propagation constant (ζ is real by definition); the amplitudes v_1 and v_2 are then wave amplitudes. The function $\mathcal{E}(\tau)$ plays the role of the coupling coefficient. In the absence of an $\mathcal{E}$-field,

$$v_1 \propto \exp - i\zeta\tau \tag{2.1}$$

and

$$v_2 \propto \exp + i\zeta\tau. \tag{2.2}$$

The wave v_1 propagates in the $-\tau$ direction, the wave v_2 in

the $+\tau$ direction (assuming the physicist's definition of phase-delay as represented by the factor $\exp i\zeta\tau$ $(\zeta > 0)$). The amplitudes v_1 and v_2 are functions of ζ and τ. Consider briefly the Fourier transform

$$\int_{-\infty}^{\infty} d\zeta\, e^{-i\zeta y}\, v_1(\zeta, \tau) = V_1(y, \tau). \tag{2.3}$$

If ζ is taken to be a propagation constant, $\zeta = \omega/u$ with u the phase velocity of the uncoupled wave, ω the frequency, then y may be interpreted as a time variable $(y = ut)$. This further interpretation endows the waves v_1 and v_2 with dispersion-free propagation at group velocity u, in the absence of $\mathcal{E}$. The original self-induced transparency problem involving interactions of electromagnetic pulses with the nonlinear medium requires that $\mathcal{E}(\tau)$ has to vanish at $|\tau| \to \infty$. Hence, equations (1.13) and (1.14) describe coupling of waves in an interaction region extending from $-\infty < \tau < +\infty$, with vanishing interaction in the limit $|\tau| \to \infty$.

In the region where $\mathcal{E} \neq 0$, the forward and backward waves are coupled. The coupling is lossless in the sense that (for real ζ)

$$\frac{d}{d\tau}\left(|v_1(\zeta, \tau)|^2 + |v_2(\zeta, \tau)|^2\right) = 0 \tag{2.4}$$

as can be demonstrated easily from Eqs. (1.13) and (1.14). In

(2.4) waves (1) and (2) may be assigned powers $|v_1(\zeta, \tau)|^2$ and $|v_2(\zeta, \tau)|^2$. According to (2.4), both waves carry power in the same direction-- say the $+\tau$ direction. Because they have oppositely directed group velocities, their energies must be of opposite sign (Pierce, 1974).

The concept of negative small signal energy is widely used in plasma physics (Sturrock, 1961). Negative energy commonly occurs in energy conservation principles derived from the linearized equations of motion of a nonlinear system which contains an energy "reservoir" (such as the kinetic energy of a moving plasma or an electron beam (Pierce, 1974)). Excitation of a wave (usually a socalled slow wave (Sturrock, 1961)) may lower the overall energy of the system, a fact that manifests itself in terms of a negative energy attributed to the wave. The energy is quadratic in the excitation amplitude of the wave. If a negative energy-wave is coupled to a positive energy wave, both wave amplitudes may grow. The growth of positive energy is balanced by the growth of the negative energy, net small signal energy is conserved. One example of such a system is the Backward-Wave oscillator (Kleen, 1958).

More familiar may be the example of parametric interaction (Yariv, 1976) of two waves of frequencies ω_1 and ω_2 with a pump wave of frequency ω_p, so that $\omega_1 + \omega_2 = \omega_p$. The phase matching condition of the (colinear) propagation vectors $\bar{k}_1$ and $\bar{k}_2$ is then $\bar{k}_p = \bar{k}_1 + \bar{k}_2$. In the steady state, when phase matching is not realized, one may define

$$\zeta \equiv \frac{1}{2}\left[(k_1 + k_2) - k_p\right].$$

The equations of parametric coupling between the two waves as a function of the spatial coordinate (τ) are of the form of (1.13) and (1.14) when the "fast" spatial variations of the waves are removed and only the slowly varying variations of "envelopes" are considered. The energy densities must be reinterpreted as photon number densities, the power flows as photon number flows and energy conservation as photon number conservation. To be more specific, in a parametric process of the type where a pump photon ω_p produces a "signal" photon at frequency ω_1 and an "idler" photon at frequency ω_2, the number of signal photons generated either spontaneously, or by induced emission, must be equal to the number of idler photons. The wave amplitudes, v_1 and v_2 may be so normalized that $|v_1|^2$ and $|v_2|^2$ are proportional to the number of photons per unit length in the interacting wave (1) and (2). Then (with τ taken as the distance variable)

$$\frac{\partial}{\partial\tau}|v_1|^2 \pm \frac{\partial}{\partial\tau}|v_2|^2 = 0$$

are the Manley Rowe conservation relations applied to this parametric process (Manley and Rowe, 1959; Weiss, 1957). A parametric instability occurs with the + sign in the above equation, when the group velocities of waves (1) and (2) are oppositely directed.

The waves v_1 and v_2 have further properties somewhat

analogous to lossless coupling of electromagnetic waves that obey reciprocity relations. Indeed, from (1.13) and (1.14) it is easily shown that, given a solution (f is treated as a column matrix of components f_1 and f_2)

$$f = \begin{pmatrix} f_1 \\ f_2 \end{pmatrix}$$

then

$$\bar{f} \equiv \begin{pmatrix} f_2^* \\ -f_1^* \end{pmatrix}$$

is also a solution for the same ζ (if ζ is real). Further, these two solutions are physically different. Indeed, have f describe the coupling of wave v_2 to v_1 via $\xi(\tau)$ with boundary conditions as indicated schematically in Fig. 25a. The solution $\bar{f}$ is the one shown in Fig. 25b. The function $\bar{f}$ in relation to f is like the time reversed solution of electromagnetic waves used to demonstrate reciprocity.

One may generalize (2.4) to show conservation of "cross power", i.e. prove the conservation law

$$\frac{d}{d\tau}\,(f_1 g_1^* + f_2 g_2^*) = 0 \qquad (2.5)$$

where f and g are any two solutions of (1.13) and (1.14). Using

the property that

$$\bar{g} = \begin{pmatrix} g_2^* \\ -g_1^* \end{pmatrix}$$

is a solution, if g is one, (2.5) becomes

$$\frac{d}{d\tau}(f_1 g_2 - f_2 g_1) = 0. \tag{2.6}$$

This is known as conservation of the Wronskian (Gardner et al., 1967).

Thus far we have studied general properties of the scattering problem. One may use (1.13) and (1.14) to find solutions v_1 and v_2 for given $\mathcal{E}$. More relevant to the solution of the self-induced transparency problem is the inverse scattering problem: given v_1 and v_2, what coupling function $\mathcal{E}(\tau)$ produces this particular v_1 and v_2.

The S.I.T. problem calls for a very special kind of solution $v_1(\zeta, \tau)$, $v_2(\zeta, \tau)$. Indeed, ζ is the parameter describing the detuning of the two level systems from the carrier frequency ω_o. If there is to be no loss, $|v_1(\zeta, \tau)| = 1$, $|v_2(\zeta, \tau)| = 0$ for $\tau \to \infty$; i.e. every two-level system has to start from the ground state before the arrival of the pulse and must return into the ground state after passage of the pulse. This requirement in turn calls for a scattering well $\mathcal{E}(\tau)$ which produces no reflection, $(v_2 = 0)$ for an incident "wave" $v_1(\zeta, \tau)$ for any ζ !

There are wells that are capable of doing this. The Schroedinger equation for a secant hyperbolic well has a continuum of eigenstates that are traveling waves outside the well and experience only a phase shift as they pass through the well (Morse and Feshbach, 1953). In the next section we set up a method for obtaining the shapes of reflection-free wells for the Zakharov-Shabat equations.

III. The Inverse Scattering Problem

We have pointed out that the solution of self-induced transparency calls for the determination of a reflection-free well. The inverse scattering theory determines the shape of a scattering well from the scattering data. The requirement that there be no reflection is sufficient to find shapes of reflection-free wells.

We shall develop the method of inverse scattering by simple physical reasoning. Consider a given scattering well $\mathcal{E}(\tau)$ with the particular solution $f(\zeta, \tau)$ that approaches the limit as $\tau \to -\infty$

$$\lim_{\tau \to -\infty} f(\zeta, \tau) = \begin{pmatrix} 1 \\ 0 \end{pmatrix} e^{-i\zeta\tau}. \tag{3.1}$$

The function $f(\zeta, \tau)$ represents an experiment in which a wave v_1 is incident from $\tau \to +\infty$, partly coupled to the reflected wave v_2 and partly transmitted.

Next consider $\bar{f}$ defined by

$$\bar{f} \equiv \begin{pmatrix} f_2^* \\ -f_1^* \end{pmatrix}$$

which is obtained by time reversal of f. It is independent of f

because it is the solution to a different boundary value problem.

Finally, introduce a third solution $g(\zeta, \tau)$ defined by its limit at $\tau \to +\infty$:

$$\lim_{\tau\to\infty} g(\zeta, \tau) = \begin{Bmatrix} 0 \\ 1 \end{Bmatrix} e^{i\zeta\tau}. \tag{3.2}$$

Figure 26 shows the experiment represented by g. A mode (wave) v_2 is incident from the left upon the interaction region, partly reflected (coupled to the backward wave v_1) and partly transmitted. $g(\zeta, \tau)$ may be written as a linear superposition of the two independent solutions of the (second order) Zakharov-Shabat equation system.

$$g(\zeta, \tau) = a(\zeta)\, f(\zeta, \tau) + b(\zeta)\, \bar{f}(\zeta, \tau). \tag{3.3}$$

The inverse scattering theory enables one to construct the scattering well from the information on $b(\zeta)$ and $a(\zeta)$. We shall now go through the derivation in a "physical" way. Consider the scattering experiments represented by g, f, and $\bar{f}$. Remember $\xi (\Leftrightarrow \omega/v)$ is interpreted as a propagation constant of a dispersion free wave and hence is proportional to the frequency. $g(\zeta, \tau)$ is, at first, defined on the real ζ-axis-- for a steady state scattering experiment. For a given well, the function $g(\zeta, \tau)$

may be continued analytically into the upper half of the complex ζ-plane. This can be interpreted simply in terms of an experiment using a wave source (of v_2) on the left side of the well with an amplitude growing exponentially with time. Each point in the upper half of the ζ-plane may be thought to have associated with it the space (τ-) dependence of the incident transmitted and scattered waves. We show such plots schematically in Fig. 27. Fig. 27a shows $g(\zeta, \tau)$ for a point in the upper half of the ζ-plane. Shown are the space (τ-) dependences of (α) the well $\varepsilon(\tau)$, (β) the exciting wave g_2 of dependence $\lim_{\tau \to -\infty} \exp i\zeta\tau$, and ($\gamma$) the reflected wave g_1 which is caused by reflection of the well and is confined to a finite region of space.

As Im ζ is increased, the incident wave decays more steeply with increasing τ, and as $|\zeta| \to \infty$ the reflected wave g_1 vanishes. Indeed, the faster the increase with time, (the greater Im ζ), the shorter the duration of the interaction and the weaker is the excitation of the reflection g_1. In the limit of $\mathrm{Im}(\zeta) \to \infty$ the reflected wave g_1 decreases to zero. The same can be said about a spatially very rapidly varying wave, $|\zeta|$ very large. The reflection vanishes not only for $\mathrm{Im}(\zeta) \to \infty$ but for $|\zeta| \to \infty$ in general. Fig. 5b shows an analogous schematic sketch of the experiment described by $f(\zeta, \tau)$ a wave incident upon the well from the right. Like in the case of $g(\zeta, \tau)$, the reflection $f_2(\zeta, \tau)$ becomes weaker and weaker as $|\zeta|$ becomes larger and larger and vanishes in the limit $|\zeta| \to \infty$.

If the well $\varepsilon(\tau)$ is chosen "deep and wide enough", the feedback provided by the well will permit trapped solutions growing with time at a characteristic rate $\text{Im}\ \zeta_k\ (> 0)$, where ζ_k may assume one or more discrete values, depending upon the depth and width of the well. A trapped solution is one for which there is no external excitation $g_2 \to 0$ as $\tau \to -\infty$. The excitation within the well decays away from the well in both directions. With a fixed amplitude of g_2 on the right hand side of the well, the amplitude of the excitation within the well remains finite for $\zeta \to \zeta_k$.

Indeed, in order to keep the excitation amplitude of the well fixed when the "resonance", represented by the trapped solution, is approached, the source amplitude has to decrease until it vanishes at $\zeta = \zeta_k$. The trapped solution is shown schematically in Fig. 6. Power is carried out of the well to supply the increasing energy storage outside the well-- the energy being supplied by the growth of positive energy in g_2 at the expense of the negative energy in g_1 via the instability within the well. The same applies to $f(\zeta, \tau)$ and indeed $g(\zeta, \tau)$ and $f(\zeta, \tau)$ cease to be linearly independent at $\zeta = \zeta_k$ because they both describe the same trapped solution.

Finally consider $\bar{f}(\zeta, \tau)$. For real ζ, the function is the time reversed version of f (compare Fig. 25b). Before we continue it analytically into the upper half plane we must understand the physical situation represented by the solution $\bar{f}$. According to Fig. 25b, waves are incident from both sides of the well. The

well is excited by <u>two</u> sources. The sources are so phased that the "reflected" wave $\bar{f}_1$ on the left hand side is suppressed. This is the solution that is to be continued analytically into the upper half plane. A sketch is shown in Fig. 27c. In the lower half plane $\bar{f}(\zeta, \tau)$ represents an excitation of the well by two sources decaying exponentially in time, again phased so as to cancel the wave $\bar{f}_1$ as $\tau \to -\infty$. (See Fig. 27d.) Trapped solutions exist in the lower half plane. Indeed solutions of the Zakharov Shabat equations occur in complex conjugate pairs. Therefore $\bar{f}$ must contain the trapped solution decaying in time, at $\zeta = \zeta_k^*$ in the lower half ζ-plane. $\bar{f}_2$ is constrained on the left hand side of the well, when ζ approaches ζ_k^*; no singularity occurs in $\bar{f}$ because a decaying trapped solution receives power from the energy in the collapsing tails outside the well and the condition $\bar{f}_1^* \to e^{+i\zeta^*\tau}$ in the limit $\tau \to -\infty$, imparts the tail with a finite amplitude.

We are now ready to exploit the scattering (thought) experiments represented by g, f and $\bar{f}$, through the use of complex function theory. The function $g(\zeta, \tau) \exp - i\zeta\tau$ is well behaved throughout the entire upper half ζ-plane; as $|\zeta| \to \infty$ it approaches $\begin{bmatrix} 0 \\ 1 \end{bmatrix}$. $b(z)$ in turn approaches $\lim_{|\zeta|\to\infty} b(\zeta) = 1$, because in this limit no reflection occurs and $\bar{f}$ becomes equal to g asymptotically. We multiply (3.3) on both sides by

$$(\exp - i\zeta\tau)/b(\zeta). \tag{3.4}$$

In the upper half plane, the left hand side has poles at $\zeta = \zeta_k$ in the upper half plane and approaches $\begin{bmatrix} 0 \\ 1 \end{bmatrix}$ in the limit $|\zeta| \to \infty$. Because the left hand side is equal to the right hand side, the latter has the same poles and same limiting behavior in the upper ζ-plane.

Next, we define the function $\bar{f}(\zeta, \tau) \exp - i\zeta\tau$ in the lower half plane. This function in turn approaches $\begin{bmatrix} 0 \\ 1 \end{bmatrix}$ as $|\zeta| \to \infty$, and has no singularities. The discontinuity between the two functions in the two half planes on the real ζ-axis, $\zeta = \xi$, is:

$$\frac{a(\xi)}{b(\xi)} f(\xi, \tau) \exp - i\xi\tau.$$

We appeal next to complex function theory. If a complex function is well behaved throughout the entire complex ζ-plane with the exception of a finite number of poles and a discontinuity on the real axis then the function can be written in terms of a sum of contributions of the poles and in terms of an integral representing the discontinuity along the real axis. This property of complex functions is in one to one correspondence with potential theory in two dimensions. If a two dimensional electrostatic potential has a finite number of point (line) charge sources and has certain discontinuities along a curve (surface), these discontinuities

being produced by surface sources, then the potential may be found using the appropriate Green's function.

The formal evaluation is presented in Zakharov-Shabat (1972). Here we shall confine ourselves to the special case of a reflection free well, $a(\xi) \to 0$. Then

$$\frac{g(\zeta, \tau)}{b(\zeta)} \exp - i\zeta\tau = \bar{f}(\zeta, \tau) \exp - i\zeta\tau \qquad (3.5)$$

everywhere. Strictly speaking, $a(\xi)$ cannot be set equal to zero, it can only be made to approach zero, because otherwise the two sides of (3.5) cannot be balanced when $|\zeta| \to \infty$ as can be seen from the asymptotic behaviors of $g(\zeta, \tau)$, $f(\zeta, \tau)$ and $\bar{f}(\zeta, \tau)$.

The only singularities left are the zeros of $b(\zeta)$ where $g(\zeta_k, \tau)$ becomes proportional to $c_k f(\zeta_k, \tau)$. Suppose $g(\zeta, \tau)/b(\zeta)$ has simple singularities at ζ_k, so that it may be written, taking advantage of the fact that $g(\zeta_k, \tau) \propto f(\zeta_k, \tau)$ at $\zeta = \zeta_k$,

$$\frac{g(\zeta, \tau)}{b(\zeta)} \exp - i\zeta\tau = \sum_{k=1}^{N} \frac{C_k f(\zeta_k, \tau)}{\zeta - \zeta_k} \exp - i\zeta_k\tau + \begin{pmatrix} 0 \\ 1 \end{pmatrix}. \qquad (3.6)$$

Then, from (3.5)

$$\sum_{k=1}^{N} \frac{C_k f(\zeta_k, \tau)}{\zeta - \zeta_k} \exp - i\zeta_k\tau = \bar{f}(\zeta, \tau) \exp - i\zeta\tau - \begin{pmatrix} 0 \\ 1 \end{pmatrix}. \qquad (3.7)$$

AD-A067 214 MASSACHUSETTS INST OF TECH CAMBRIDGE RESEARCH LAB OF--ETC F/G 20/14
SHORT PULSE PROPAGATION IN THE SUBMILLIMETER REGION.(U)
JAN 79 H A HAUS DAAG29-77-C-0043

UNCLASSIFIED ARO-15323.1-P NL

2 OF 2
AD A067 214

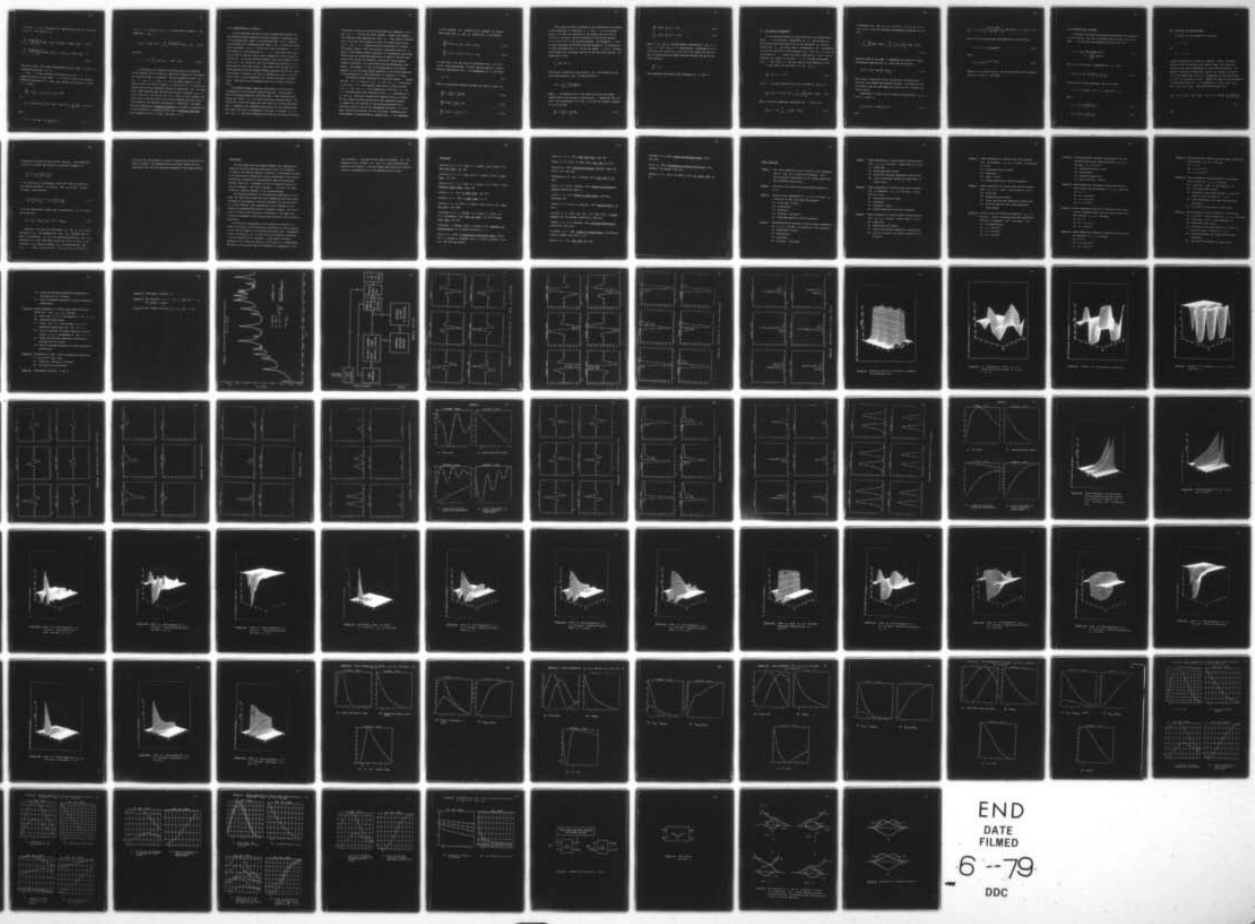

END
DATE FILMED
6-79
DDC

If we set $\zeta = \zeta_j^*$, we obtain 2N equations for the 2N functions $f_1(\zeta_j, \tau)$ and $f_2^*(\zeta_j^*, \tau)$

$$\sum_{k=1}^{N} \frac{C_k f_1(\zeta_k, \tau)}{\zeta_j^* - \zeta_k} \exp - i\zeta_k\tau = f_2^*(\zeta_j^*, \tau) \exp - i\zeta_j^*\tau \qquad (3.7)$$

$$\sum_{k=1}^{N} \frac{C_k^* f_2^*(\zeta_k^*, \tau)}{\zeta_j - \zeta_k^*} \exp + i\zeta_k^*\tau = - f_1(\zeta_j, \tau) \exp + i\zeta_j\tau - 1. \qquad (3.8)$$

The unity in Eq. (3.8) takes care ofthe fact that $\exp - i\zeta\tau\, f_2(\zeta, \tau)$ approaches unity for $|\zeta| \to \infty$.

From f one may evaluate the scatter-free well $\varepsilon(\tau)$ by comparing results in the limit $\zeta \to \infty$. From (1.14) and the assumed asymptotic behavior of f (Fig. 27b) we have in the limit of large $\zeta = \xi$ (real)

$$\frac{\partial f_2}{\partial \tau} - i\xi f_2 = - \frac{1}{2} \varepsilon^* f_1 \cong - \frac{1}{2} \varepsilon^* e^{-i\xi\tau}$$

or

$$f_2 = - \frac{1}{2} \exp i\xi\tau \int_\tau^\infty \varepsilon^*(\tau) \exp - 2i\xi\tau \, d\tau \cong - \frac{1}{4i\xi} \exp - i\xi\tau \, \varepsilon^*(\tau).$$

Thus

$$\varepsilon(\tau) = - 4i\xi \exp - i\xi\tau \lim_{\xi \to \infty} f_2^*(\xi, \tau). \qquad (3.9)$$

From (3.7) we evaluate $f_2^*(\xi, \tau)$ in the limit of large ξ, by replacing ζ by ξ:

$$f_2^*(\xi, \tau) \exp - i\xi\tau = \sum_{k=1}^{N} \frac{C_k f_1(\zeta_k, \tau)}{\xi} \exp - i\zeta_k\tau \qquad (3.10)$$

and thus

$$\mathcal{E}(\tau) = - 4i \sum_{k=1}^{N} C_k f_1(\zeta_k, \tau) \exp - i\zeta_k\tau. \qquad (3.11)$$

In concluding this section one should mention one subtlety of the approach that is often not explicitly brought out, but which our approach helps to illuminate. We have pointed out that $f(\zeta, \tau)$ $\exp - i\zeta\tau$ and $\bar{f}(\zeta, \tau) \exp - i\zeta\tau$ do not behave properly in the complex plane, but only in concert, in the sum (3.5). To cancel the singularities of the individual terms the coefficient a/b is essential. When analyzing the reflection-free well, although $a(\zeta) \to 0$ on the real axis, we have not set $a(\zeta)$ equal to zero, because that would make it strictly zero in the entire complex plane and lead to a breakdown of the analytic continuation. Physically, this means that the conditions of causal excitation as utilized in construction of the solutions of a scattering well and a reflection-free well are compatible only in a limit, the limit $a \to 0$.

IV. Invariance of ζ with z

In the preceding sections we have reviewed the solution of the Zakharov-Shabat equations and given physical interpretations to the mathematical steps. We recognized that S.I.T. implies the existence of a reflection free "well" $\xi(\tau)$ so that the lower level amplitude $v_1(\zeta, \tau)$ starts with unity magnitude at $\tau = +\infty$ and returns to unity magnitude at $\tau \to -\infty$. Such wells exist and one of them is the well known secant hyperbolic to be reviewed in section VI. It is not obvious, however, that such reflection-free wells $\xi(\tau)$ are consistent with the propagation equation (1.12), which has not been used as yet. When Lamb (1973) solved the 2π-pulse problem using the Zakharov-Shabat equations he did not prove consistency in general, but only by substitution of the solution into (1.12). Later, Ablowitz et al. (1974a) provided a general proof. The proof will be presented here in a slightly modified form.

The Zakharov-Shabat equations were shown to be the direct consequence of the two-level systems equations. The parameter ζ was the detuning parameter, obviously real. When solutions were sought for "wells" $\xi(\tau)$ of given reflection characteristics ($\bar{E}$-fields that excite the upper and lower level by a given amplitude) the ζ parameter was extended analytically into the complex plane. This meant the study of responses of the well to "waves" $v_1(\zeta, \tau)$ and $v_2(\zeta, \tau)$ excited by exponentially growing the decaying sources.

No physical connection can be made between the responses $v_1(\zeta, \tau)$ and $v_2(\zeta, \tau)$ and the two level systems. Indeed, for complex ζ the responses grew exponentially with $|\tau|$. This finds no counterpart in the two level system for which the normalization holds $|v_1|^2 + |v_2|^2 = 1$, a normalization not maintained for complex ζ. This means, however, that the analytic continuation into the ζ-plane of the Zakharov-Shabat equations is a mathematical procedure which cannot be interpreted physically in terms of the two level system, even though the parametric oscillator analog permits "physical pictures" to be associated with the mathematical procedure. The complex ζ has a new significance, not directly apparent in the two level system equations or the Bloch equations. A reinterpretation of these equations is, therefore, in order.

The Zakharov-Shabat equations for any given complex ζ define the well $\mathcal{E}(\tau)$ in terms of $v_1(\zeta, \tau)$ and $v_2(\zeta, \tau)$. Conversely, a given well $\mathcal{E}(\tau)$ and boundary conditions at infinity define $v_1(\zeta, \tau)$ and $v_2(\zeta, \tau)$. The propagation of the well, i.e. its τ, z dependence are then reflected in the τ, z dependences of v_1 and v_2. Nonlinear differential equations that are soluble by the inverse scattering method have the remarkable property in common that the solution of the scattering problem for a particular value of one of the independent variables (z in our case) implies the solution for all its values. Mathematically this property is demonstrated by showing that ζ is independent

of this variable (z). Ablowitz et al. proceed as follows. They assume that v_1 and v_2 evolve with z as follows.

$$\frac{\partial v_1}{\partial z} = A(\zeta, z, \tau)v_1 + B(\zeta, z, \tau)v_2 \tag{4.1}$$

$$\frac{\partial v_2}{\partial z} = C(\zeta, z, \tau)v_1 + D(\zeta, z, \tau)v_2. \tag{4.2}$$

In order that (4.1) and (4.2) be consistent with (1.13) and (1.14), cross derivatives $\partial^2/\partial\tau\partial z$ must be equal to $\partial^2/\partial z\partial\tau$. From the requirement that ζ be independent of z one finds

$$A = -D \tag{4.3}$$

where an integration constant has been set equal to zero, and

$$\frac{\partial A}{\partial \tau} = -\left\{\frac{1}{2}\xi C - \frac{1}{2}\xi^* B\right\} \tag{4.4}$$

$$\frac{\partial B}{\partial \tau} + 2i\zeta B = \frac{1}{2}\xi_z - A\xi \tag{4.5}$$

$$\frac{\partial C}{\partial \tau} - 2i\zeta C = -\frac{1}{2}\xi_z^* - A^*. \tag{4.6}$$

These equations must correspond to the equations of the system, if the hypothesis of invariance of ζ with z is to be proven correct. To cast the equations of the system into the form of (4.5)-(4.7) we take a Hilbert transform of the Bloch equations (1.17) and (1.18) in the following manner. The parameter ζ used in those equations is the real detuning parameter. To distinguish it from the generalized ζ, we use the symbol ξ for it. Further, we introduce the line shape function of the two level systems $g(\xi)$ normalized so that

$$\int_{-\infty}^{\infty} g(\xi)\, d\zeta = 1.$$

The Hilbert transform of any function $f(\xi)$ with respect to the line shape function $g(\xi)$ is then defined as

$$H(f) \equiv \frac{i}{4} \int_{-\infty}^{\infty} \frac{f(\xi)\ g(\xi)}{\zeta - \xi}\, d\xi$$

where ζ is assumed to be in the upper half plane and proper indentation of the contour is implied when ζ approaches the real axis. By transforming (1.17) and (1.18) and the complex conjugate of (1.18) we find

$$\frac{\partial A}{\partial \tau} = - \left(\frac{1}{2} \mathcal{E} C - \frac{1}{2} \mathcal{E}^* B \right) \qquad (4.7)$$

$$\frac{\partial B}{\partial \tau} + 2i\zeta B - \frac{1}{2}\langle\lambda\rangle = -\xi A \tag{4.8}$$

$$\frac{\partial C}{\partial \tau} - 2i\zeta C + \frac{1}{2}\langle\lambda^*\rangle = -\xi^* A \tag{4.9}$$

where A, B, and C are the Hilbert transforms of $N(\xi, z, \tau)$, $\lambda(\xi, z, \tau)$ and $\lambda^*(\xi, z, \zeta)$ respectively. Comparison of (4.7), (4.8) and (4.9) with (4.4), (4.5) and (4.6) shows that the two sets of equations can be made identical through the use of the field equation:

$$\frac{\partial \xi}{\partial z} = \langle\lambda\rangle.$$

This completes the proof of the invariance of ζ with z.

V. The Spatial Dependence

In the preceding section we have shown that the complex parameter ζ is an invariant (independent of z). The solution of the problem being described fully by the constants C_k and the eigenvalues ζ_k. The latter being z-independent, the z-dependence is contained entirely in the constants C_k^*. The C_k's in turn are independent of τ ! Using this fact, equations for $C_k(z)$ may be obtained very simply in the limit $\tau \to -\infty$. We need to evaluate $f_1(\zeta, \tau)$ and $f_2^*(\zeta, \tau)$ and then use the field equation (1.12).

In this limit, we find from (3.1) for $f_1(\zeta, \tau)$

$$\lim_{\tau \to -\infty} f_1(\zeta, \tau) = e^{-i\zeta\tau}. \tag{5.1}$$

$f_2^*(\xi, \tau)$ follows directly from (3.5) in terms of $f_1(\zeta_k, \tau)$

$$\lim_{\tau \to -\infty} f_2^*(\xi, \tau) \exp - i\xi\tau = \sum_{k=1}^{N} \frac{C_k}{\xi - \zeta_k} \exp - 2i\zeta_k\tau. \tag{5.2}$$

Next we need the asymptotic expression for $\mathcal{E}$ from (3.11)

$$\lim_{\tau \to -\infty} \mathcal{E} = -4i \sum_{k=1}^{N} C_k \exp - 2i\zeta_k\tau. \tag{5.3}$$

Introducing (5.3), and $v_1 = f_1$ of (5.1), $v_2 = f_2$ of (5.2), into (1.12) we get the following differential equations for the C_k's:

$$\sum_{k=1}^{N} \frac{\partial C_k}{\partial z} \exp - 2i\zeta_k\tau = \sum_{k=1}^{N} \frac{i}{2} C_k \left\langle \frac{1}{\xi - \zeta_k} \right\rangle \exp - 2i\zeta_k\tau. \tag{5.4}$$

Equating terms of the same τ dependence one obtains a simple differential equation for C_k which has the solution

$$C_k(z) = C_k(0) \exp \frac{iz}{2} \left\langle \frac{1}{\xi - \zeta_k} \right\rangle . \tag{5.5}$$

This result, along with (3.11), allows one to construct the ξ-field for any assumed distribution of poles. We consider first the general case and then apply the result to the 2π-pulse and zero-pi pulse.

Combining (3.7) and (3.8) we obtain an equation for $f_1(\zeta_j, \tau)$ exp $i\zeta_j\tau$ which is

$$\sum_j D_{ij} f_1(\zeta_j, \tau) \exp i\zeta_j\tau = 1 \tag{5.6}$$

with

$$D_{ij} \equiv \delta_{ij} + \sum_k \frac{C_k^*(z)\, C_j(z)}{(\zeta_i - \zeta_k^*)(\zeta_k^* - \zeta_j)} \exp i(2\zeta_k^* - \zeta_i - \zeta_j)\tau. \quad (5.7)$$

When (5.6) is inverted and introduced into (3.11) we find

$$\mathcal{E}(\tau, z) = -4i \,\mathrm{Trace}[MD^{-1}] \quad (5.8)$$

where

$$M_{ij} \equiv C_j(z)\, e^{-i(\zeta_i + \zeta_j)\tau}. \quad (5.9)$$

Equation (5.8) looks like Eq. (16) of Lamb (1973) but his definitions of M and D are wrong.

VI. Solution for 2π-Pulse

The number of assumed singularities determines the complexity of the solution. We start by assuming the existence of only one pole j and find the corresponding solution from (5.8):

$$\mathcal{E}(\tau) = 4iC_j \frac{\exp - 2(i\alpha\tau - \beta\tau)}{1 + \frac{|C_j|^2}{|2\beta|^2} \exp 4\beta\tau} . \tag{6.1}$$

From (5.5) we find the z-dependence of C_j to be

$$C_j(z) = C_j(0) \exp \frac{iz}{2} \left\langle \frac{1}{\xi - \alpha - i\beta} \right\rangle . \tag{6.2}$$

Introduction of this expression into (6.1) gives

$$\mathcal{E}(\tau, z) = 4\beta \exp - 2i\alpha(\tau - \tau_1) \operatorname{sech} 2\beta(\tau - \tau_o)$$

where

$$\alpha\tau_1 = \frac{1}{4} \left\langle \frac{\xi - \alpha}{(\xi - \alpha)^2 + \beta^2} \right\rangle \tag{6.3}$$

$$\beta\tau_o = \frac{1}{4} \left\langle \frac{\beta}{(\xi - \alpha)^2 + \beta^2} \right\rangle . \tag{6.4}$$

VII. Solution for Zero-Pi Pulse

We assume now the presence of two poles

$$\zeta_a \equiv \alpha + i\beta$$

and

$$\zeta_b \equiv -\alpha + i\beta$$

located symmetrically around the imaginary ζ-axis. The usual expression for the zero-pi pulse result (Lamb, 1974) when the envelope of the pulse propagates at a well defined velocity. For symmetric location of the poles, this is not possible in general as follows immediately from the z-dependence of the coefficients C_a and C_b as given by (5.5). Indeed, the speed of the envelope(s) is determined from the τ, z dependences of $C_a(z) \exp - 2i\zeta_a\tau$ and $C_b(z) \exp - 2i\zeta_b\tau$ which are obtained from (5.5).

$$C_a(z) \exp - 2i\zeta_a\tau = C_a(0) \exp - 2i(\alpha + i\beta)\tau \exp \frac{iz}{2} < \frac{\xi - \alpha + i\beta}{(\xi - \alpha)^2 + \beta^2} > \qquad (7.1)$$

and

$$C_b(z)\ \exp - 2i\zeta_b\tau = C_b(0)\ \exp - 2i(-\alpha + i\beta)\tau\ \exp \frac{iz}{2} \left\langle \frac{(\xi + \alpha) + i\beta}{(\xi + \alpha)^2 + \beta^2} \right\rangle . \tag{7.2}$$

The speeds of the functions responsible for the envelopes are obtained from

$$2\beta d\tau = \frac{1}{2} \left\langle \frac{\beta}{(\xi \mp \alpha)^2 + \beta^2} \right\rangle dz$$

respectively.

The speeds will be different, unless

$$\left\langle \frac{1}{(\xi - \alpha)^2 + \beta^2} \right\rangle = \left\langle \frac{1}{(\xi + \alpha)^2 + \beta^2} \right\rangle \tag{7.3}$$

which is true only for a symmetric line function centered with the carrier frequency of the pulse. When the line is symmetric, then the speed of "phase propagation" determined from

$$\pm\ 2\alpha d\tau = \frac{1}{2} \left\langle \frac{\xi \mp \alpha}{(\xi \mp \alpha)^2 + \beta^2} \right\rangle dz$$

is also equal for both constituents. In this case, one finds from (5.8) after some algebra

$$\mathcal{E}(\tau, z)$$

$$= 8\beta \frac{\cos 2\alpha(\tau - \tau_1) \cosh 2\beta(\tau - \tau_o) - \frac{\beta}{\alpha} \sin 2\alpha(\tau - \tau_1) \sinh 2\beta(\tau - \tau_o)}{\cosh^2 2\beta(\tau - \tau_o) + \frac{\beta^2}{\alpha^2} \sin^2 2\alpha(\tau - \tau_1) \sinh^2 2\alpha(\tau - \tau_1)} \tag{7.4}$$

where

$$\beta\tau_o \equiv \frac{1}{4} z < \frac{\beta}{(\xi - \alpha)^2 + \beta^2} > \tag{7.5}$$

$$\alpha\tau_1 \equiv \frac{1}{4} z < \frac{\xi - \alpha}{(\xi - \alpha)^2 + \beta^2} > . \tag{7.6}$$

This is the same result in a simpler form than the one obtained by Lamb (1974).

When the poles are not picked symmetrically with respect to the $\mathrm{Im}(\zeta)$ axis, new solutions may be generated. In particular, one is interested in finding solutions that do not split up into 2π pulses and possess a spectrum not centered with the material line. Whether such solutions exist may be decided with the aid of (5.8). In limit $\tau \to \infty$, the expression for $\mathcal{E}(z, \tau)$ contains $\tau - z$ dependences only in the combination $C_i(z) \exp - 2i\zeta_i\tau$ or its complex conjugate. This combination gives a very special

propagation velocity of the envelope $\exp 2\beta_i\tau$. The propagation velocity (or rather its inverse) is given by (compare 7.5)

$$\frac{\Delta\tau}{\Delta z} = \frac{1}{4} \left\langle \frac{1}{(\xi - \alpha_i)^2 + \beta_i^2} \right\rangle .$$

If the solution is to describe a pulse that does not break up, the envelope speeds of $C_a \exp 2\beta_a\tau$ and $C_b \exp 2\beta_b\tau$ must be the same. This requires

$$\left\langle \frac{1}{(\xi - \alpha_a)^2 + \beta_a^2} \right\rangle = \left\langle \frac{1}{(\xi - \alpha_b)^2 + \beta_b^2} \right\rangle . \tag{7.7}$$

If we are considering a sharp line, with detuning ξ_o, the above may be written

$$\alpha_a^2 + \beta_a^2 - 2\xi_o\alpha_a = \alpha_b^2 + \beta_b^2 - 2\xi_o\alpha_b. \tag{7.8}$$

Equation (7.8) puts the eigenvalues ζ_a and ζ_b on a circle centered at ξ_o. The exponentials $\exp - i\zeta_k\tau$ obtained for the case of no detuning, $\xi_o = 0$, are simply multiplied by $\exp - i\xi_o\tau$. Equations (5.7) and (5.8) show clearly the effect of such a multiplication; D_{ij} does not change, M_{ij} is multiplied by $\exp - 2i\xi_o\tau$ -- a simple frequency shift. The spectrum is shifted by

precisely the right amount to center it again with the line of the material medium. The assumed detuning has been removed by the requirement that the two envelopes propagate at the same velocity.

Conclusions

We have shown that the Zakharov-Shabat (Z-S) equations are identical with the two-level equations of the S.I.T. problem. In order to be aided by physical intuition in the general solution of the equations we showed that they are analogous to the spatial differential equations of the parametric amplifier-oscillator problem, where the ζ-parameter of the Z-S equations plays the role of frequency. The "time" variable τ of S.I.T. is interpreted as a spatial variable in the analog problem.

The analytic extension of the scattering functions into the upper and lower half planes and their properties were made understandable by the physical intuition developed for the excitation of a given "twoport" from transmission lines connected to the twoport by exponentially growing or decaying sources. The occurrence of zeros of the reflection coefficient in the upper half ζ-plane corresponded to the growing oscillations of the parametric oscillator.

The analytic continuation of the scattering equation containing the zeros of the reflection coefficients as poles enabled one to find the shape of the scatter-free wells, the τ-dependence of the E-field of S.I.T. at one value of the spatial coordinate z of the original S.I.T. problem. It was shown (following Ablowitz et al.) that the position of the poles is z-independent. This fact, and the fact that the residues are independent of the

time variable τ was used to get simply the spatial (z-) dependence of the E-field. 2π- and 0-π pulse solutions were obtained very directly. We also showed that there is no soliton solution corresponding to an off-resonant zero-pi pulse.

References

Ablowitz, M. J., D. J. Kaup, A. C. Newell, and H. Sequr, 1973, Phys. Rev. Lett., 31, 125.

Ablowitz, M. J., D. J. Kaup, and A. C. Newell, 1974a, J. Math. Phys., 15, 1852.

Ablowitz, M. J., D. J. Kaup, A. C. Newell, and H. Segur, 1974b, Studies in Appl. Math., LIII, 249.

Balanis, G. N., 1972, J. Math. Phys., 13, 1001.

Faddeyev, L. D., 1962, J. Math. Phys., 4, 72.

Gardner, C. S., J. Green, M. Kruskal, and R. Miura, 1967, Phys. Rev. Lett., 19, 1095.

Grieneisen, H. P., J. Goldhar, N. A. Kurnit, A. Javan, and H. R. Schlossberg, 1972, Bull. Am. Phys., 17, 681 and Appl. Phys. Lett., 21, 559.

Grieneisen, J. Goldhar, and N. A. Kurnit, 1973, Coherence and Quantum Optics, Ed. by Mandel and Wolff, p. 5.

Kleen, W. J., 1958, in Electronics of Microwave Tubes, Transl. by P. A. Lindsay, A. Reddish, and C. R. Russel (Academic Press, Inc., New York and London).

Lamb, Jr., G. L., 1973, Phys. Rev. Lett., 31, 196.

Manley, J. M., and H. E. Rowe, 1959, Proc. IRE, 47, 2115.

Marcuse, D., 1970, Quantum Electronics, Harcourt, Brace and World, Inc., New York.

McLaughlin, D. W., and J. Corones, 1974, Phys. Rev. A, 10, 2051.

Morse, P. M., and H. Feshbach, 1953, Methods of Theoretical Physics, McGraw-Hill Book Co.

Pierce, J. R., 1974, Almost All About Waves, MIT Press, Cambridge, MA.

Rothman, L. S., and R. A. McClathey, 1976, Applied Optics, 15, 2616.

Sturrock, P. A., 1958, Phys. Rev., 112, 1488; 1961, in Plasma Physics, Ed. by Drummond, McGraw-Hill, New York.

Townes, C. H., A. L. Schwalow, 1955, Microwave Spectroscopy, McGraw-Hill, New York.

Vuylsteke, A. A., 1960, Elements of Maser Theory, van Nostrand, Toronto, London, New York, p. 177.

Weiss, M. T., 1957, Proc. IRE, 45, 1012.

Whitham, G. B., 1974, Linear and Nonlinear Waves, Wiley, New York.

Yariv, A., 1976, Introduction to Optical Electronics, Holt, Rinehart, and Winston, New York.

Zakharov, V. E., and A. B. Shabat, 1972, Sov. Phys. JETP, 34, 62.

Figure Captions

Figure 1 The linear absorption over 1 km path in the atmosphere (due to H_2O) as a function of frequency (cm^{-1}). The curves were calculated by S. A. Clough using AFGL Line Parameter Compilation.

Figure 2 Flow Chart for Inverse Scattering Method applied to S.I.T.

Figure 3 Zero-pi pulse propagation for $t_e = t_f = 100$ psec as a function of time, with space as parameter.

(a) normalized E-field
(b) polarization
(c) population
(d) intensity (watts/cm^2)
(e) magnitude squared of Fourier spectrum.

Figure 4 Three-dimensional displays of zero-pi pulse propagation for $t_e = t_f = 10$ psec as function of time and space.

(a) normalized E-field
(b) polarization
(c) population
(d) intensity (watts/cm^2).

Figure 5 Lossy propagation of zero-pi pulse versus distance (cm); $t_e = t_f = 100$ psec; values given in (7.10).

(a) pulse area

(b) normalized pulse energy

(c) linear and nonlinear absorption coefficients

(d) ratio of nonlinear absorption coefficient to linear value.

Figure 6 Lossy propagation of zero-pi pulse, with distance (cm) as parameter; $t_e = t_f = 100$ psec; values given in (7.10).

(a) normalized electric field

(b) population

(c) intensity (w/cm^2)

(d) squared magnitude of Fourier transform.

Figure 7 Lossy propagation of zero-pi pulse versus distance (cm); $t_e = t_f = 10$ psec; values given in (7.12).

(a) pulse area

(b) normalized pulse energy

(c) linear and nonlinear absorption coefficients

(d) ratio of nonlinear and linear absorption coefficients.

Figure 8 Lossy propagation of zero-pi pulse with distance (cm) as parameter; $t_e = t_f = 10$ psec; values given in (7.12).

(a) normalized electric field

(b) population

(c) power (w/cm^2)

(d) squared magnitude of Fourier transform.

Figure 9 Lossy propagation of zero-pi pulse versus distance (cm); $t_e = t_f = 1$ nsec; values given in (7.14).

(a) pulse area

(b) normalized pulse energy

(c) linear and nonlinear absorption coefficients

(d) ratio of nonlinear and linear absorption coefficients.

Figure 10 Lossy on- and off-resonant propagation; $t_e = t_f = 100$ psec; Fourier transform magnitude squared as a function of frequency (cm^{-1}) and space (cm).

(a) on-resonance case

(b) $\Delta\omega = 0.05\ cm^{-1}$

(c) $\Delta\omega = 0.10\ cm^{-1}$

(d) $\Delta\omega = 0.20\ cm^{-1}$

Figure 11 Three-dimensional displays of propagation for off-resonant pulse versus time and distance $t_e = t_f =$ 100 psec; $\Delta\omega = 0.05\ cm^{-1}$

(a) normalized electric field

(b) polarization

(c) normalized population

(d) pulse intensity (w/cm^2).

Figure 12 Three-dimensional displays of normalized electric field versus time and distance; $t_e = t_f = 100$ psec.

(a) $\Delta\omega = 0$

(b) $\Delta\omega = 0.10\ cm^{-1}$

(c) $\Delta\omega = 0.20\ cm^{-1}$

(d) $\Delta\omega = 0.5\ cm^{-1}$.

Figure 13 Three-dimensional displays of normalized real polarizations (imaginary parts are not shown) versus time and distance; $t_e = t_f = 100$ psec.

(a) $\Delta\omega = 0$

(b) $\Delta\omega = 0.10\ cm^{-1}$

(c) $\Delta\omega = 0.20\ cm^{-1}$

Figure 14 Three-dimensional displays of population versus time and distance; $t_e = t_f = 100$ psec.

(a) $\Delta\omega = 0$

(b) $\Delta\omega = 0.10\ cm^{-1}$

(c) $\Delta\omega = 0.20\ cm^{-1}$

Figure 15 Three-dimensional displays of pulse power versus time and distance; $t_e = t_f = 100$ psec.

(a) $\Delta\omega = 0$

(b) $\Delta\omega = 0.10\ cm^{-1}$

(c) $\Delta\omega = 0.20\ cm^{-1}$

Figure 16 Lossy propagation versus distance of on-resonant zero-pi pulse for $t_e = t_f = 100$ psec.

(a) pulse area (real A and imaginary B)

(b) normalized pulse energy

(c) deviation of the pulse velocity u from the speed of light in terms of 1 - u/c

(d) loss coefficients for linear and nonlinear absorption

(e) the ratio of nonlinear to linear loss.

Figure 17 Lossy propagation versus distance of off-resonant ($\Delta\omega = 0.05\ cm^{-1}$) zero-pi pulse for $t_e = t_f = 100$ psec.

(a) pulse area (real A and imaginary B)

(b) normalized pulse energy

(c) deviation of the pulse velocity u from the speed of light in terms of 1 - u/c

(d) loss coefficients for linear and nonlinear absorption

(e) the ratio of nonlinear to linear loss.

Figure 18 Lossy propagation versus distance of off-resonant ($\Delta\omega = 0.10\ cm^{-1}$) zero-pi pulse for $t_e = t_f = 100$ psec.

(a) pulse area (real A and imaginary B)

(b) normalized pulse energy

(c) deviation of the pulse velocity u from the speed of light in terms of 1 - u/c

(d) loss coefficients for linear and nonlinear absorption

(e) the ratio of nonlinear to linear loss.

Figure 19 Lossy propagation versus distance of off-resonant ($\Delta\omega = 0.15\ cm^{-1}$) zero-pi pulse for $t_e = t_f = 100$ psec.

(a) pulse area (real A and imaginary B)

(b) normalized pulse energy

(c) deviation of the pulse velocity u from the speed of light in terms of 1 - u/c

(d) loss coefficients for linear and nonlinear absorption

(e) the ratio of nonlinear to linear loss.

Figure 20 Lossy propagation of zero-pi pulse versus distance; 18.577 cm^{-1} line; $t_e = t_f = 100$ psec.

(a) pulse area

(b) normalized pulse energy

(c) linear and nonlinear absorption coefficients

(d) ratio of nonlinear to linear absorption coefficients.

Figure 21 Lossy propagation of zero-pi pulse versus distance; 20.204 cm^{-1} line; $t_e = t_f = 100$ psec.

(a) pulse area; A, B, C, D corresponds to $|M| = 3, 2, 1, 0$

(b) normalized pulse energy

(c) linear (B, D, F, H) and nonlinear (A, C, E, G) absorption coefficients for $|M| = 3, 2, 1, 0$

(d) ratio of nonlinear to linear absorption coefficients; A, B, C, D corresponds to $|M| = 3, 2, 1, 0$

(e) linear and nonlinear absorption coefficients averaged over all M-levels

(f) ratio of averaged nonlinear to linear absorption coefficients.

Figure 22 Lossy propagation of zero-pi pulse versus distance 25.080 cm^{-1} line; $t_e = t_f = 100$ psec.

(a) pulse area; A, B corresponds to $|M| = 2, 1$

(b) normalized pulse energy

(c) linear (A, B) and nonlinear (C, D) absorption coefficients

(d) ratio of nonlinear to linear absorption coefficients A, B corresponds to $|M| = 2, 1$

(e) linear and nonlinear absorption coefficients averaged over all M-levels

(f) ratio of averaged nonlinear to linear absorption coefficients.

Figure 23 Lossy propagation of zero-pi pulse versus distance; 30.560 cm^{-1} line; $t_e = t_f = 100$ psec.

(a) pulse area; A, B, C corresponds to $|M| = 2, 1, 0$

(b) normalized pulse energy

(c) linear (B, D, F) and nonlinear (A, C, E) absorption coefficients for $|M| = 2, 1, 0$

(d) ratio of nonlinear to linear absorption coefficients, A, B, C corresponds to $|M| = 2, 1, 0$

(e) linear and nonlinear absorption coefficients averaged over all levels

(f) ratio of averaged nonlinear to linear absorption coefficients.

Figure 24 Propagation of CH_3F line in presence of absorption of 18.577 cm^{-1} H_2O line.

(a) energy as a function of distance

(b) the absorption coefficient.

Figure 25 "Experiments" defining f and $\bar{f}$.

Figure 26 "Experiment" defining g.

Figure 27 The functions $f(\zeta, \tau)$, $g(\zeta, \tau)$ and $\bar{f}(\zeta, \tau)$ in the complex ζ-plane.

Figure 28 The trapped solutions at $\zeta = \zeta_k$ and $\zeta = \zeta_k^*$.

Figure 1. Calculated using AFGL line parameters compilation
by S. A. Clough

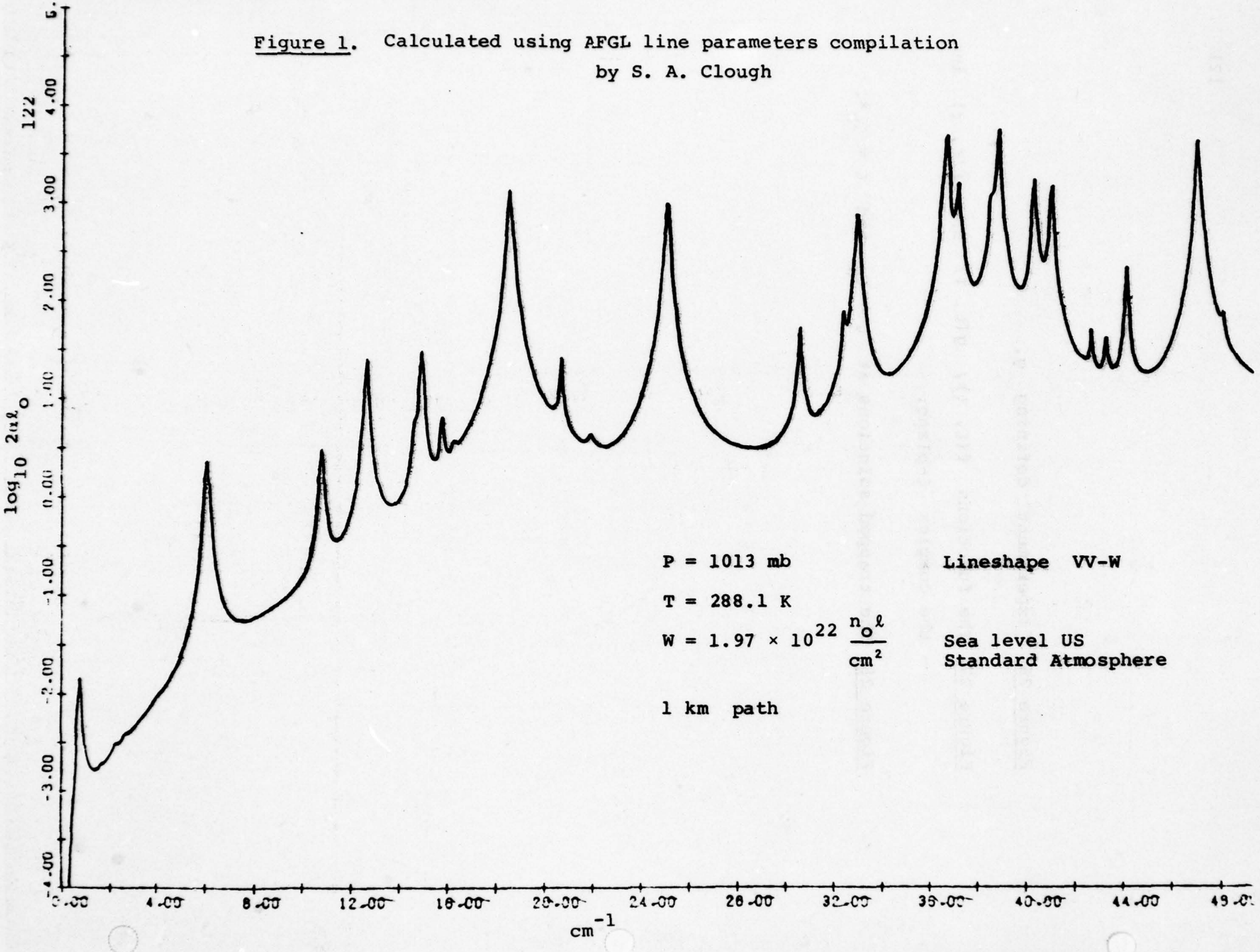

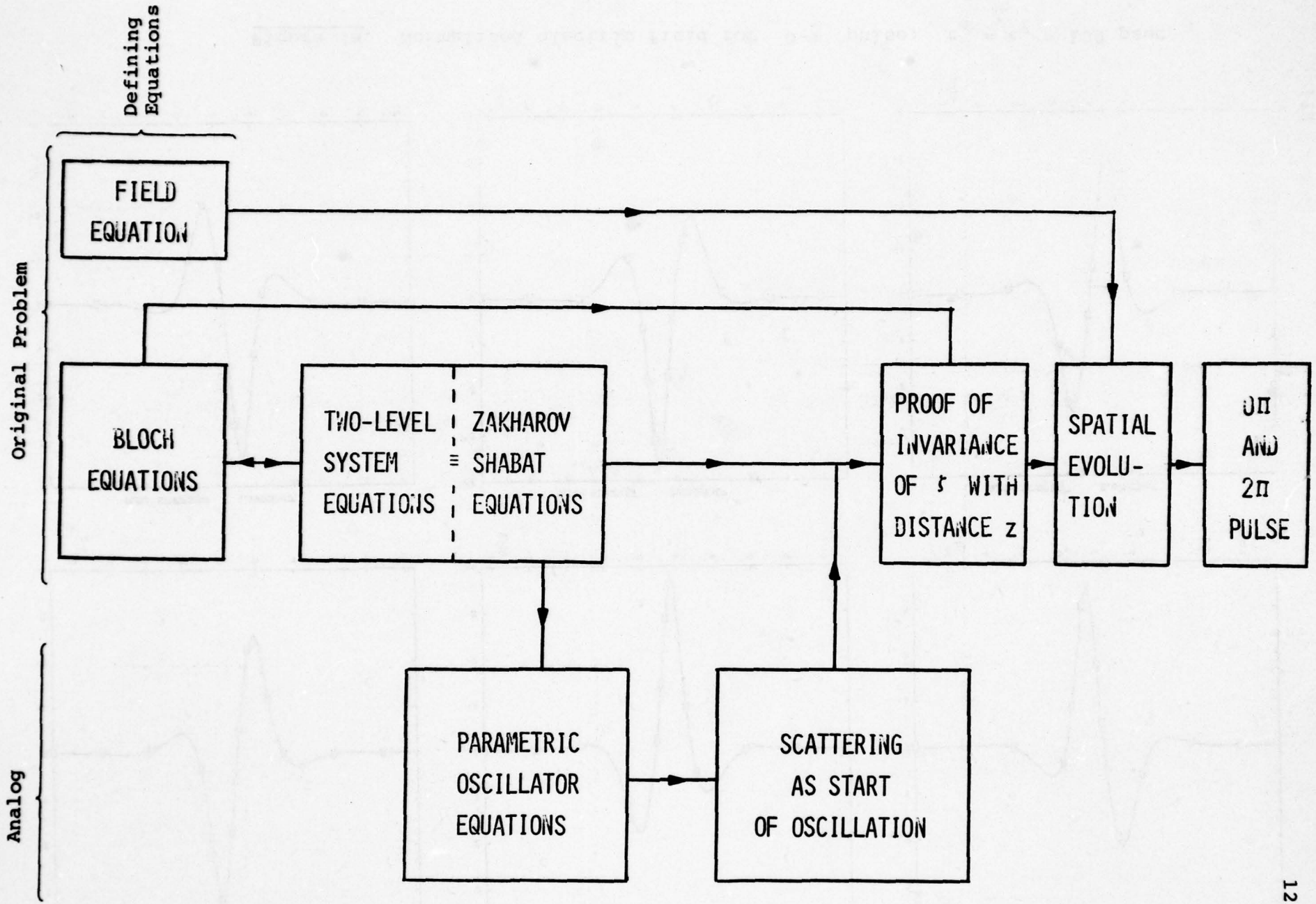

Figure 2. Flow Chart

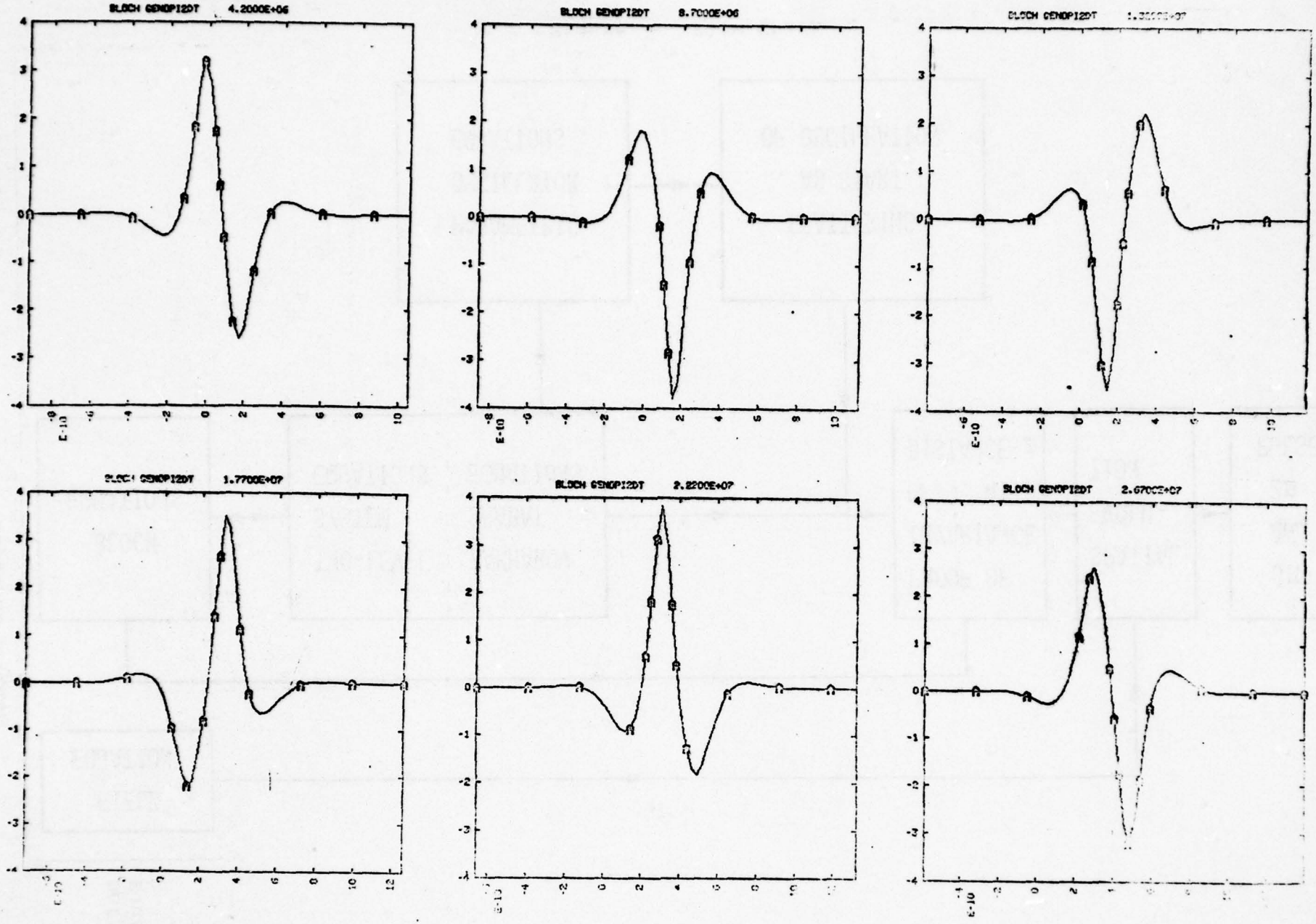

Figure 3a. Normalized electric field for 0-π pulse; $t_e = t_f = 100$ psec

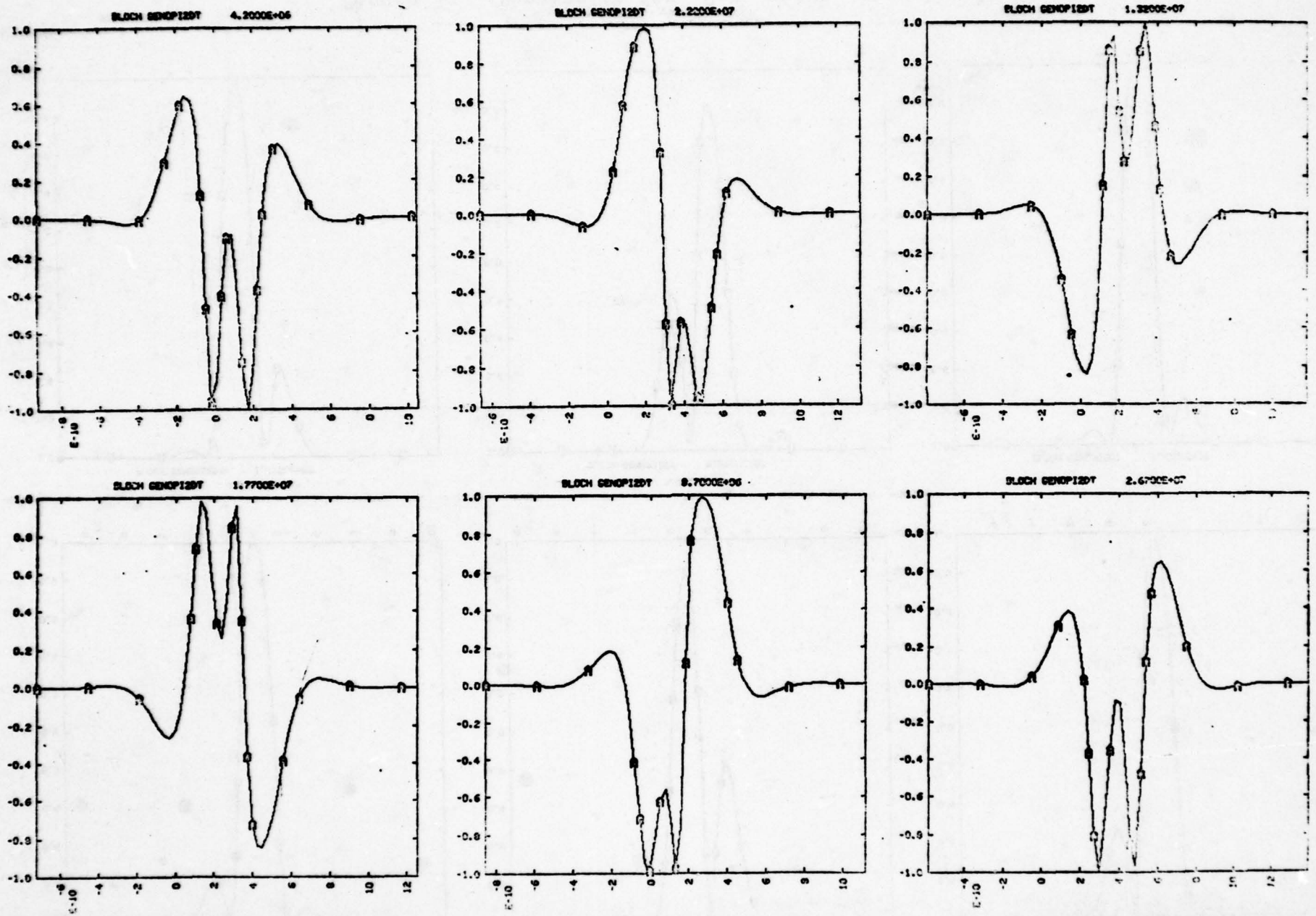

Figure 3b. Polarization for

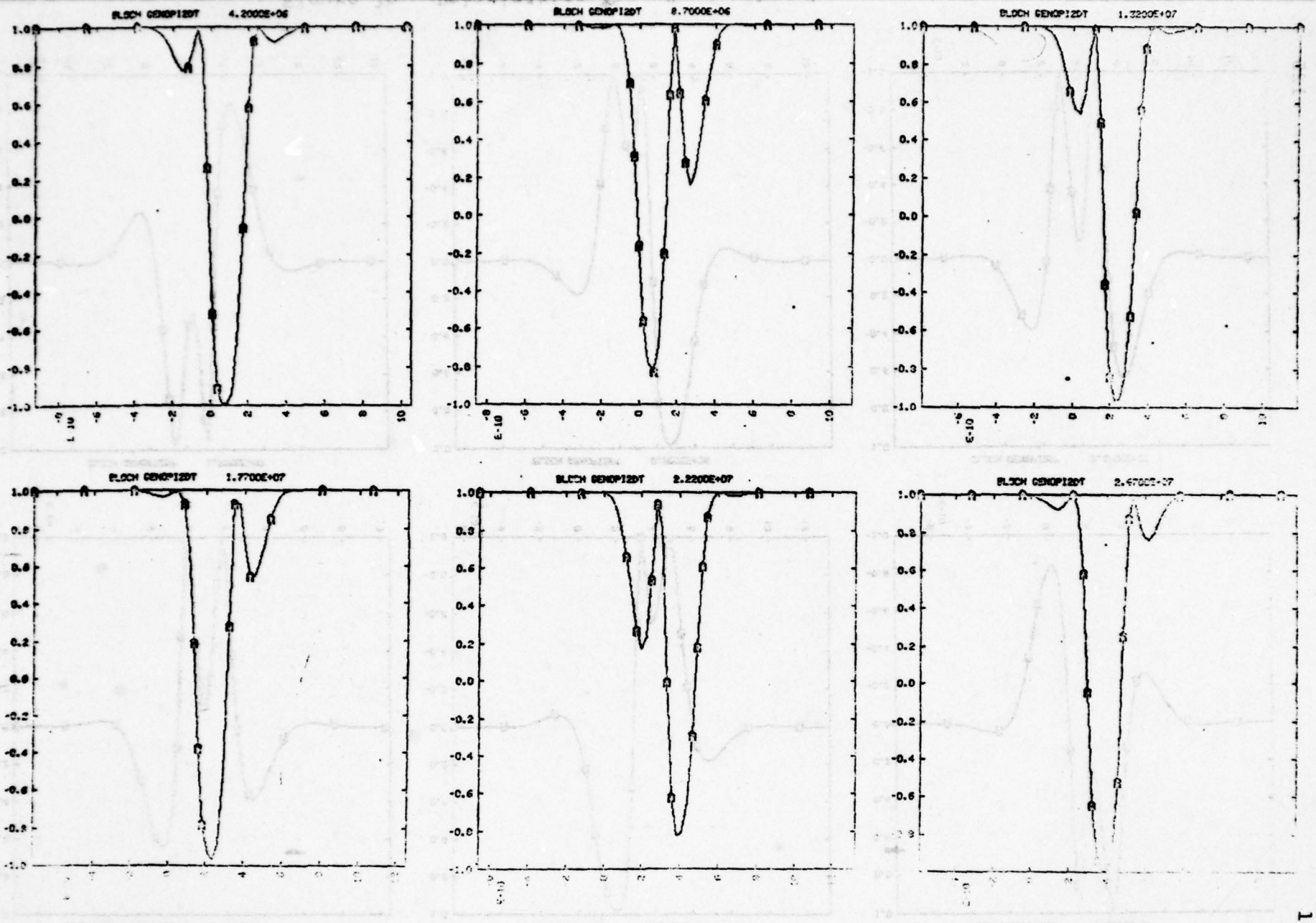

Figure 3c. Population for 0-π pulse (normalized)

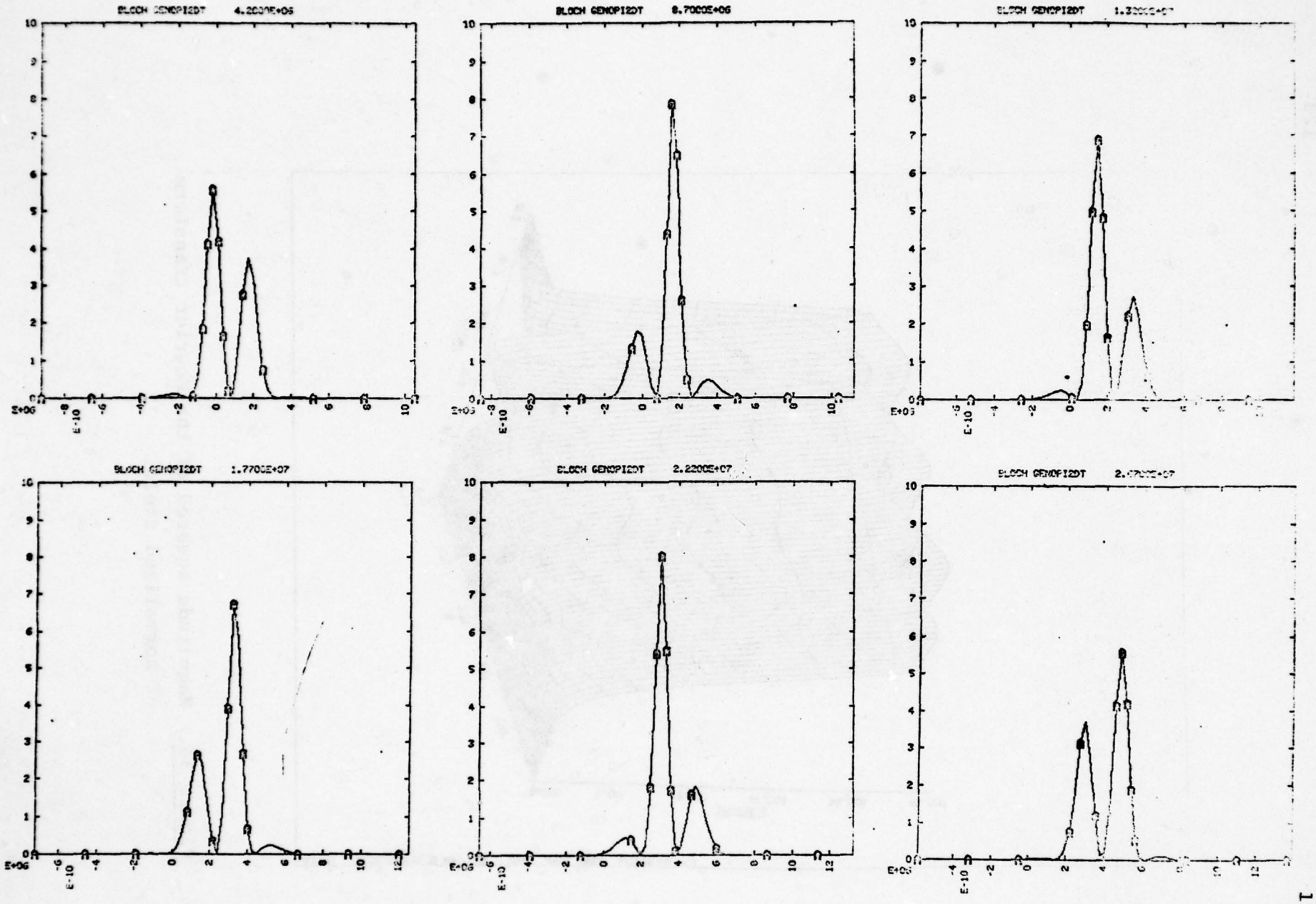

Figure 3d. Pulse power for 0-π pulse (W/cm^2)

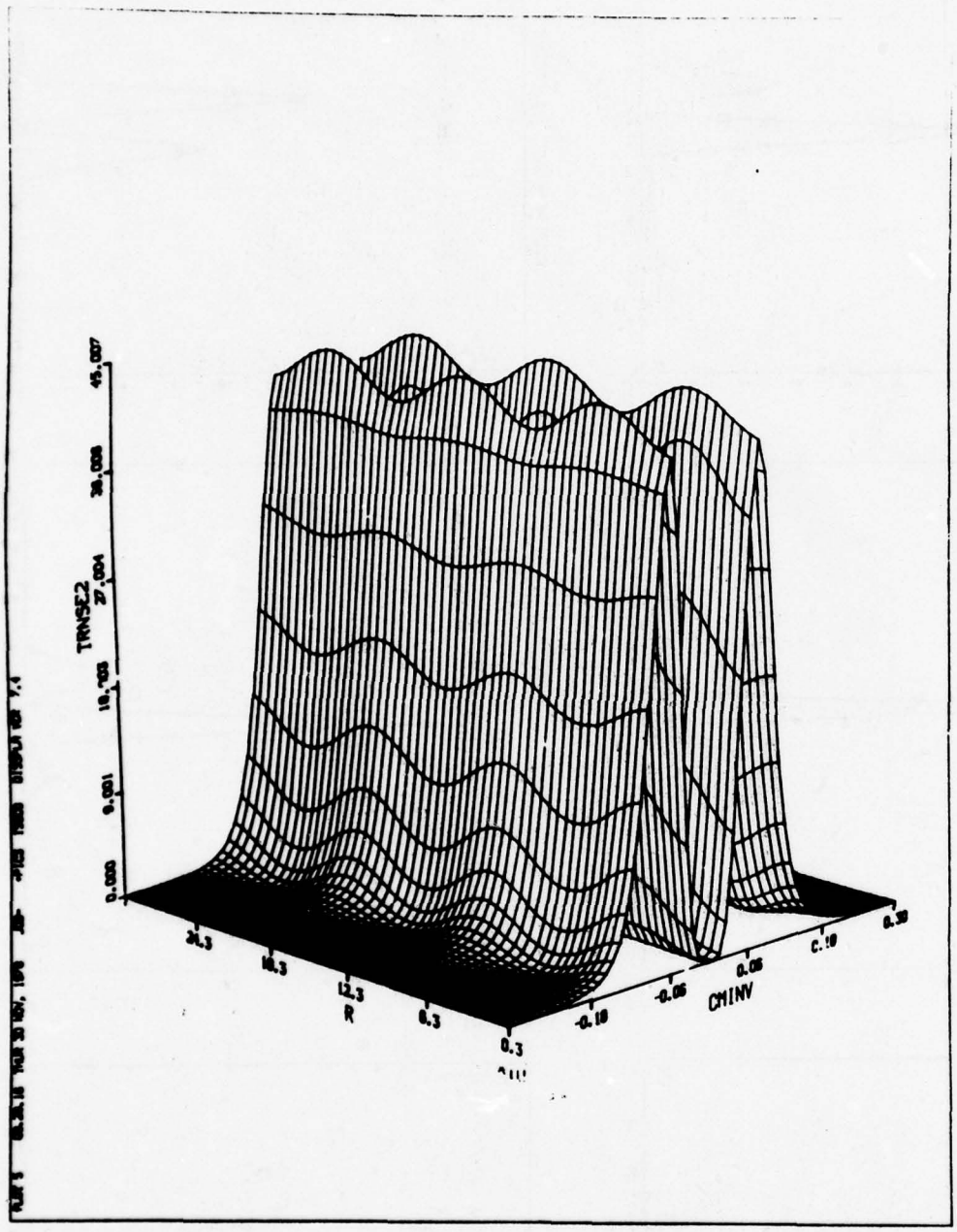

Figure 3e. Magnitude squared of the Fourier transform of normalized field.

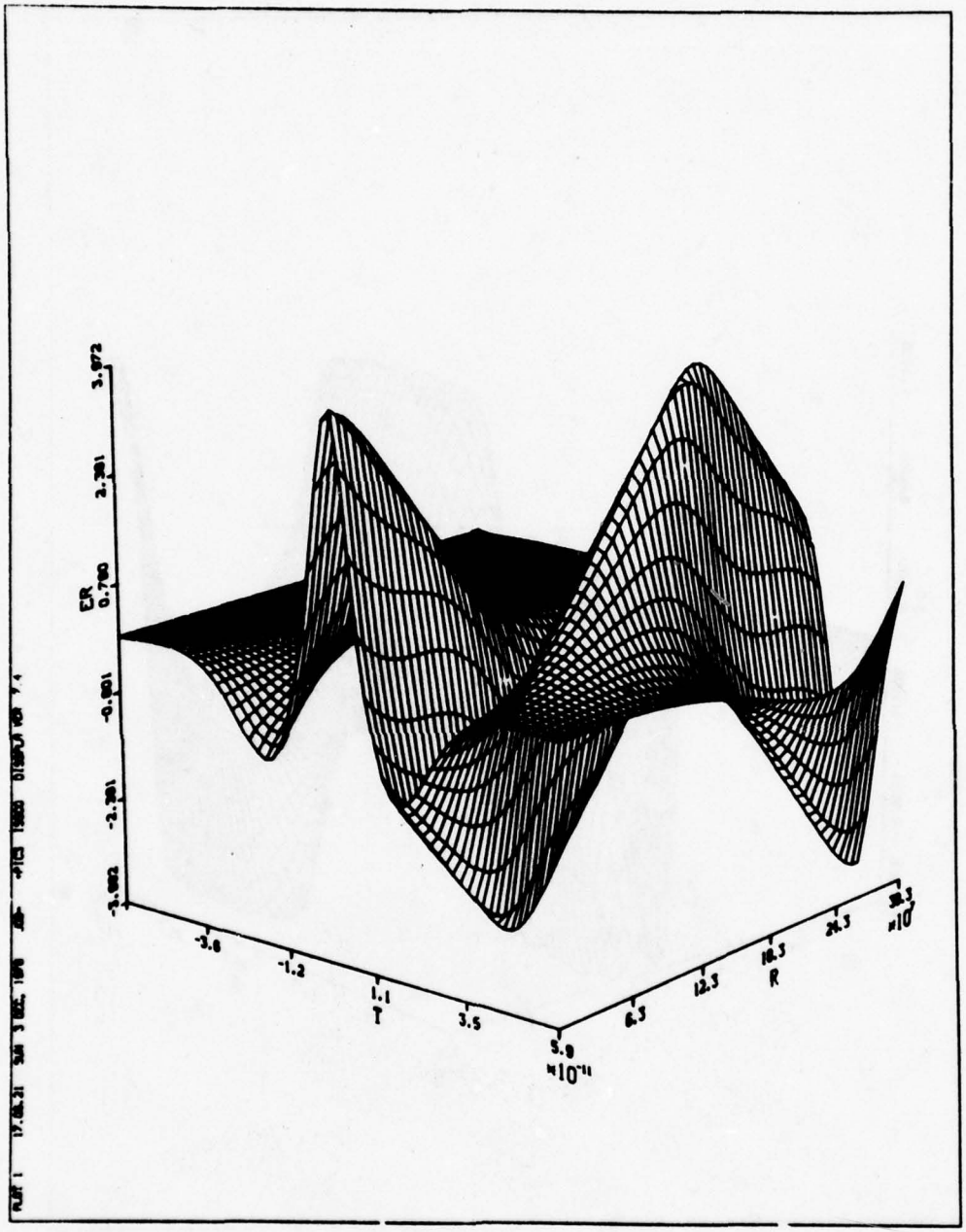

Figure 4a. 0-π propagation: 10 ps = t_e = t_f; normalized electric field; T in sec, R in cm.

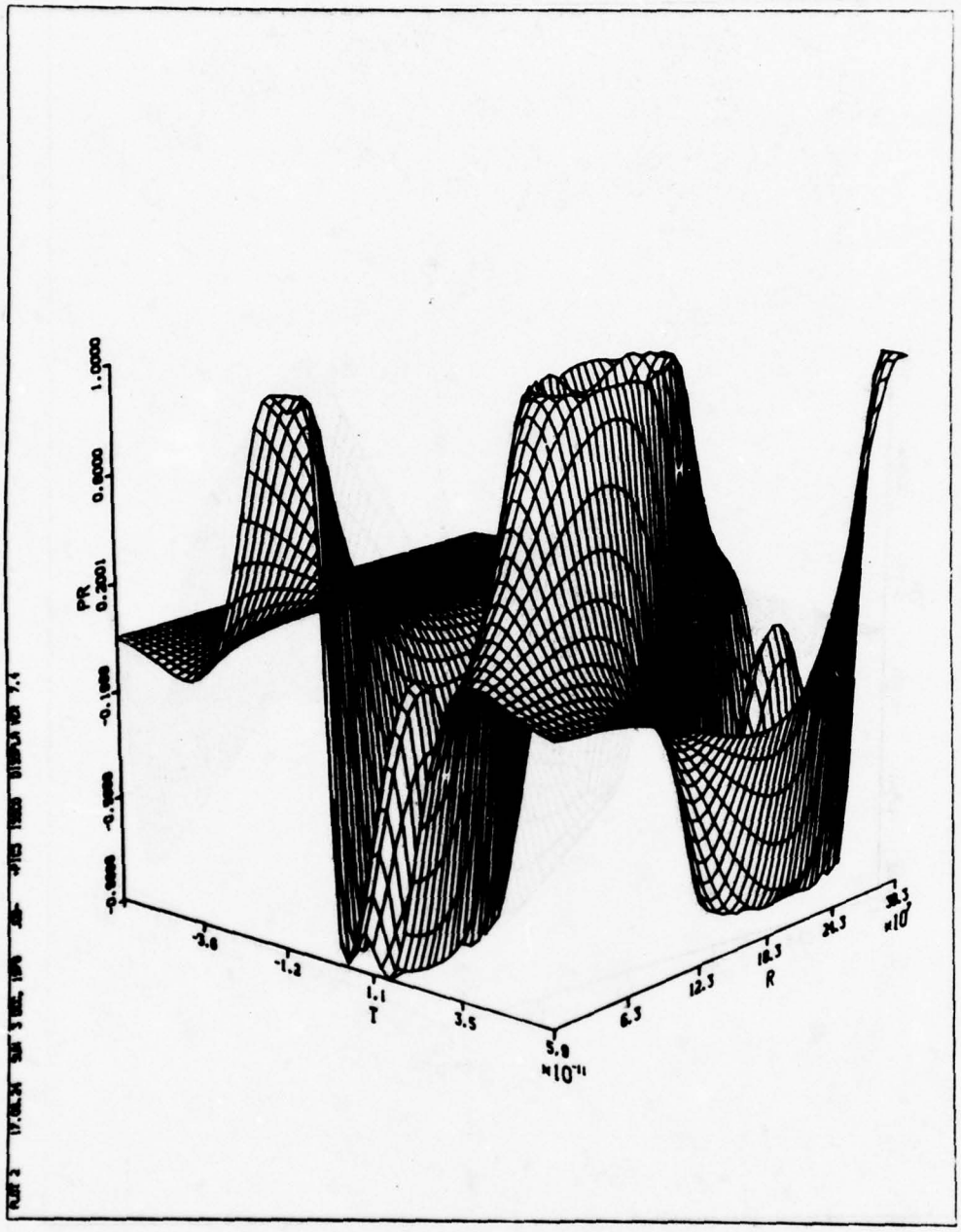

Figure 4b. Lossless 0-π polarization (normalized).

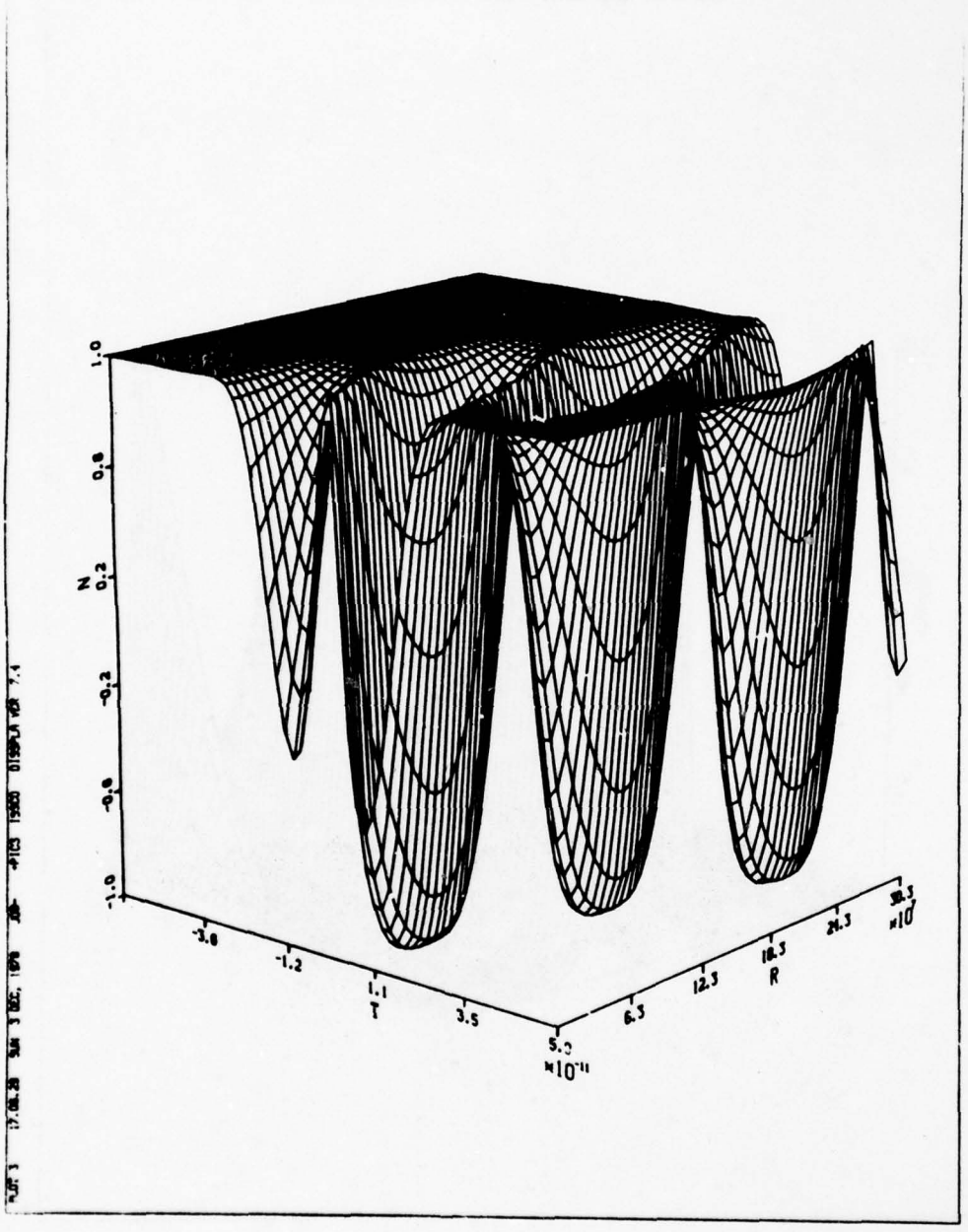

Figure 4c. Lossless 0-π propagation $t_e = t_f = 10$ ps; normalized N.

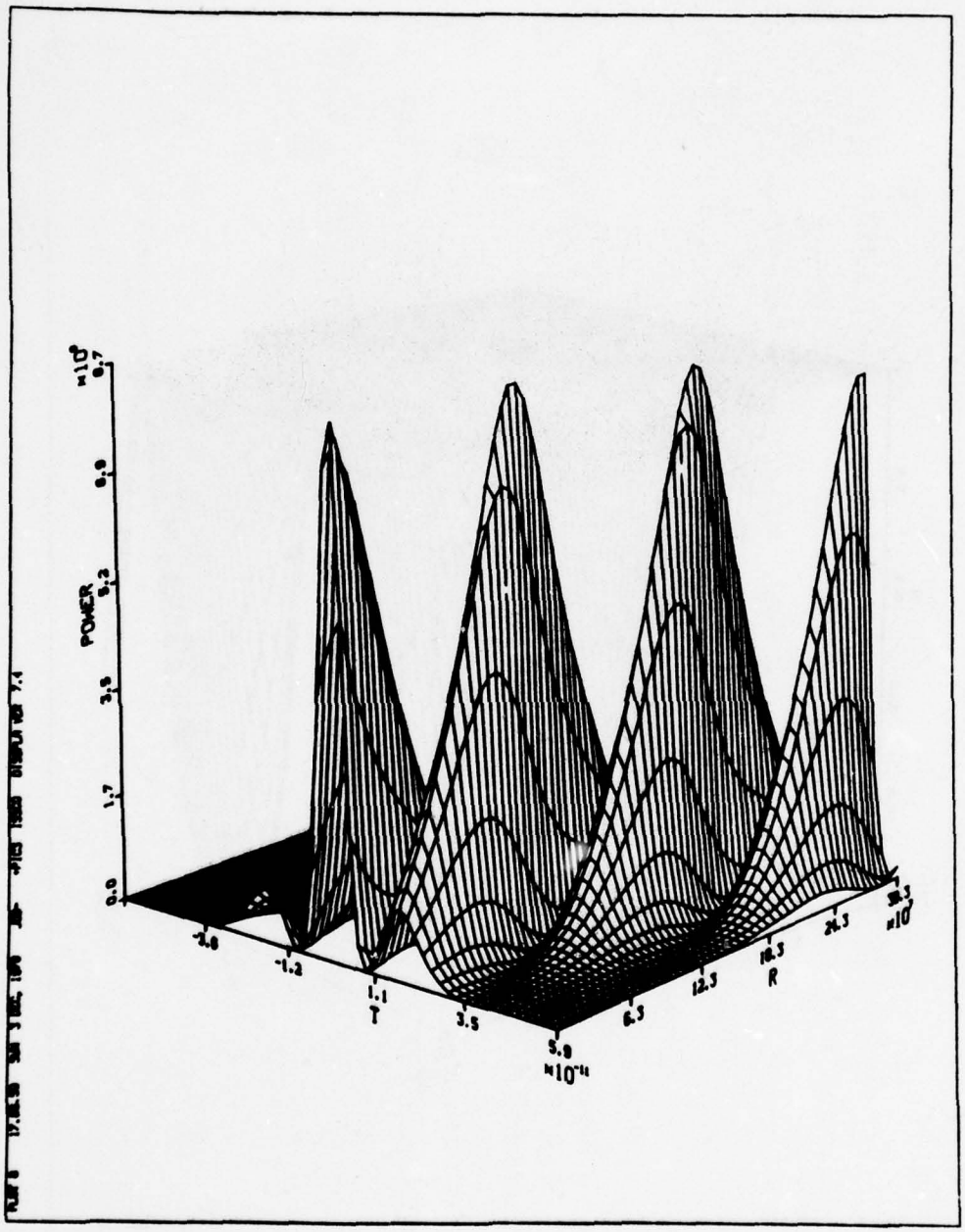

Figure 4d. Lossless 0-π propagation $t_e = t_f = 10$ ps; absolute power (W/cm^2).

Figure 5

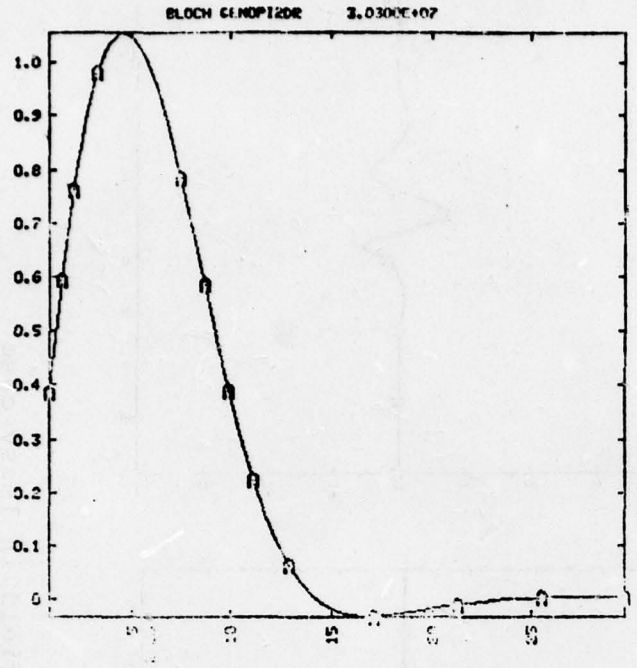

(a) Pulse area

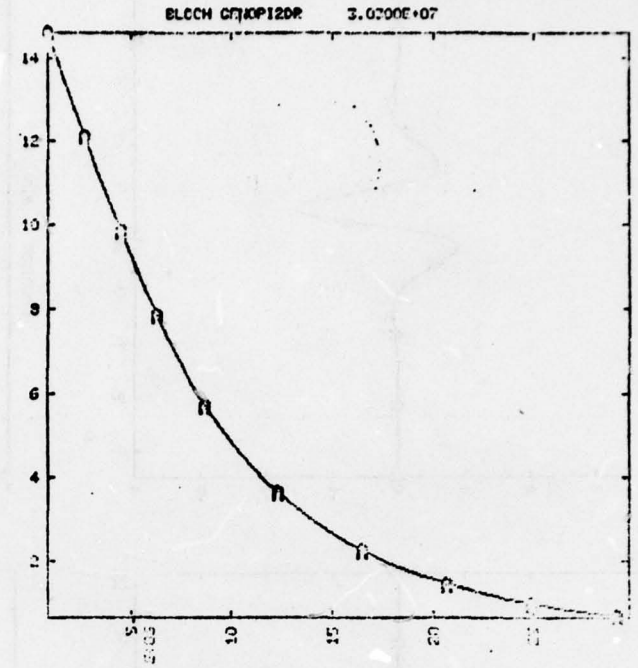

(b) normalized pulse energy

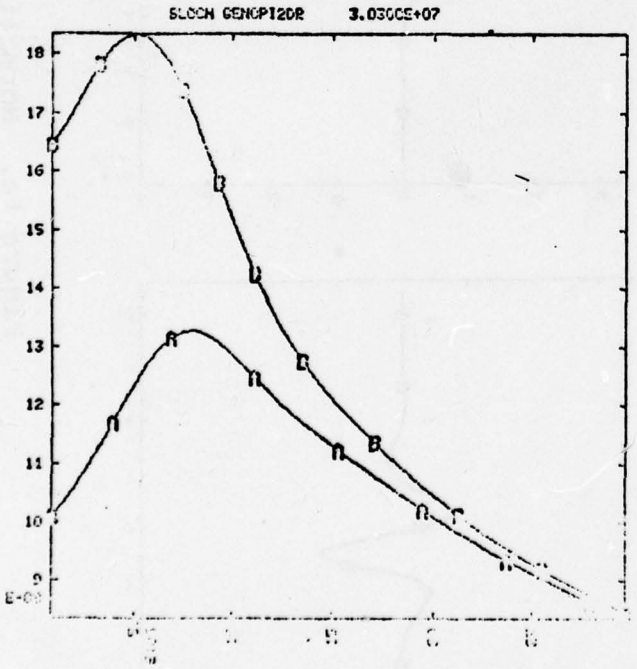

(c) linear and nonlinear absorption coefficients

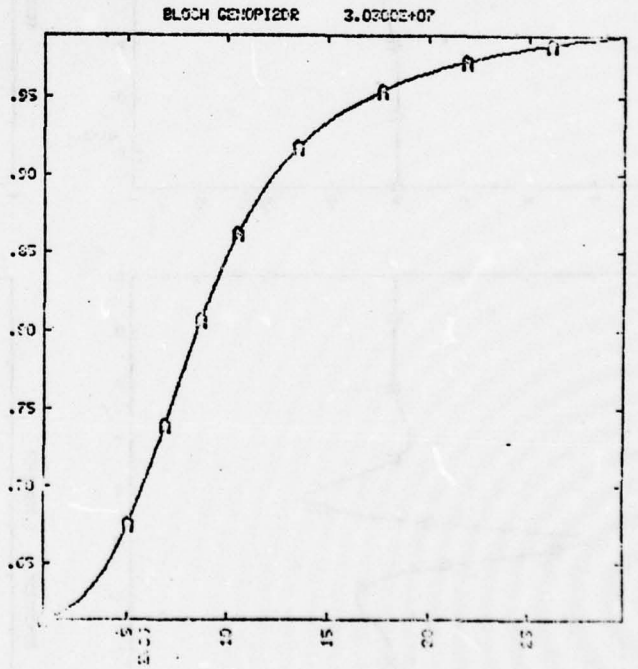

(d) ratio of nonlinear absorption coefficient to its linear value

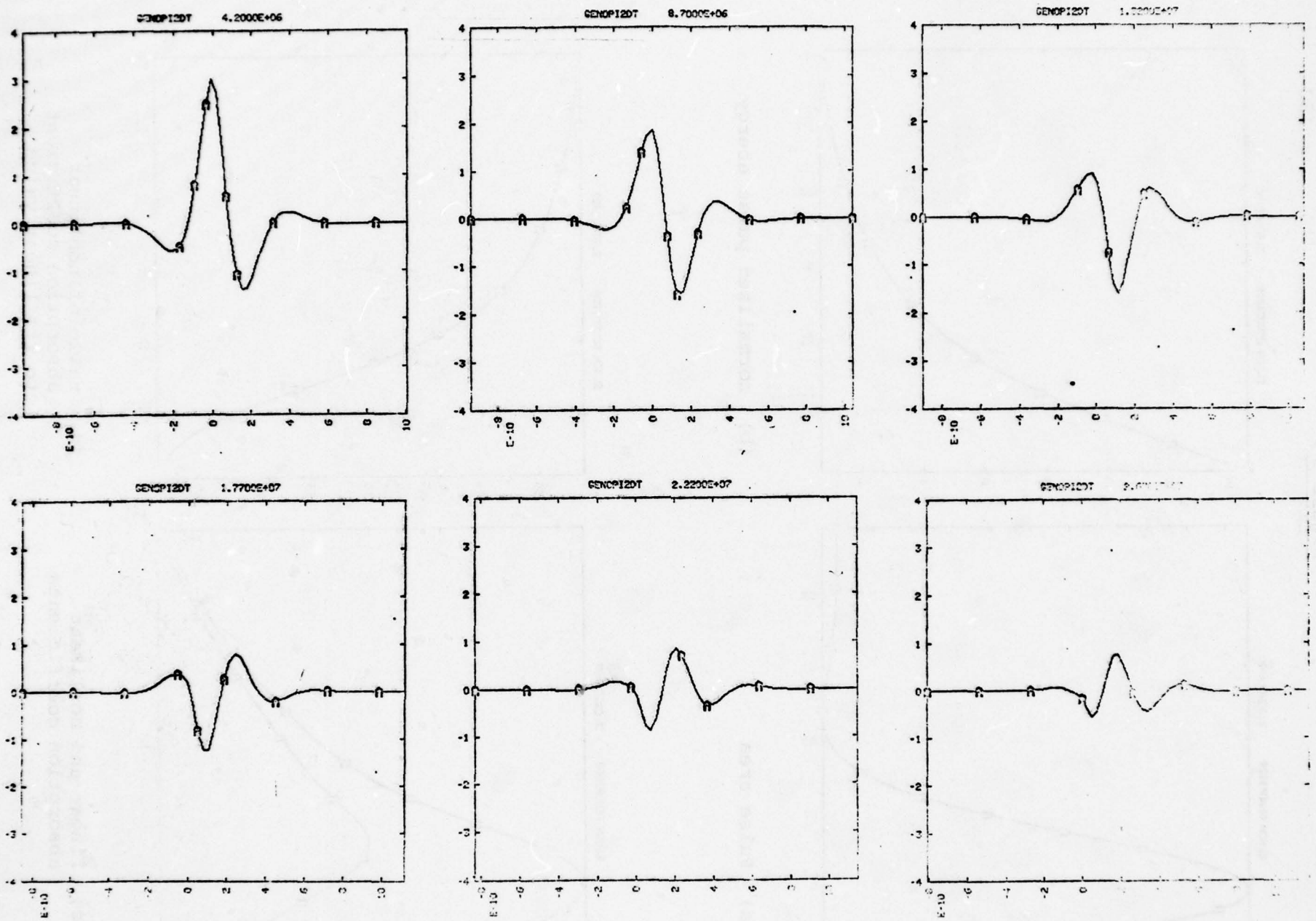

Figure 6a. Normalized electric field in lossy case

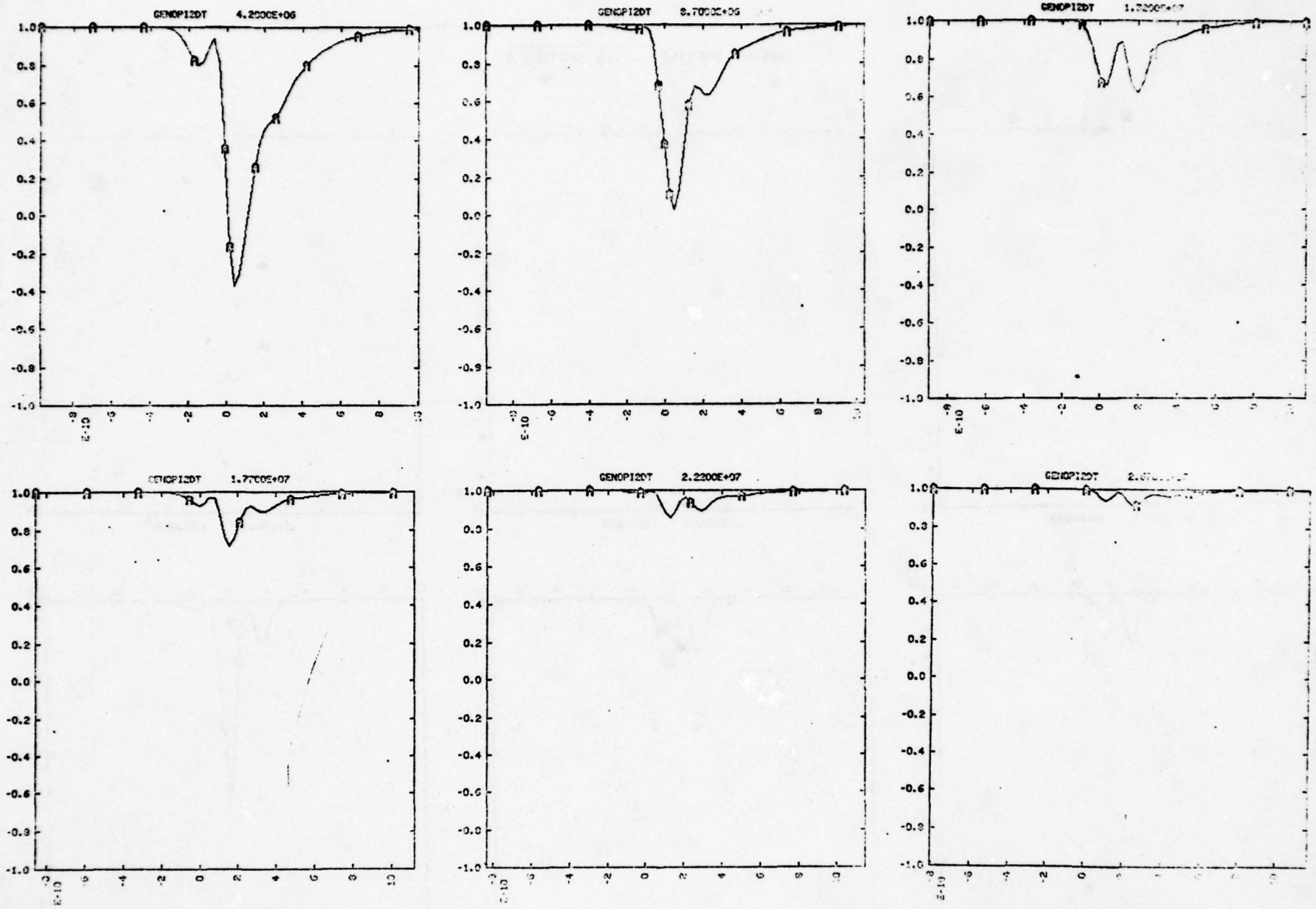

Figure 6b. Normalized population

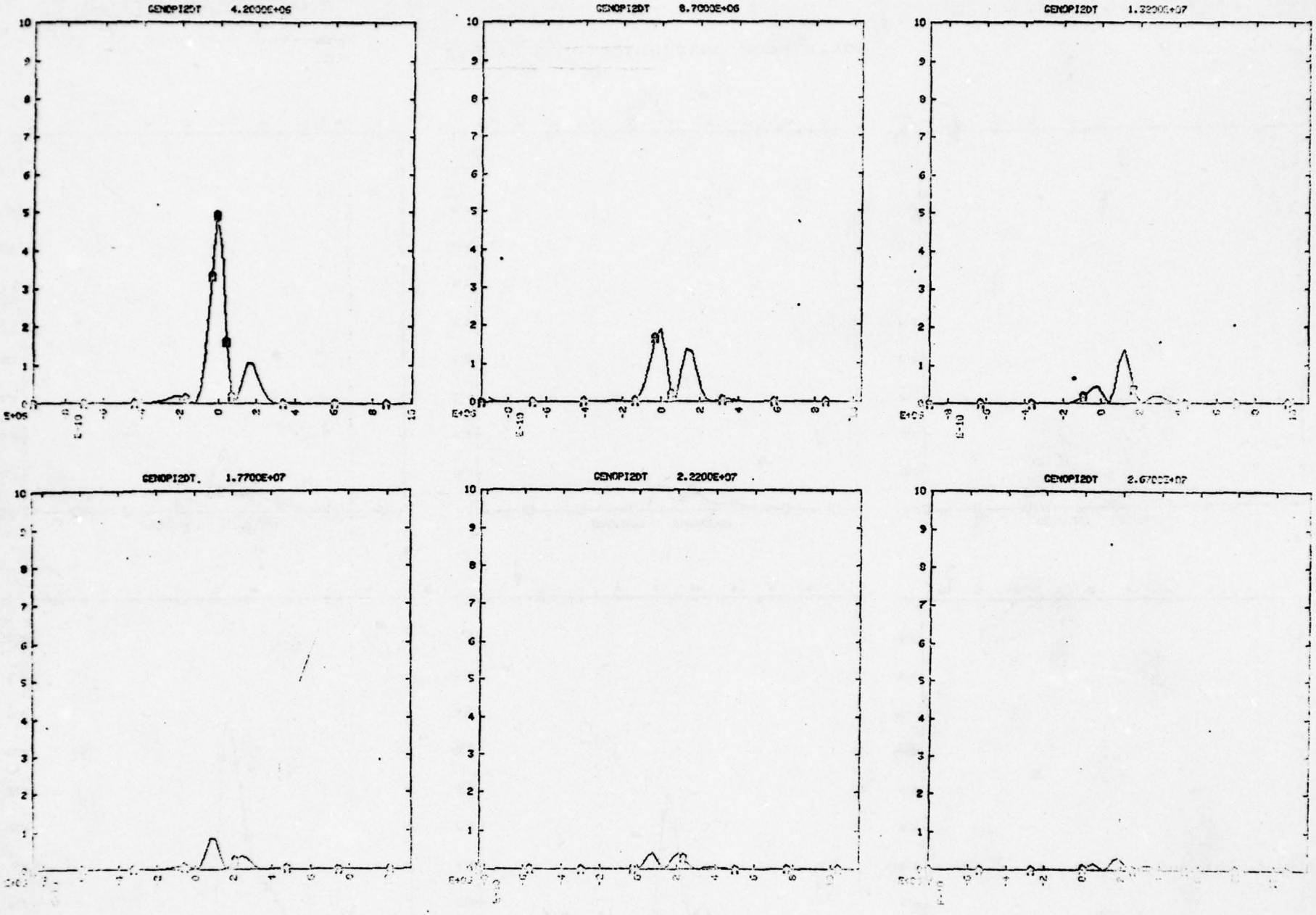

Figure 6c. Pulse power

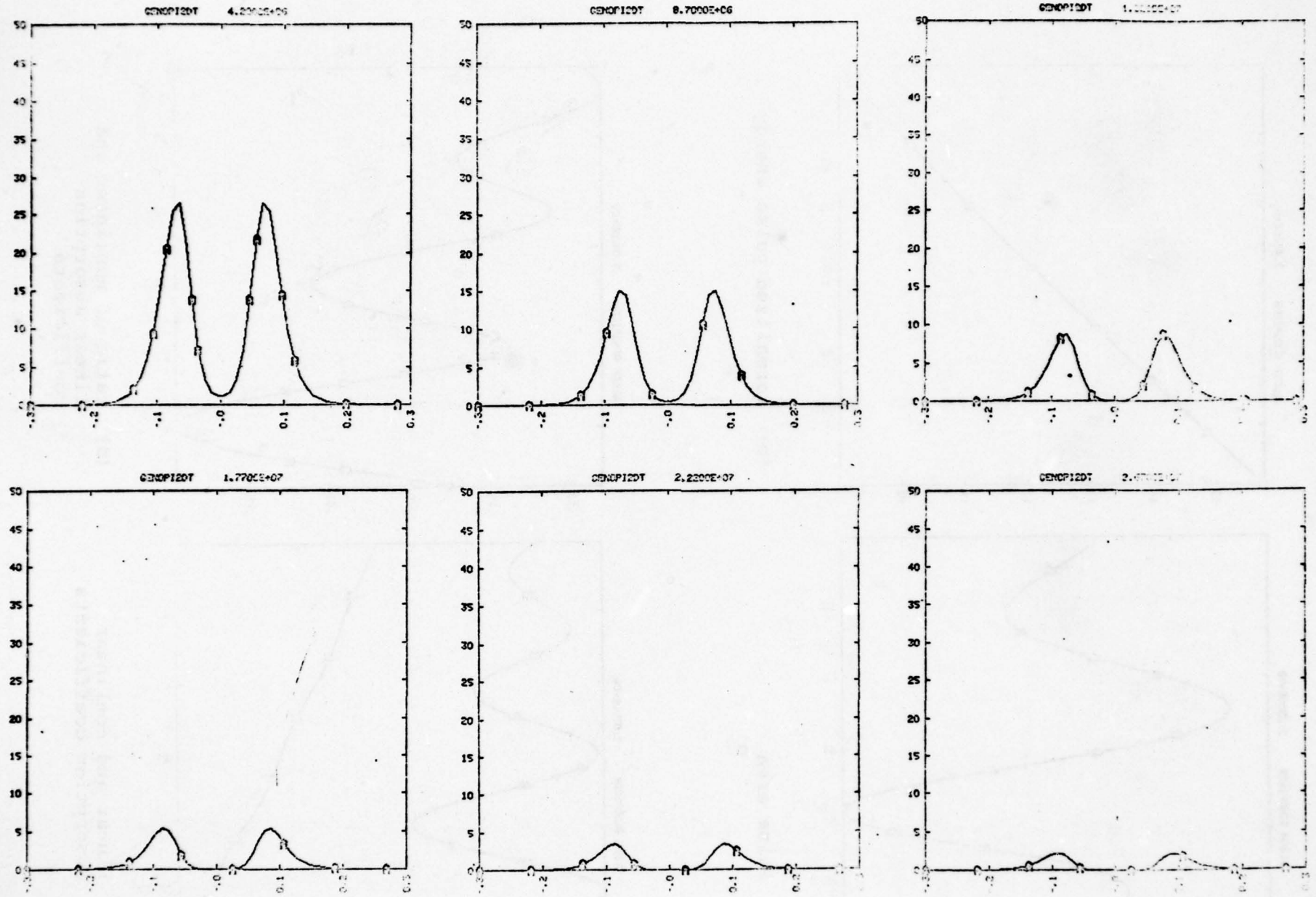

Figure 6d. Squared magnitude of Fourier transform of normalized field

Figure 7.

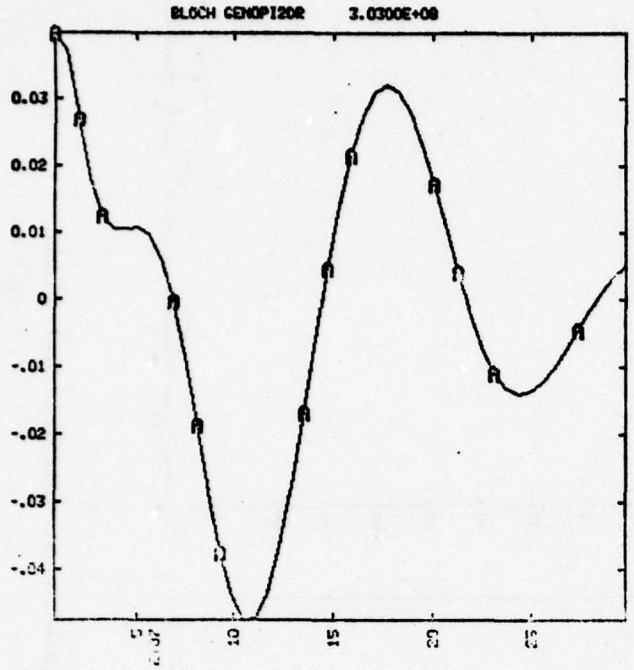

(a) Pulse area

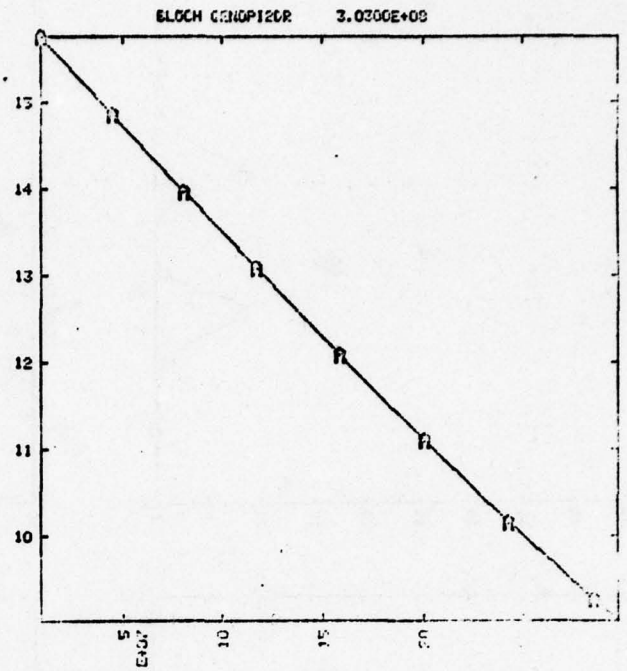

(b) normalized pulse energy

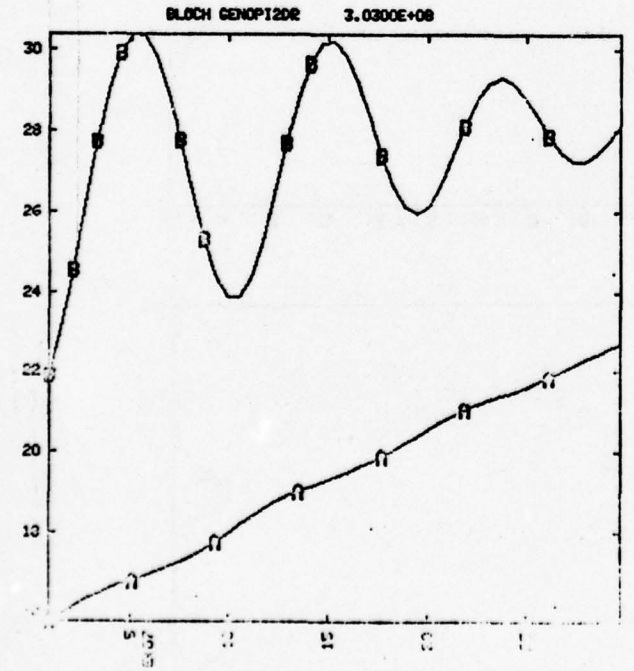

(c) linear and nonlinear absorption coefficients

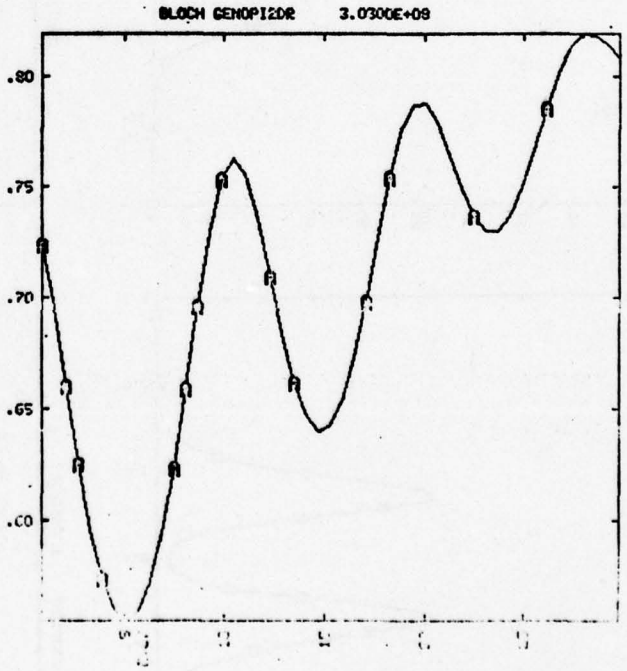

(d) ratio of nonlinear and linear absorption coefficients

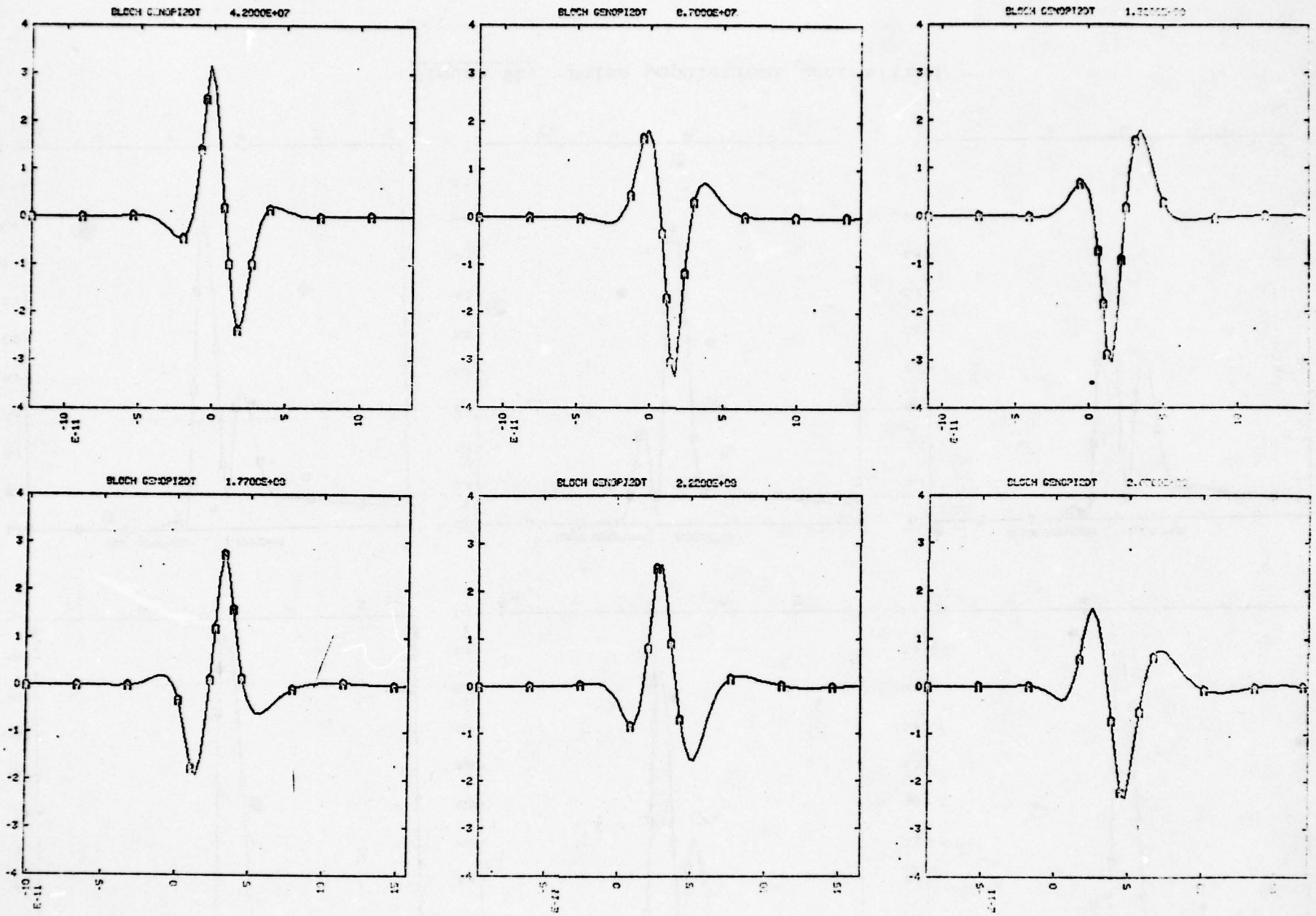

Figure 8a. Pulse normalized electric field

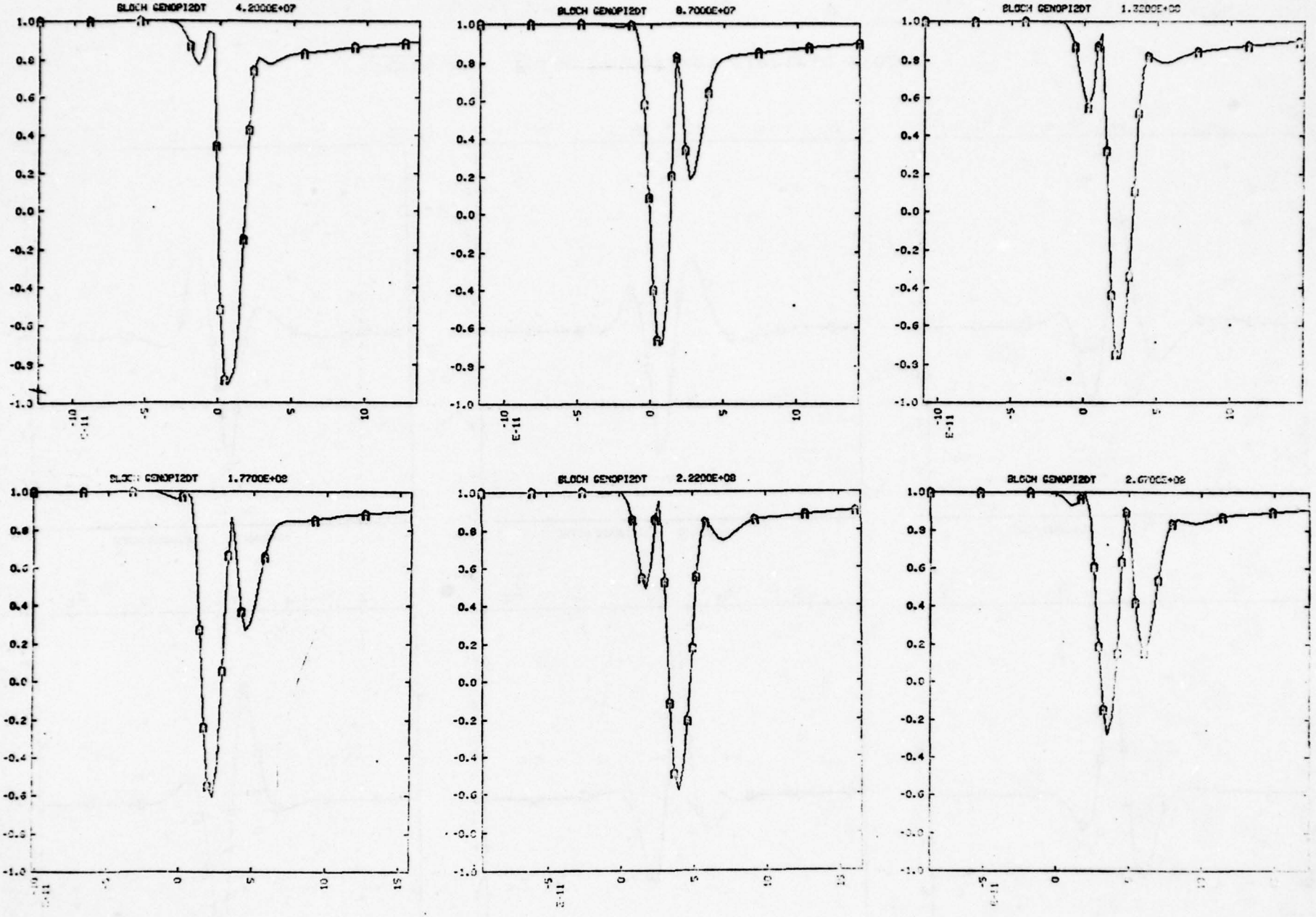

Figure 8b. Pulse populations (normalized)

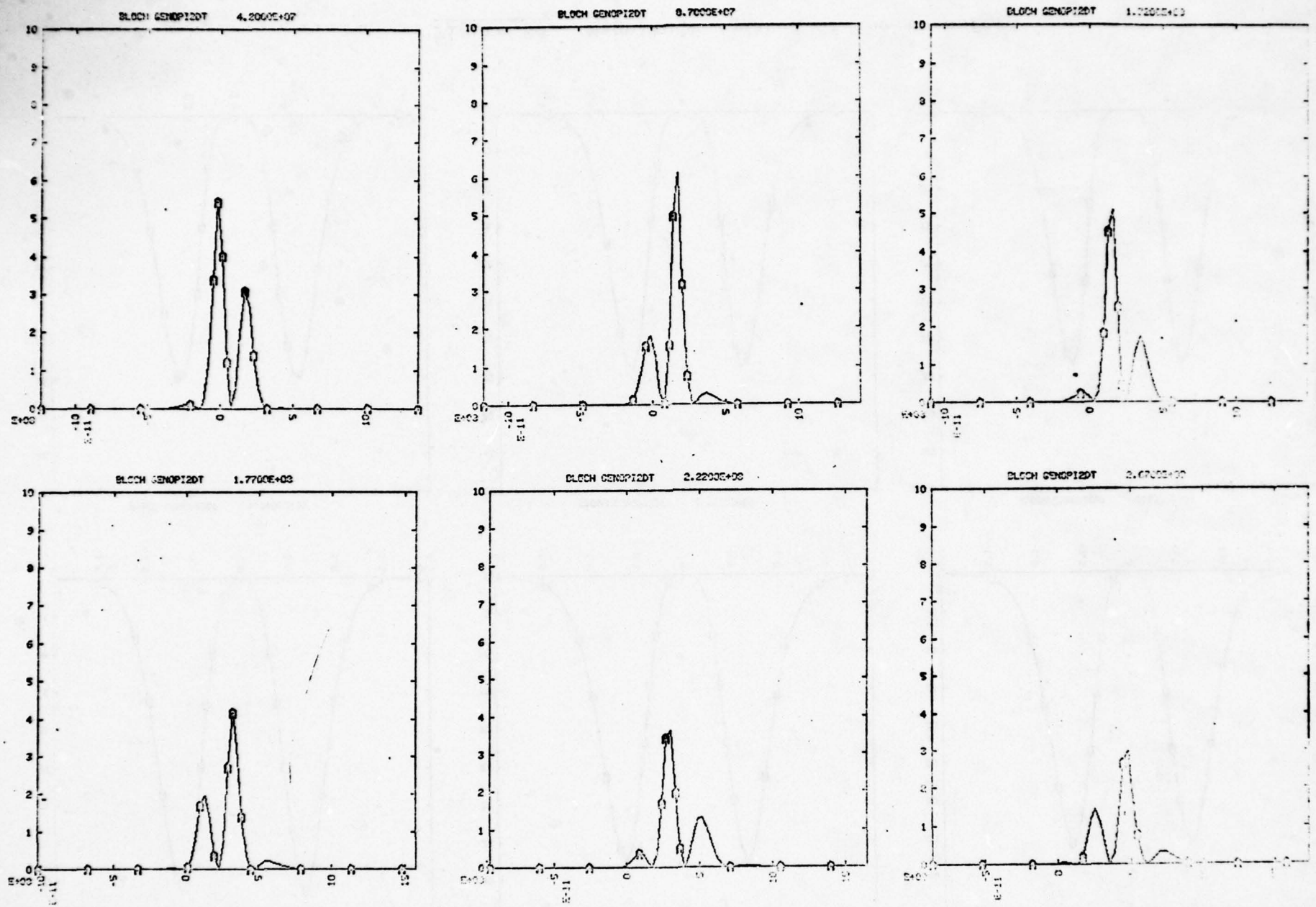

Figure 8c. Pulse power

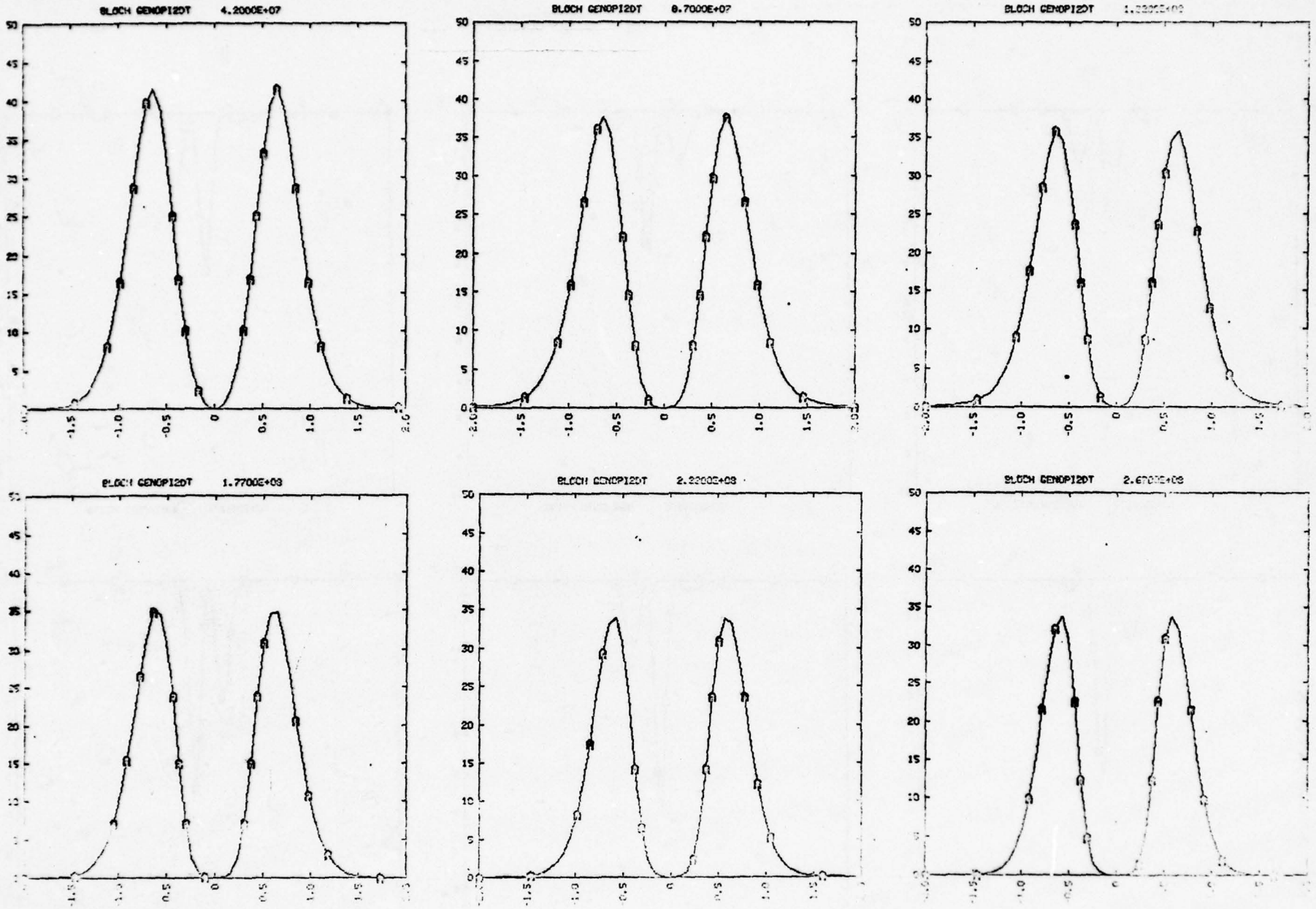

Figure 8d. Magnitude squared of the transform

Figure 9

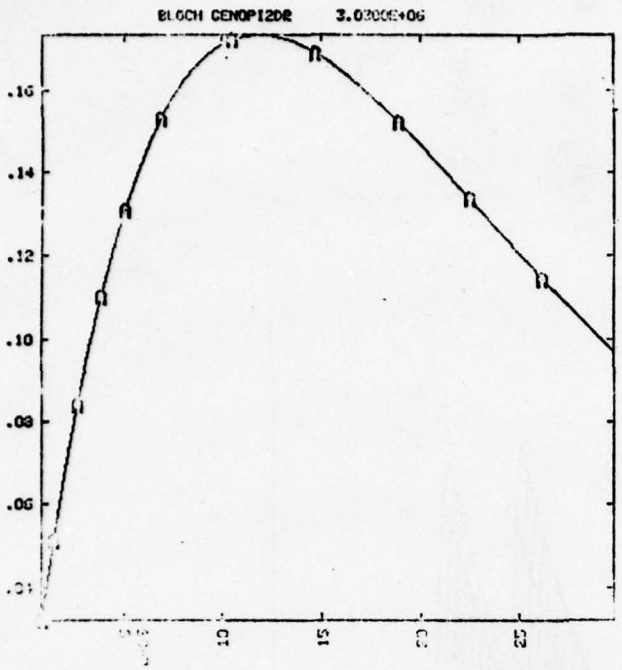

(a) Pulse area

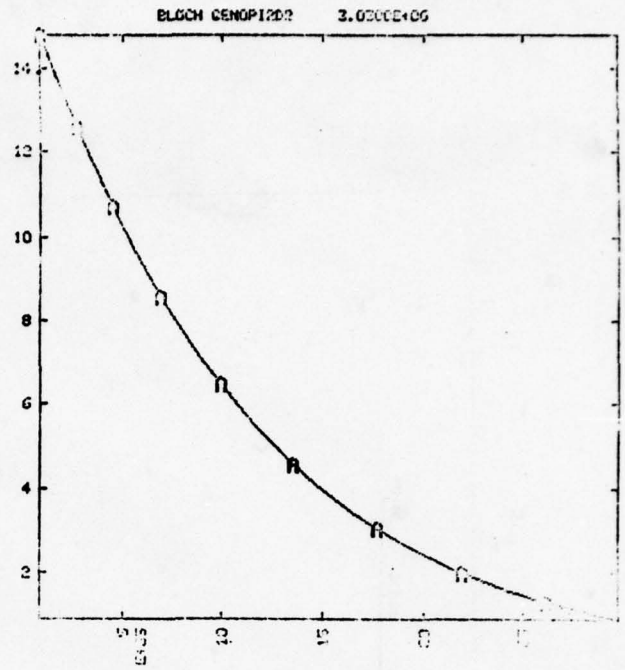

(b) normalized pulse energy

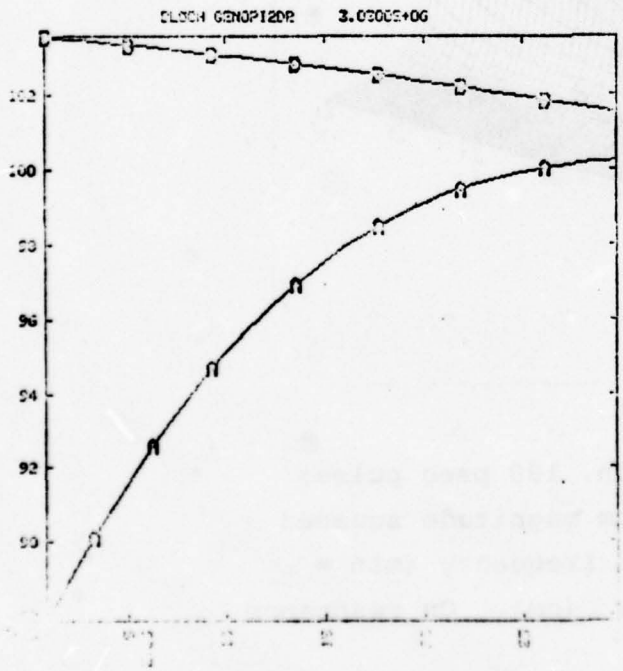

(c) linear and nonlinear absorption coefficients

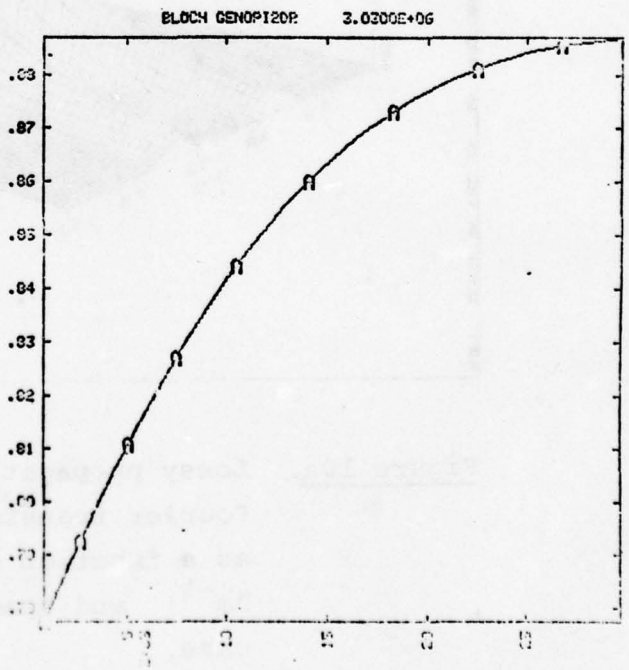

(d) ratio of nonlinear to linear absorption coefficients

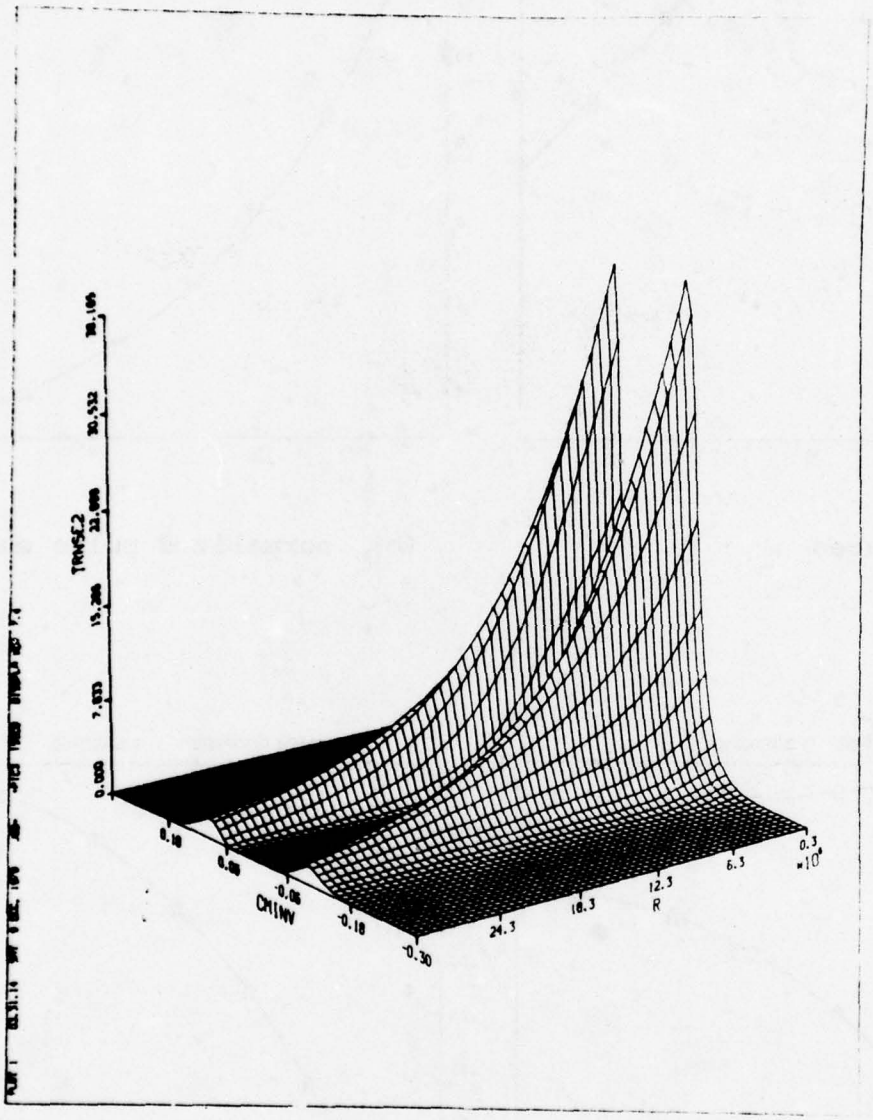

Figure 10a. Lossy propagation 100 psec pulse; Fourier transform magnitude squared as a function of frequency (min = cm^{-1}) and space (cm). On resonance case.

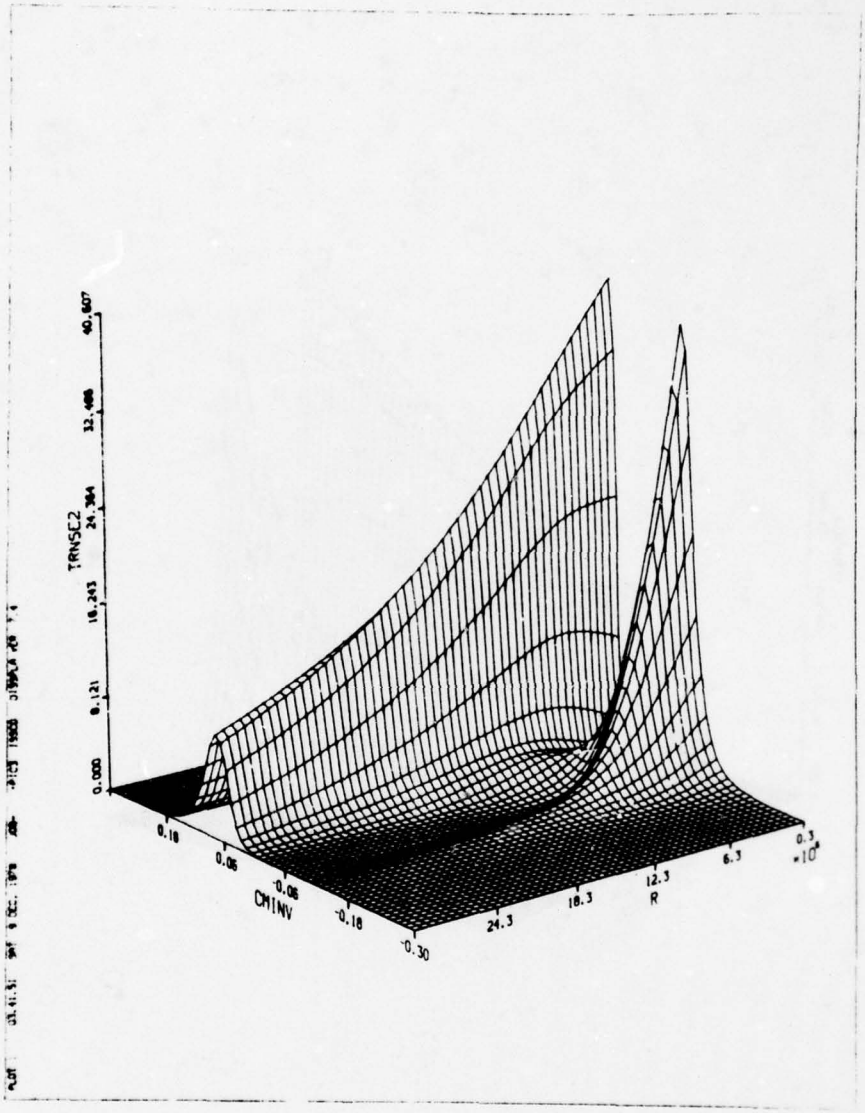

Figure 10b. Lossy propagation 100 psec pulse; $\Delta\omega = 0.05\ cm^{-1}$.

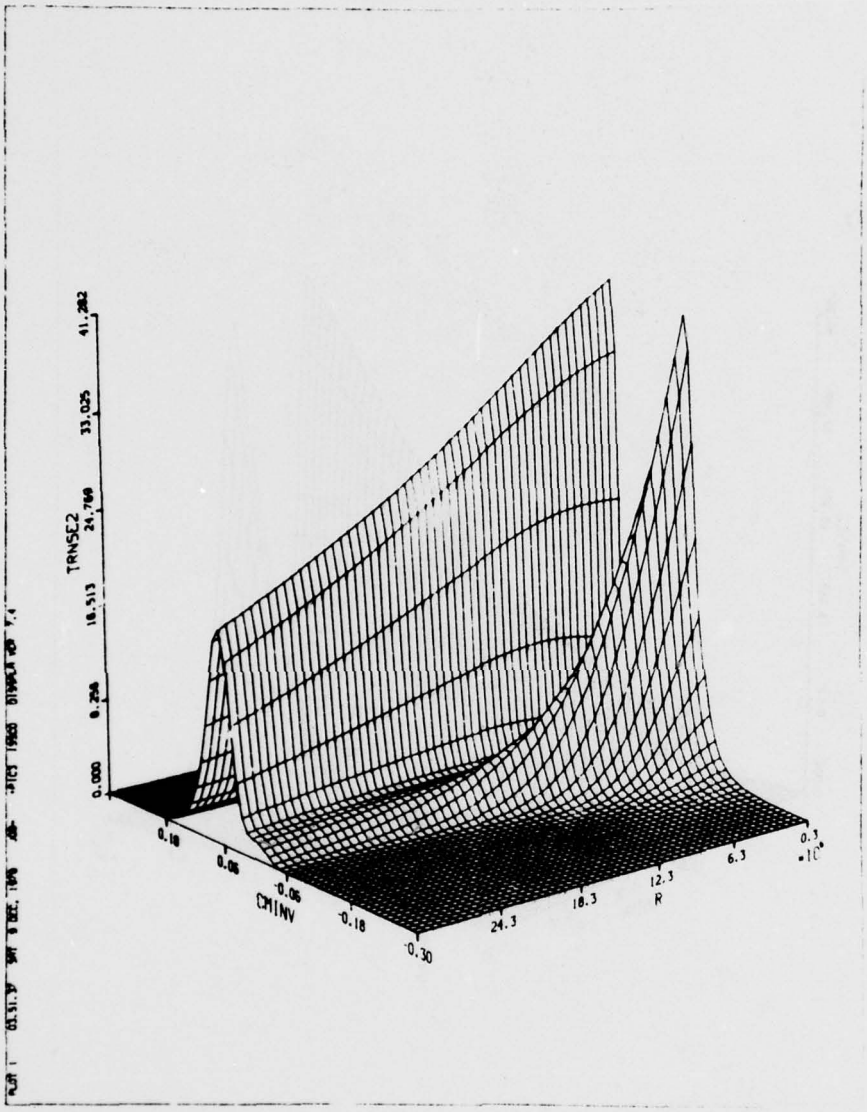

Figure 10c. Lossy propagation 100 psec pulse; $\Delta\omega = 0.10\ cm^{-1}$.

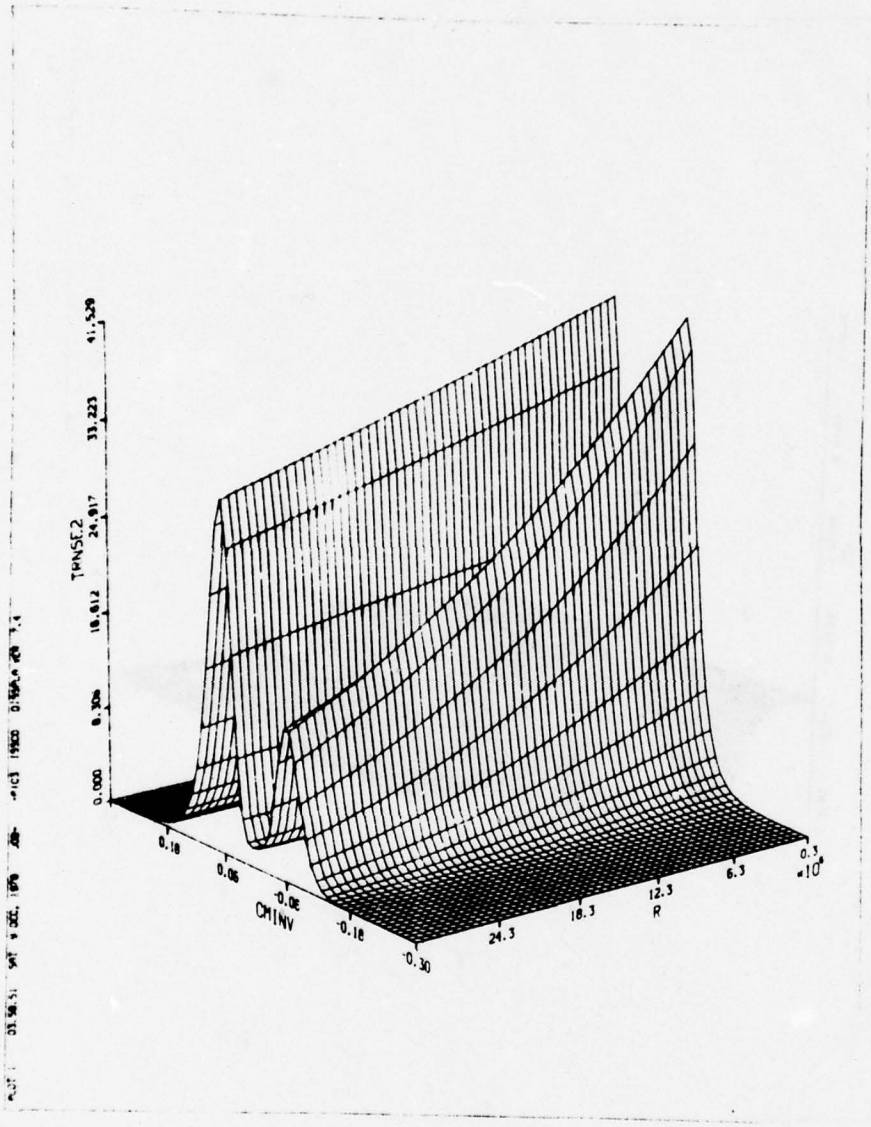

Figure 10d. Lossy propagation 100 psec pulse; $\Delta\omega = 0.20\ cm^{-1}$.

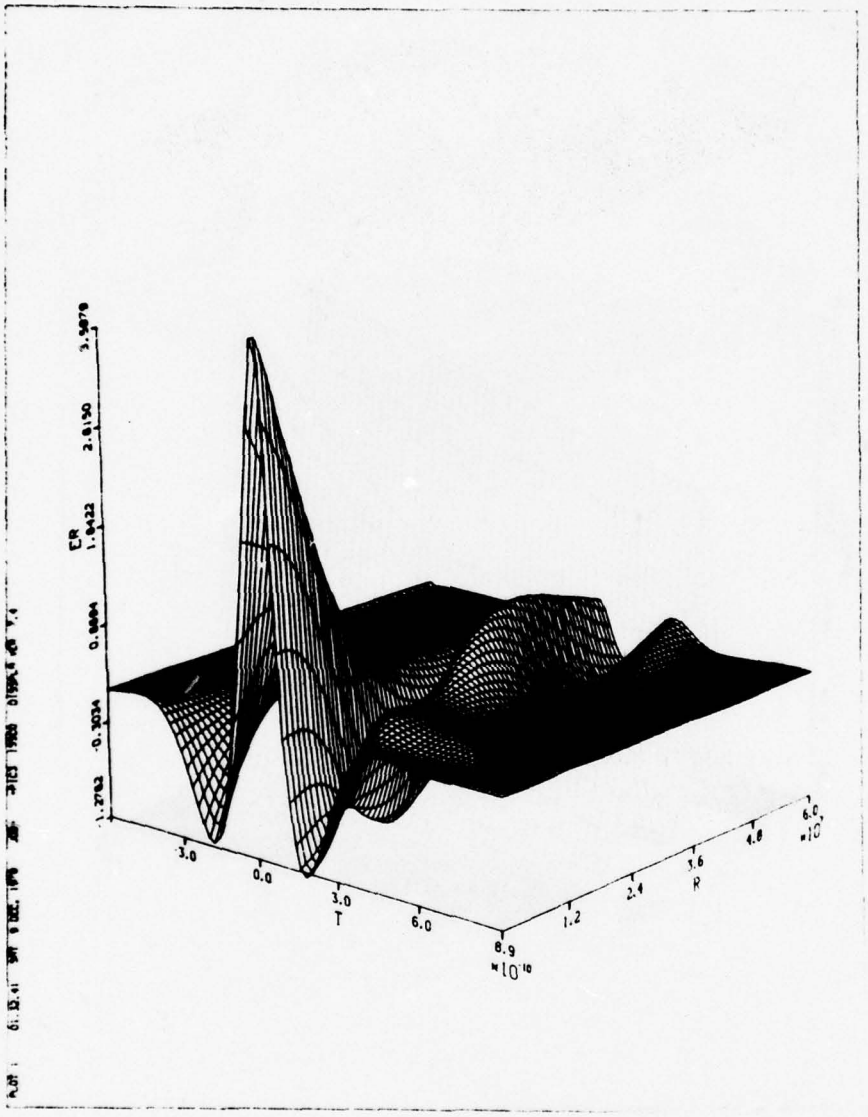

Figure 11a. Lossy 0π pulse propagation $\Delta\omega$ = 0.05 cm^{-1}; normalized electric field 100 psec = t_e = t_f.

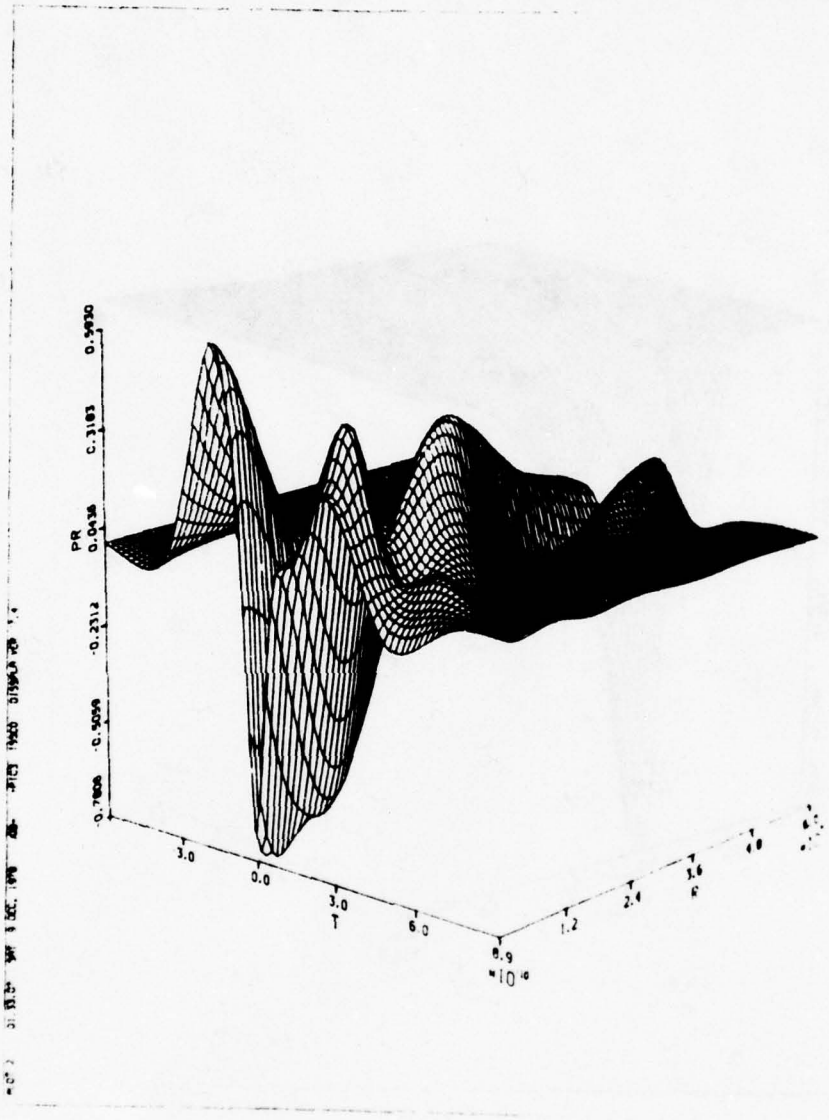

Figure 11b. Lossy 0π pulse propagation $\Delta\omega$ = 0.05 cm^{-1}; normalized polarization 100 psec = $t_e = t_f$.

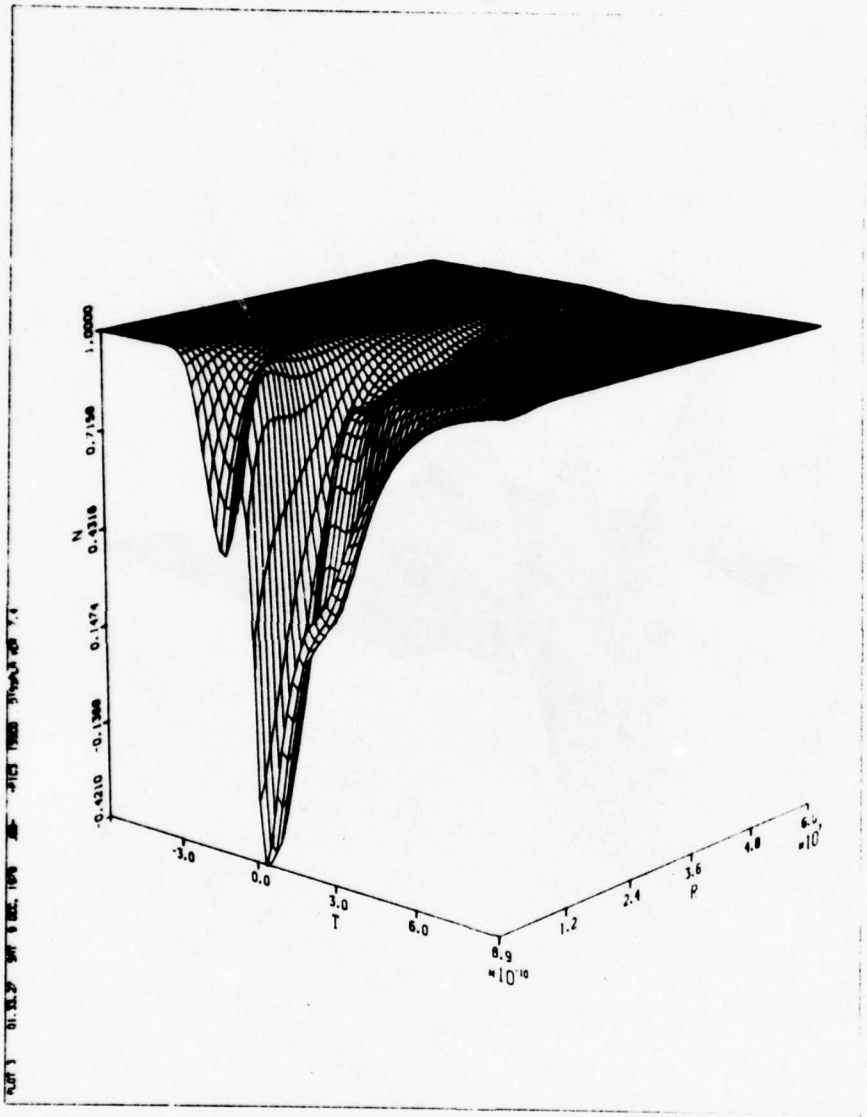

Figure 11c. Lossy 0π pulse propagation $\Delta\omega$ = 0.05 cm^{-1}; normalized population 100 psec = t_e = t_f.

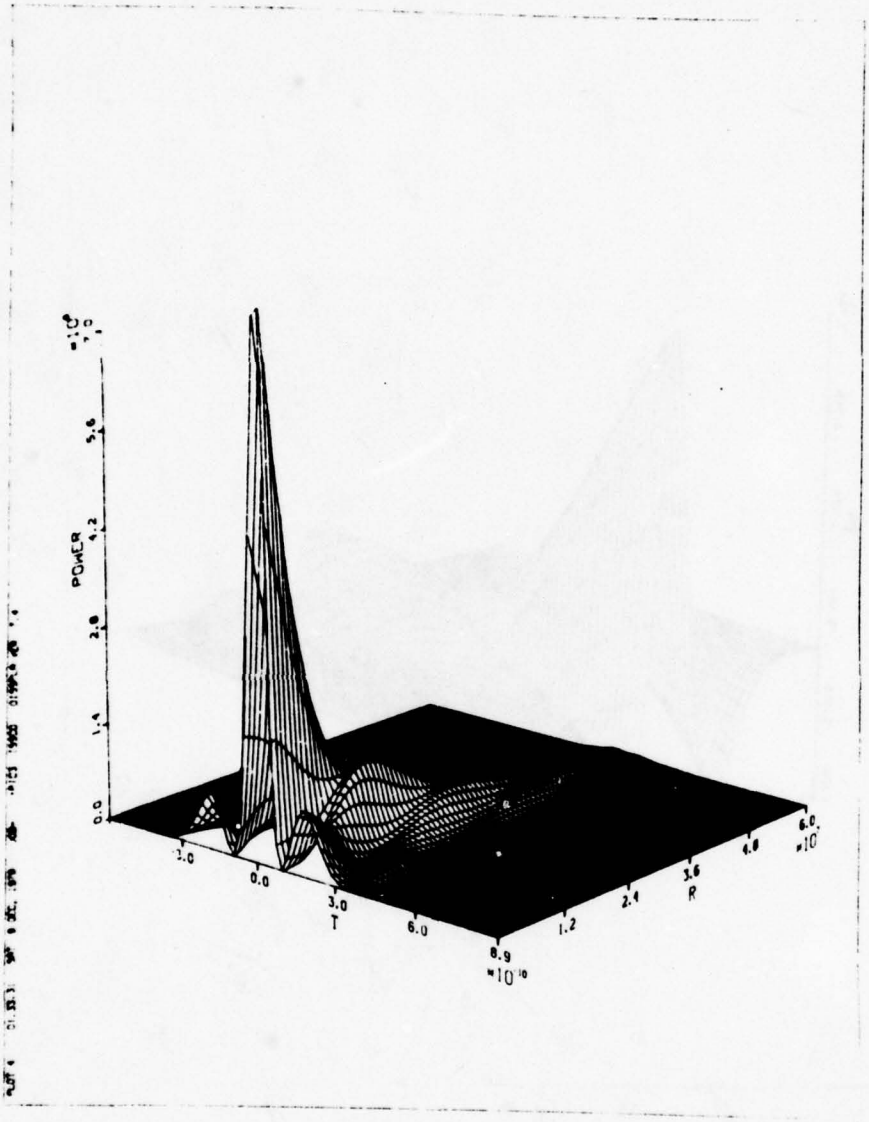

Figure 11d. Pulse power, lossy 0π pulse; $\Delta\omega = 0.05\ cm^{-1}$, $t_e = t_f = 100$ psec.

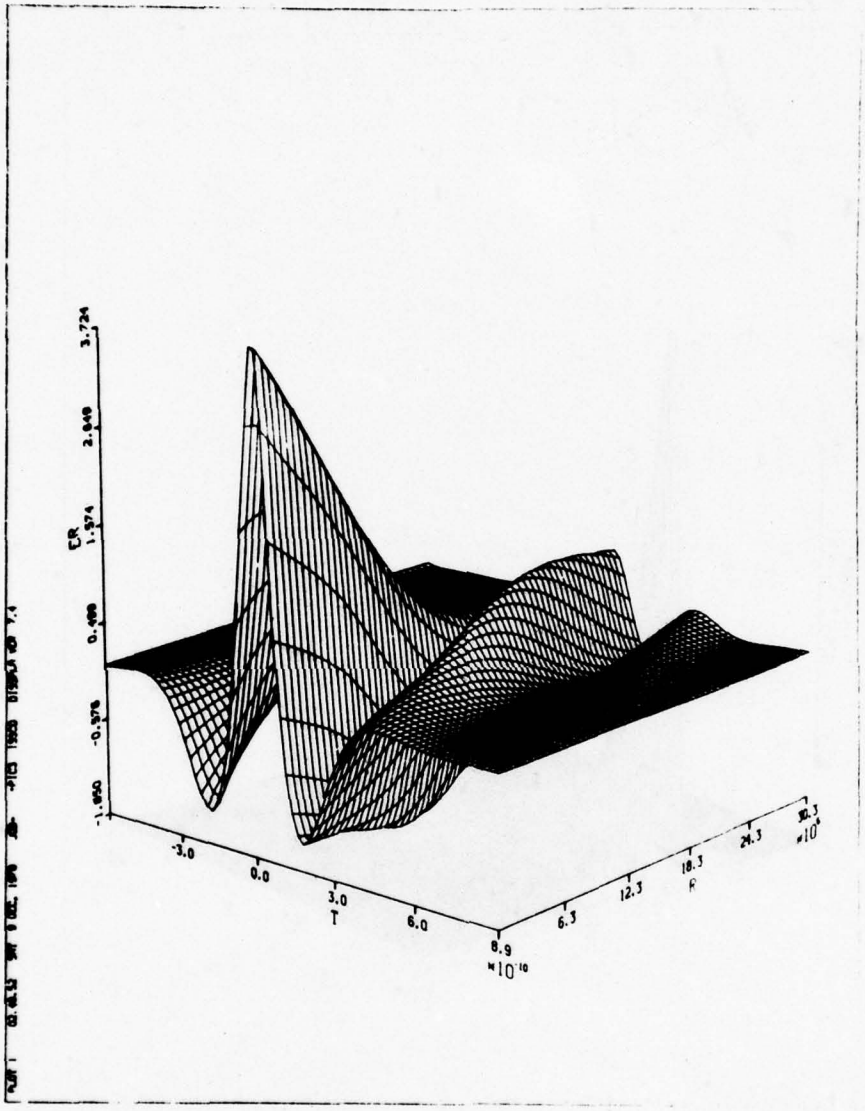

Figure 12a. Lossy 0π pulse propagation t_e = t_f = 100 psec; normalized electric field $\Delta\omega$ = 0.

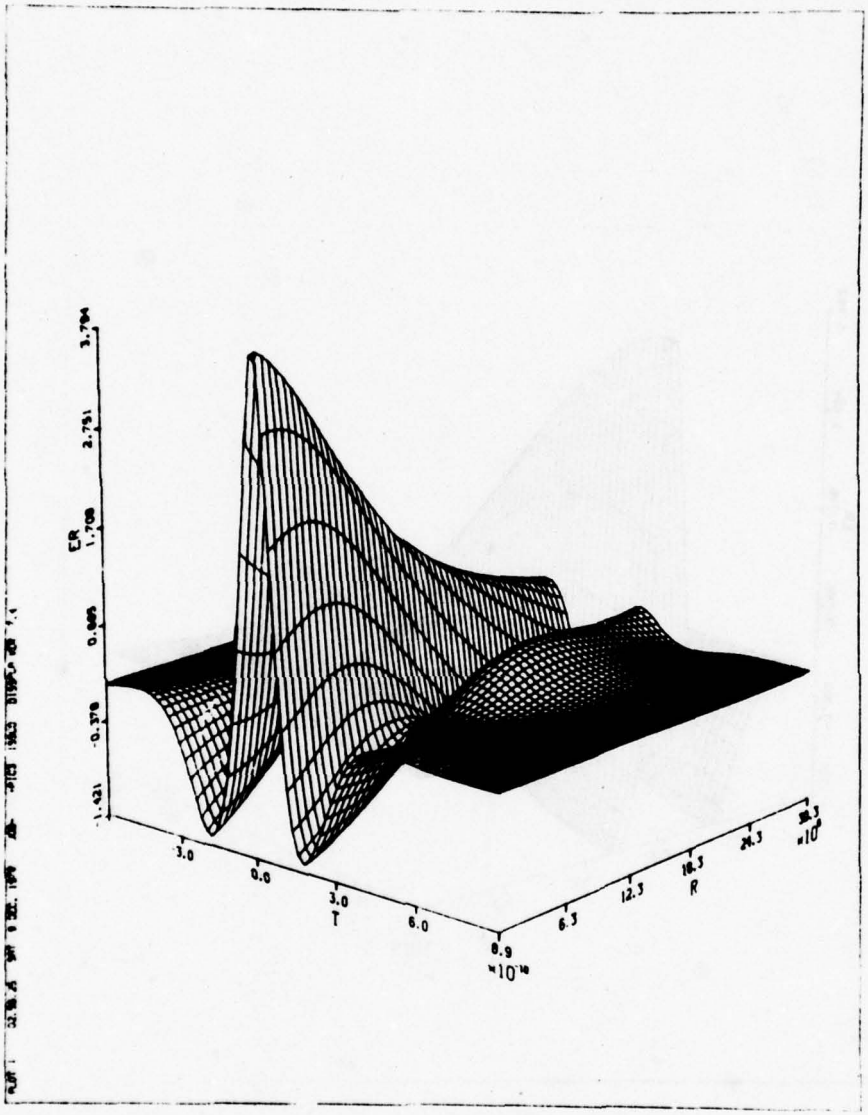

Figure 12b. Lossy 0π pulse propagation t_e = t_f = 100 psec; normalized electric field $\Delta\omega$ = 0.10 cm.

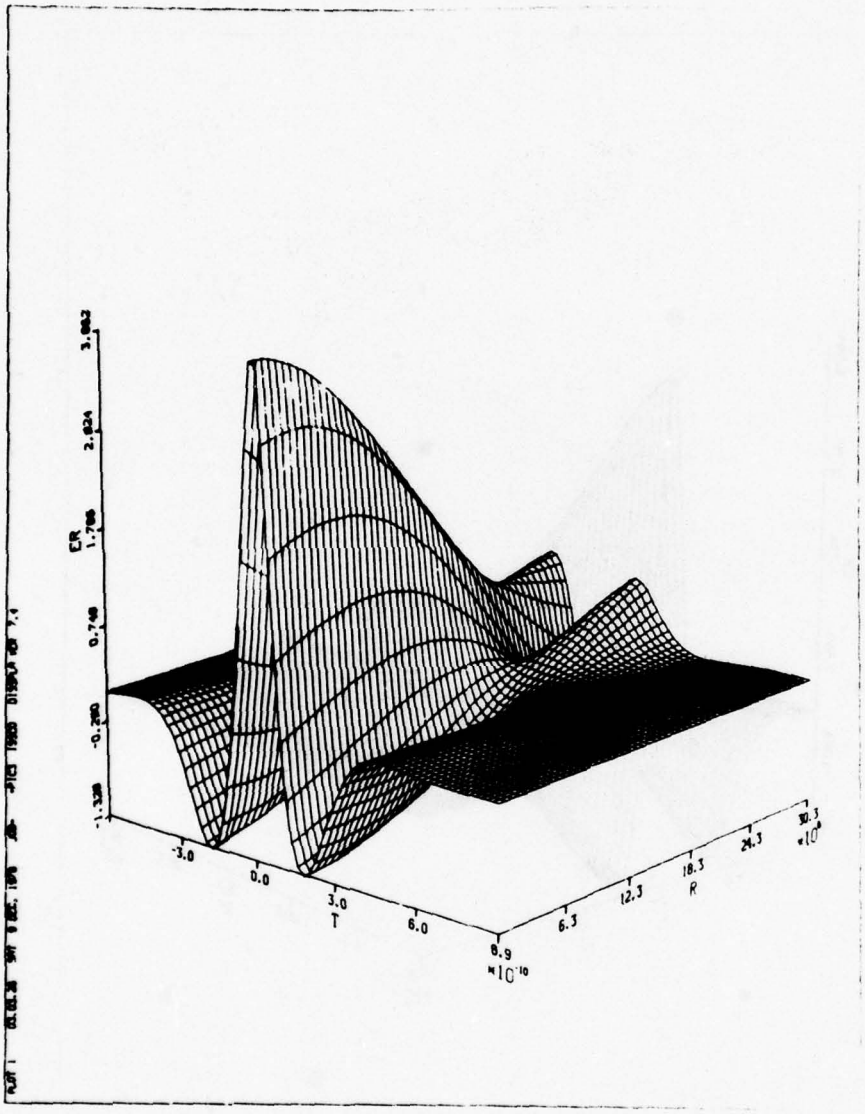

Figure 12c. Lossy 0π pulse propagation $t_e = t_f = 100$ psec; normalized electric field $\Delta\omega = 0.2$ cm^{-1}.

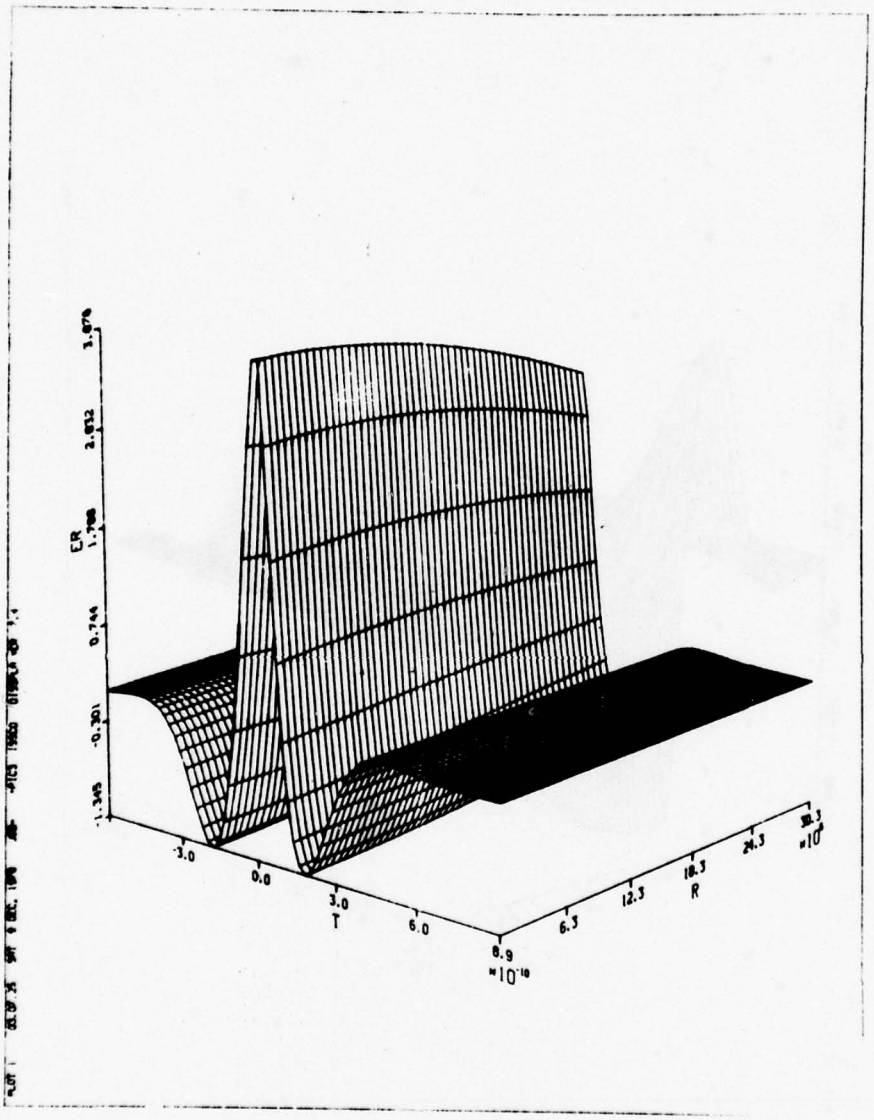

Figure 12d. Lossy 0π pulse $t_e = t_f = 100$ psec; normalized electric field $\Delta\omega = 0.6\ cm^{-1}$

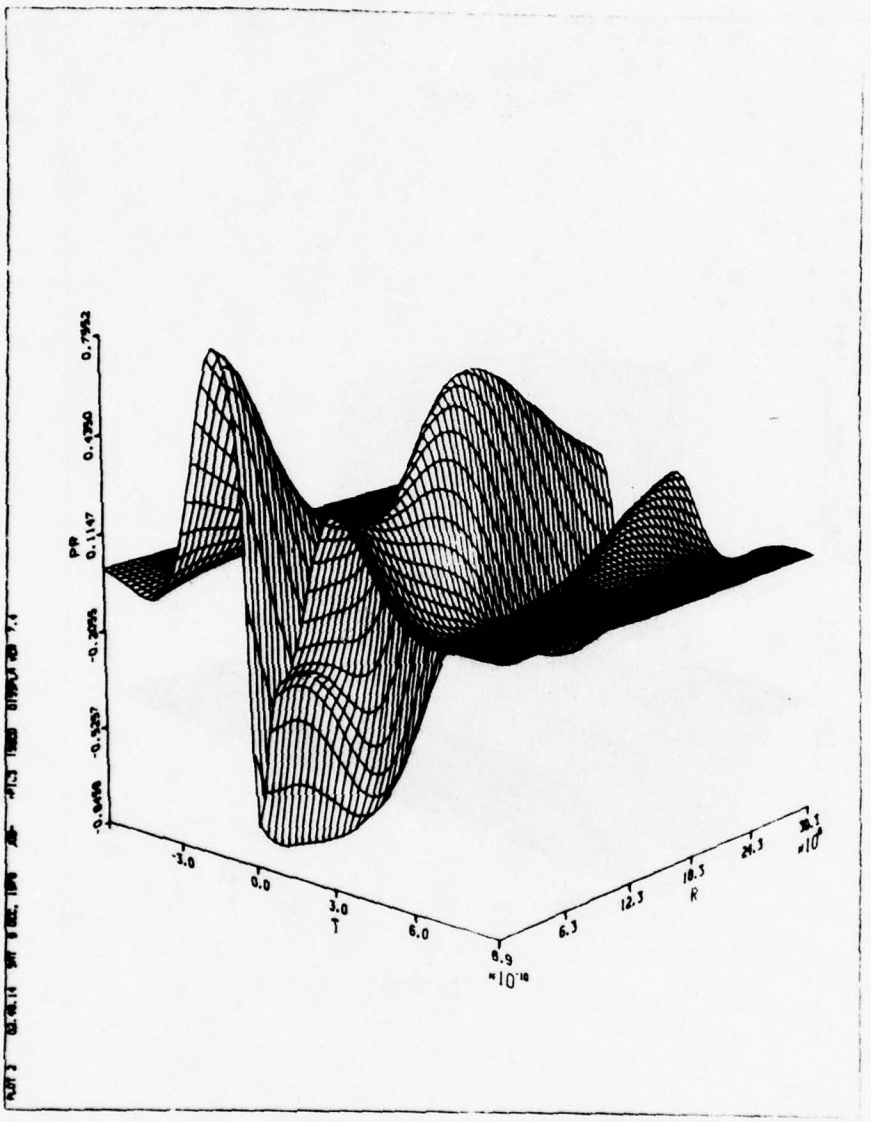

Figure 13a. Lossy 0π pulse propagation t_e = t_f = 100 psec; normalized polarization $\Delta\omega = 0$.

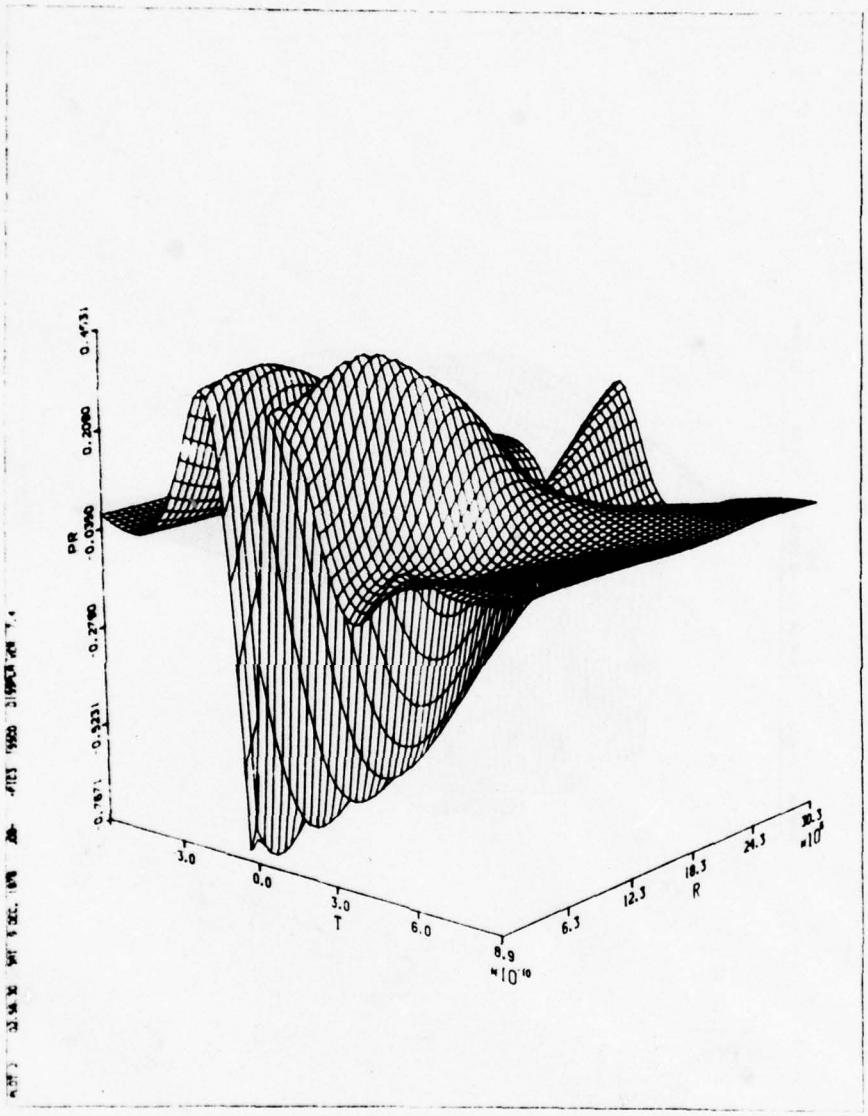

Figure 13b. Lossy 0π pulse propagation t_e = t_f = 100 psec; normalized polarization $\Delta\omega = 0.10\ cm^{-1}$

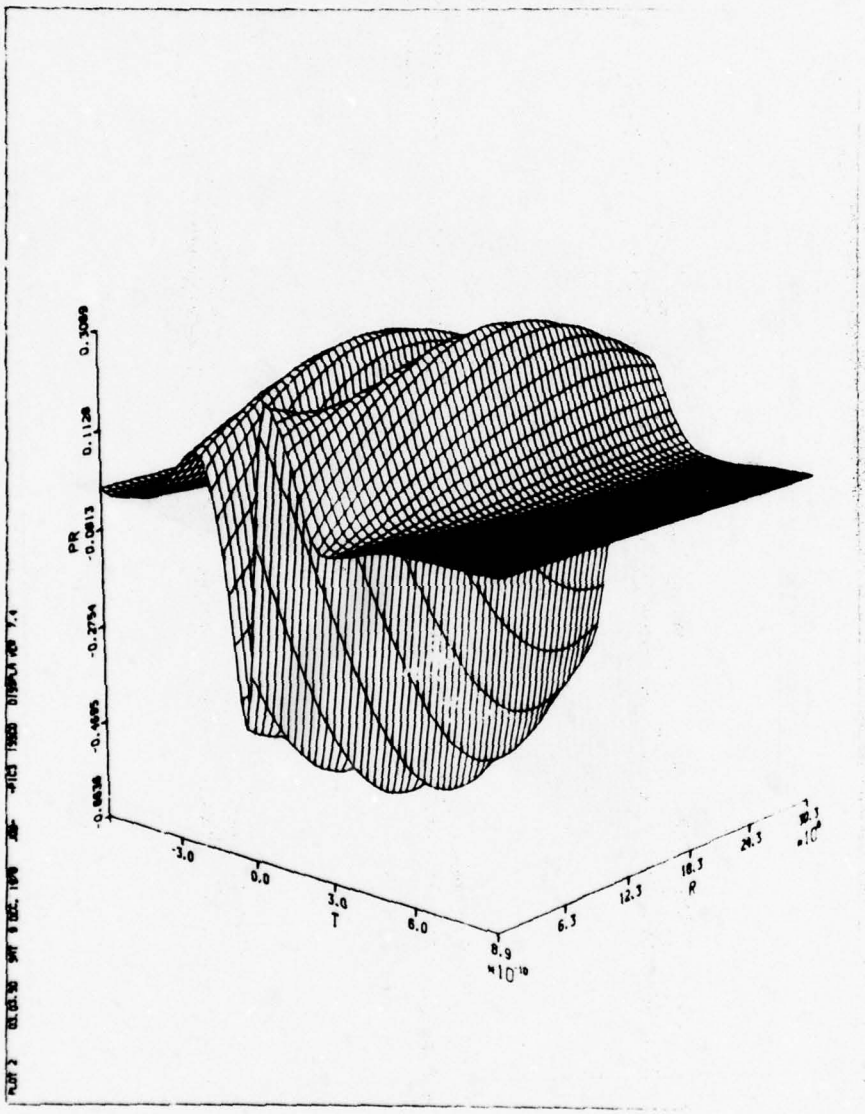

Figure 13c. Lossy 0π pulse propagation t_e = t_f = 100 psec; normalized polarization $\Delta\omega = 0.20\ cm^{-1}$.

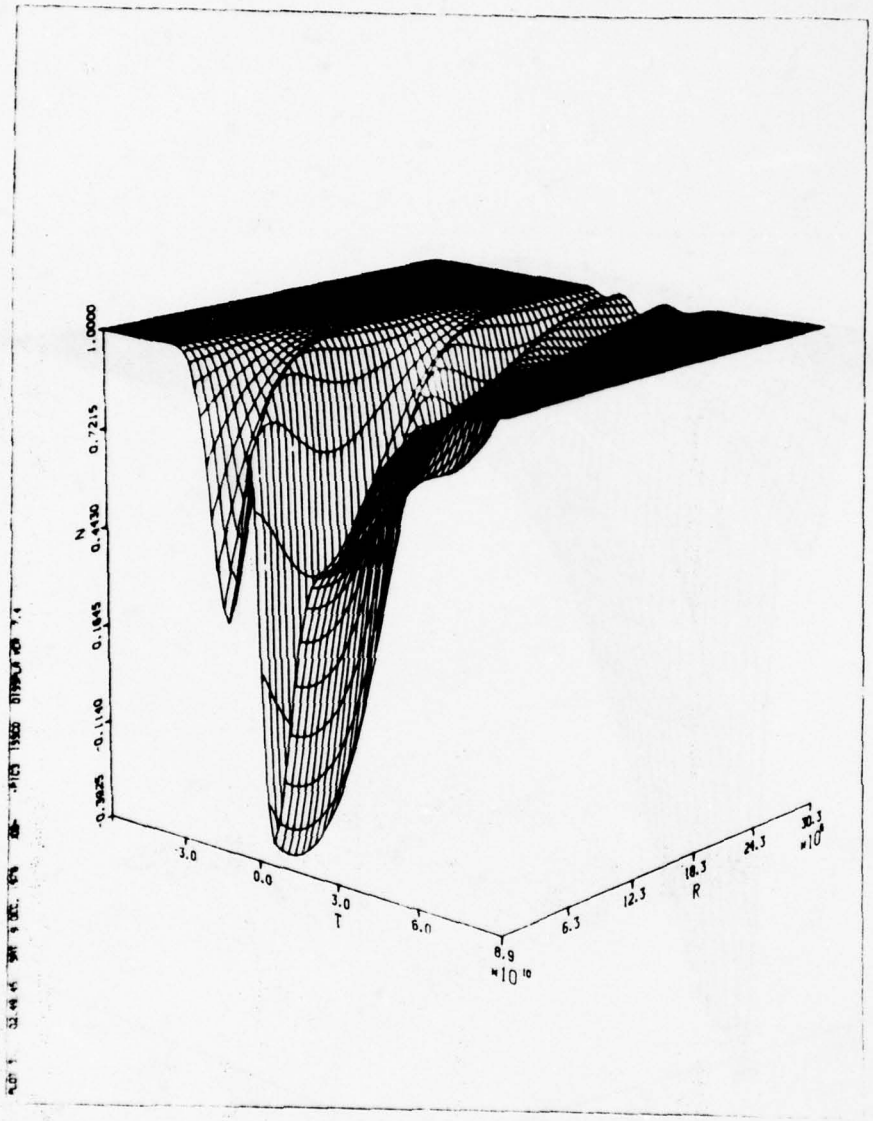

Figure 14a. Lossy 0π pulse propagation $t_e = t_f$ = 100 psec; normalized population $\Delta\omega = 0$.

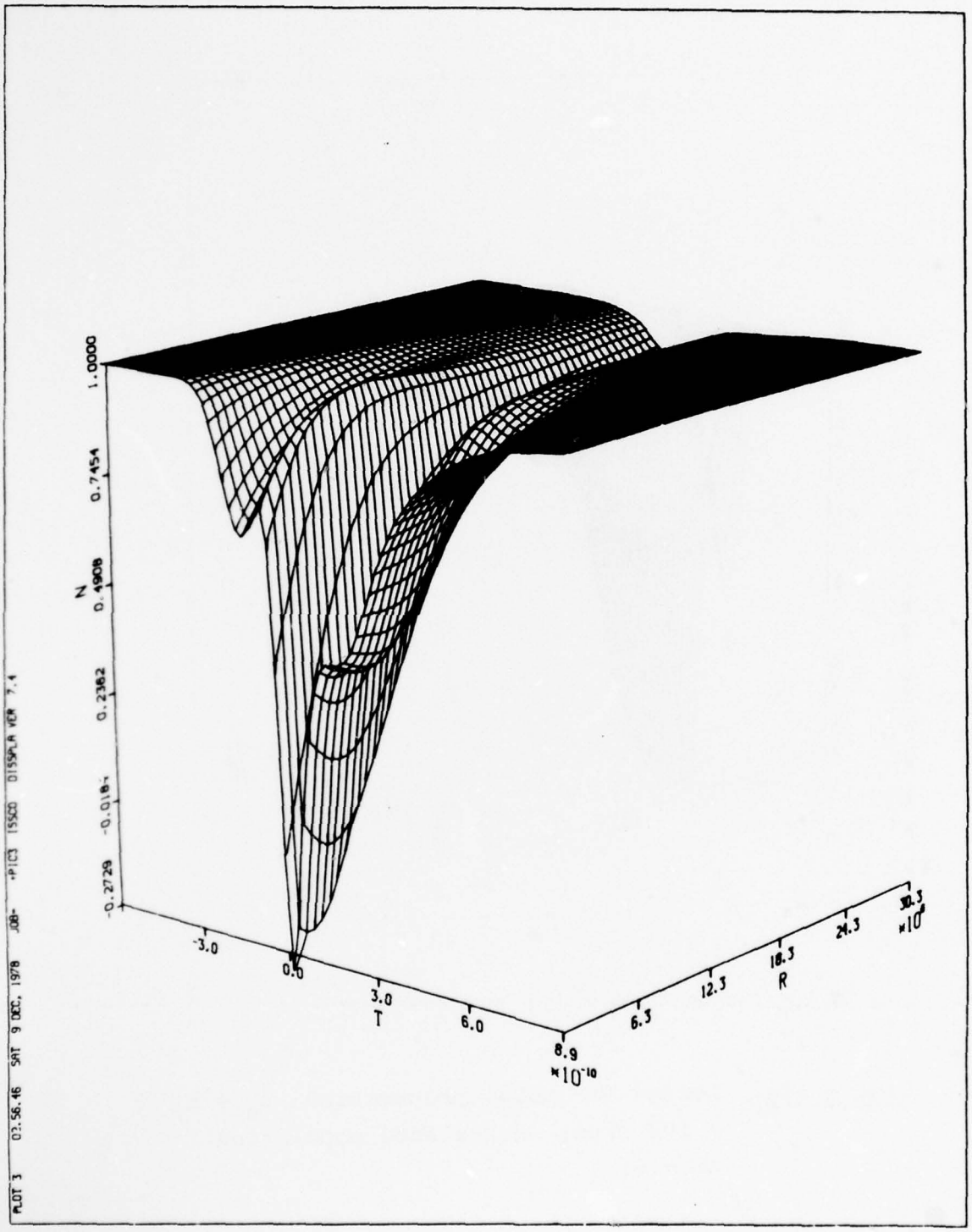

Figure 14b. Lossy 0π pulse propagation; $t_e = t_f = 100$ psec; normalized population $\Delta\omega = 0.10$ cm^{-1}.

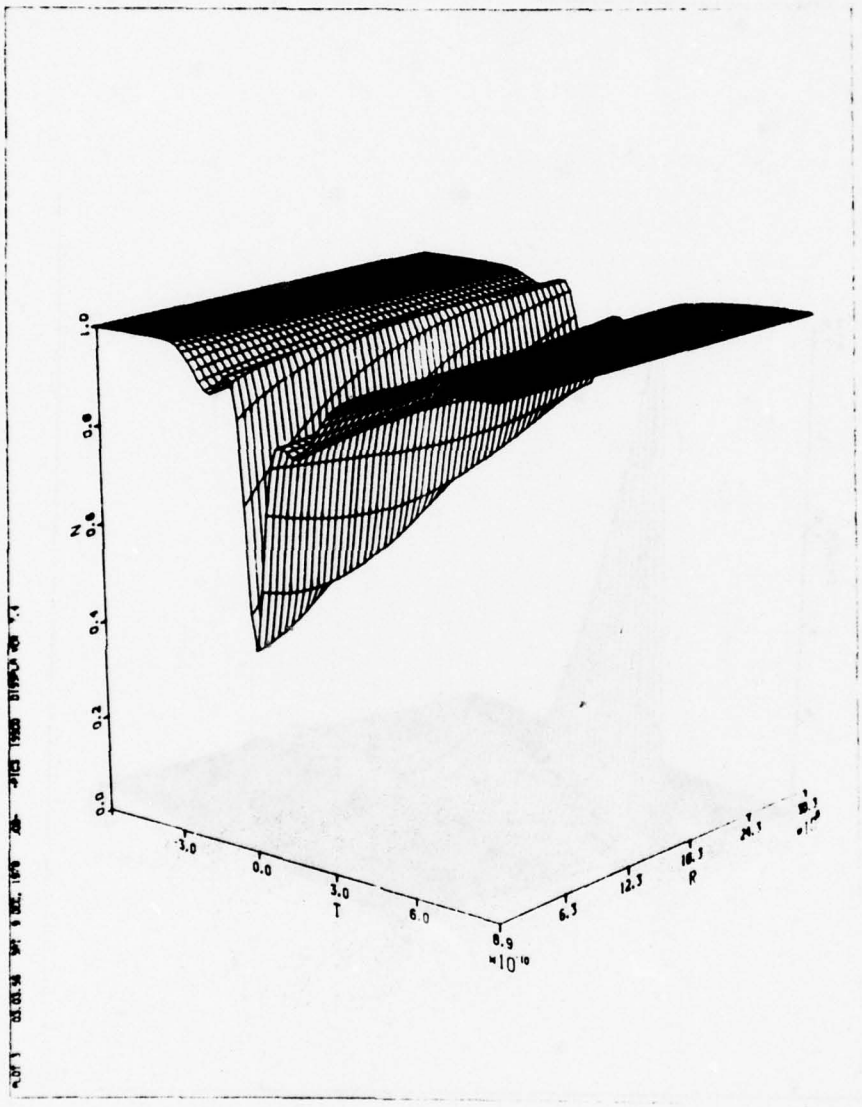

Figure 14c. Lossy 0π pulse propagation $t_e = t_f$ = 100 psec; normalized population $\Delta\omega$ = 0.20 cm^{-1}.

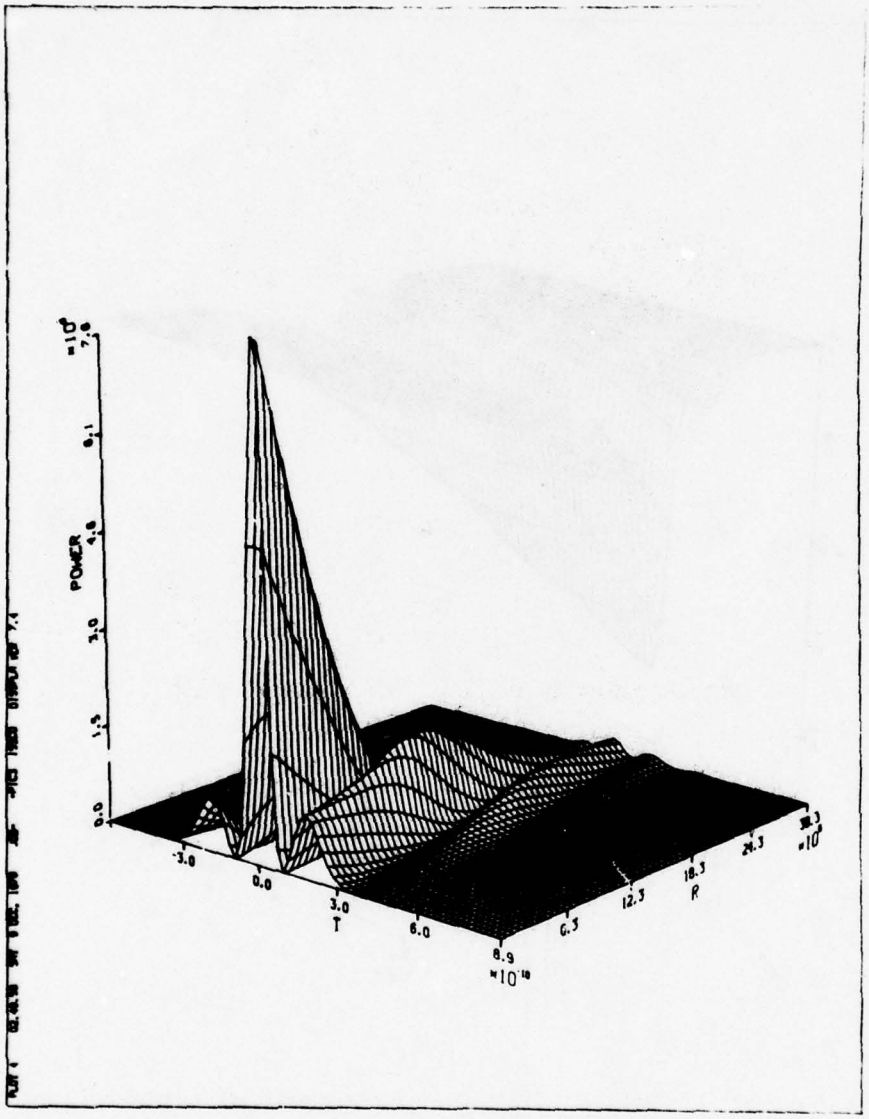

Figure 15a. Lossy 0π pulse propagation $t_e = t_f$ = 100 psec; pulse power $\Delta\omega = 0$.

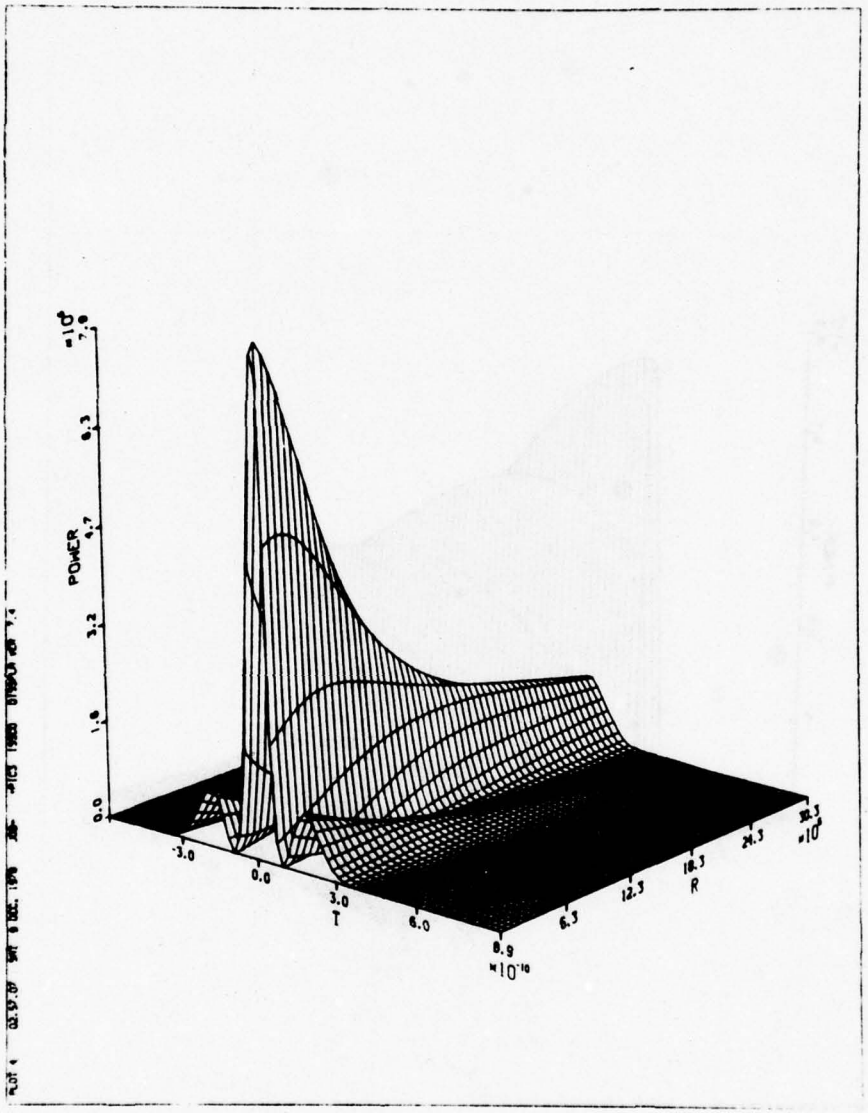

Figure 15b. Lossy 0π pulse propagation $t_e = t_f = 100$ psec; pulse power $\Delta\omega = 0.10\ cm^{-1}$.

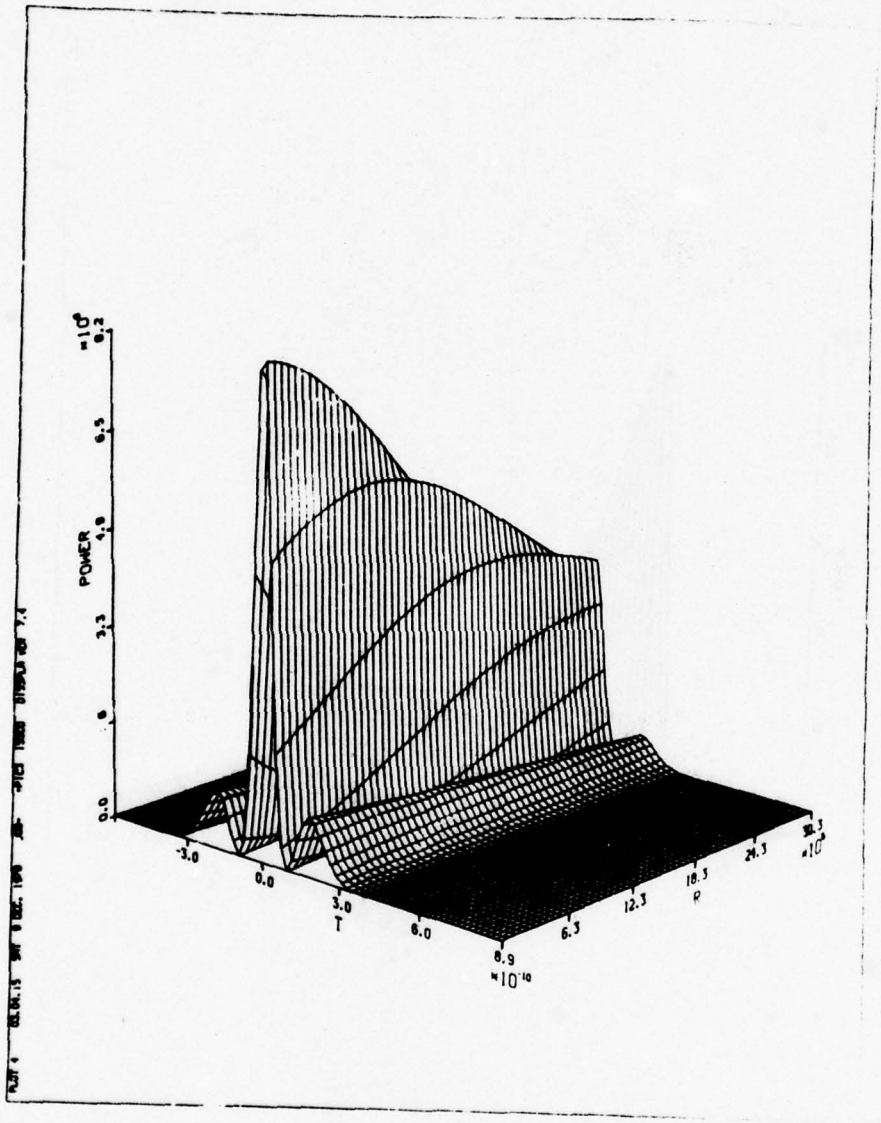

Figure 15c. Lossy 0π pulse propagation t_e = t_f = 100 psec; pulse power $\Delta\omega$ = 0.20 cm^{-1}.

Figure 16. Lossy propagation (0π pulse); $t_e = t_f = 100$ psec, $\Delta\omega = 0$ 165

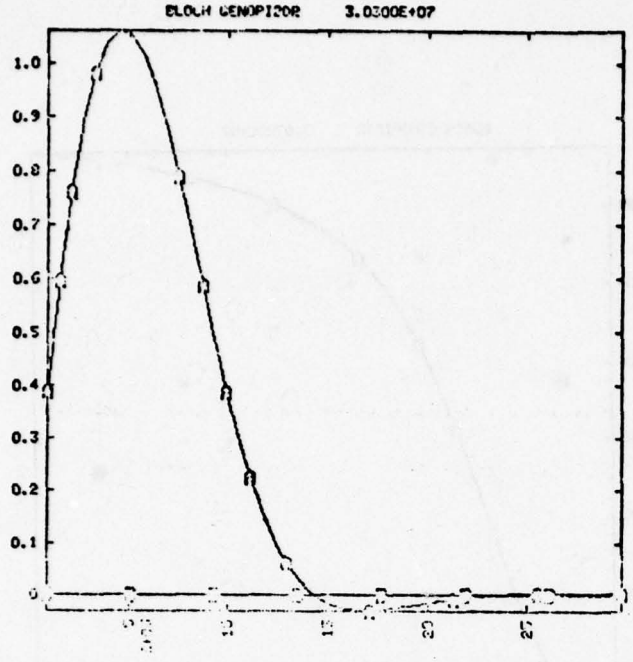

(a) Pulse area versus R(cm)

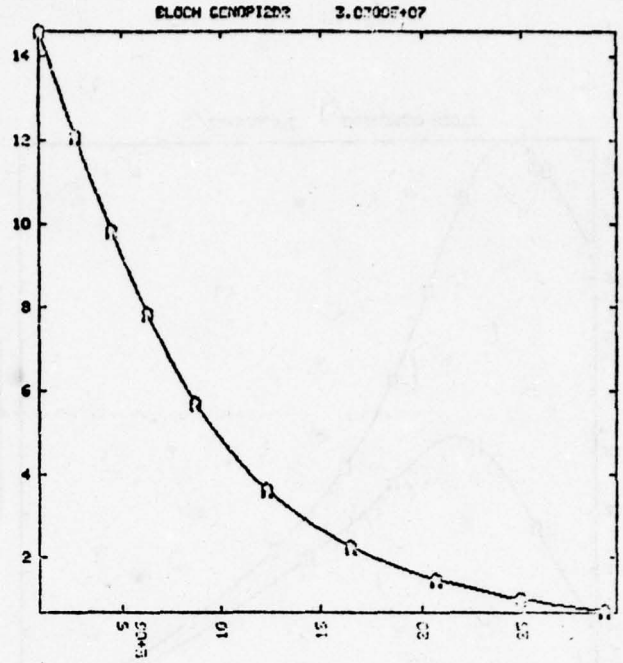

(b) Normalized energy versus R(cm)

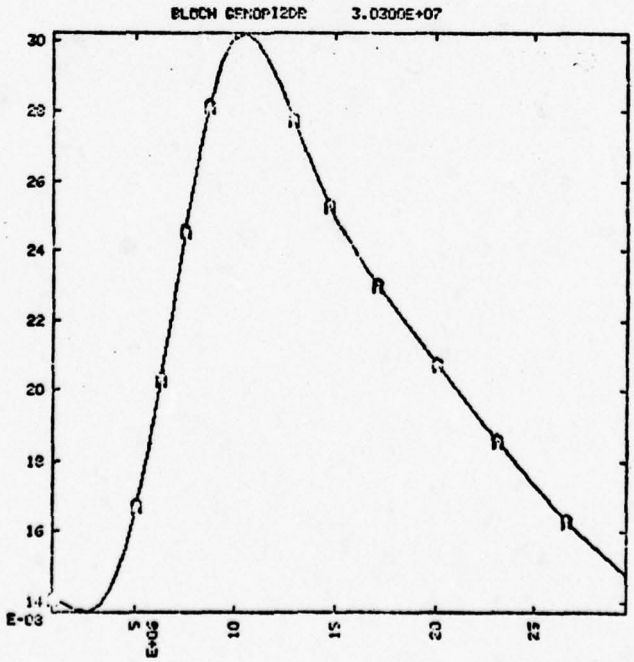

(c) (1 - v/c) versus R(cm)

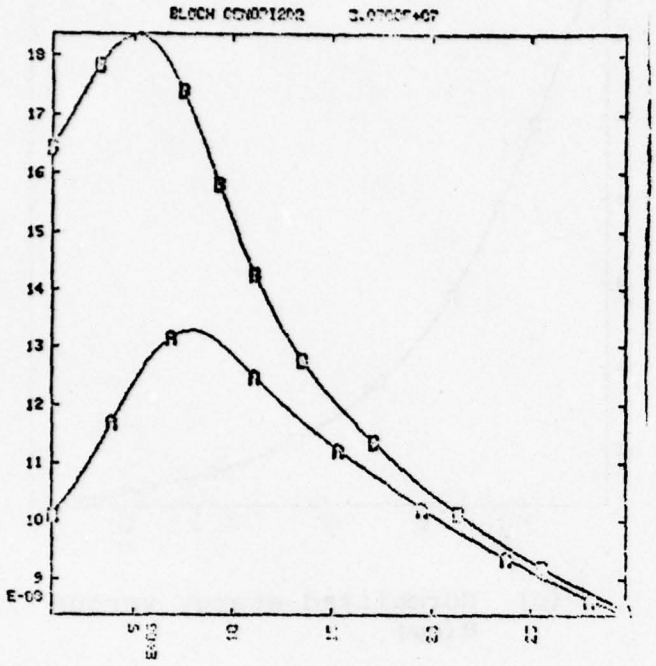

(d) Linear + nonlinear K (cm^{-1})

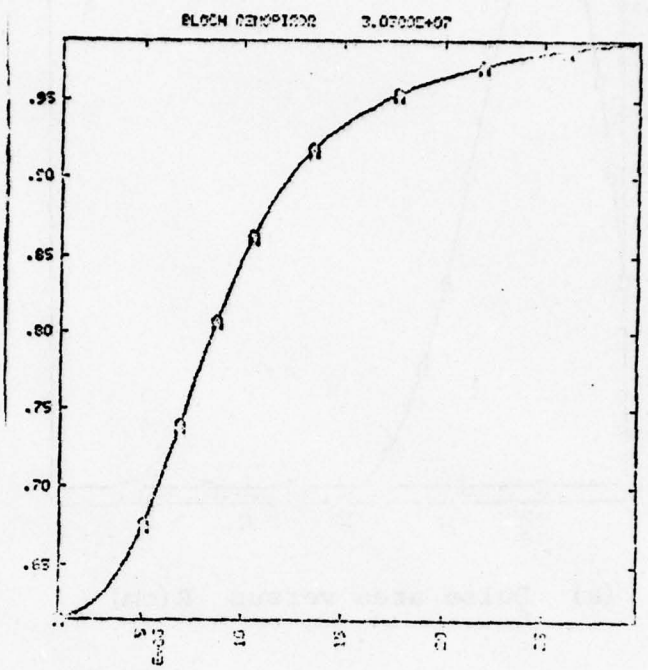

(e) K_{nonlin}/K_{lin}

Figure 17. Lossy propagation; $t_e = t_s = 100$ ps, $\Delta\omega = 0.05$ cm^{-1}

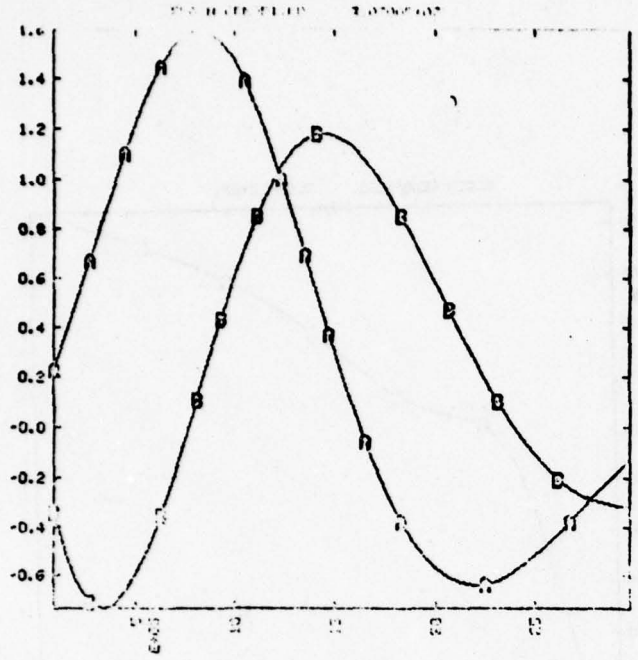

(a) Pulse area

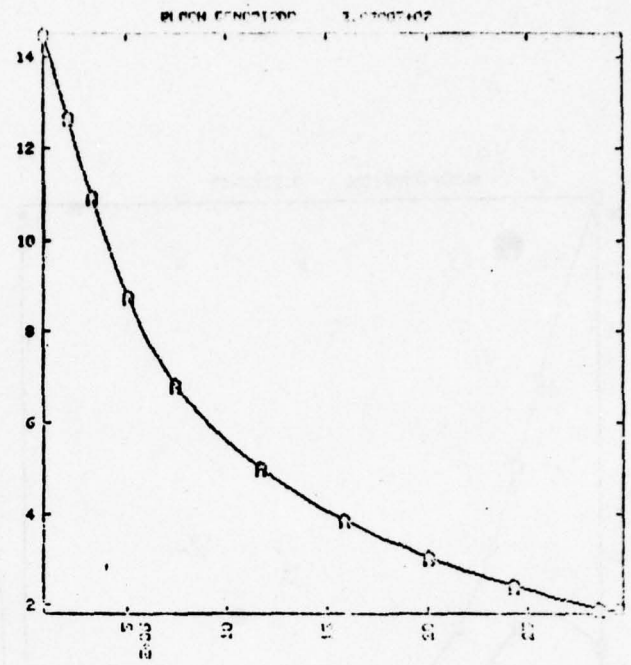

(b) energy

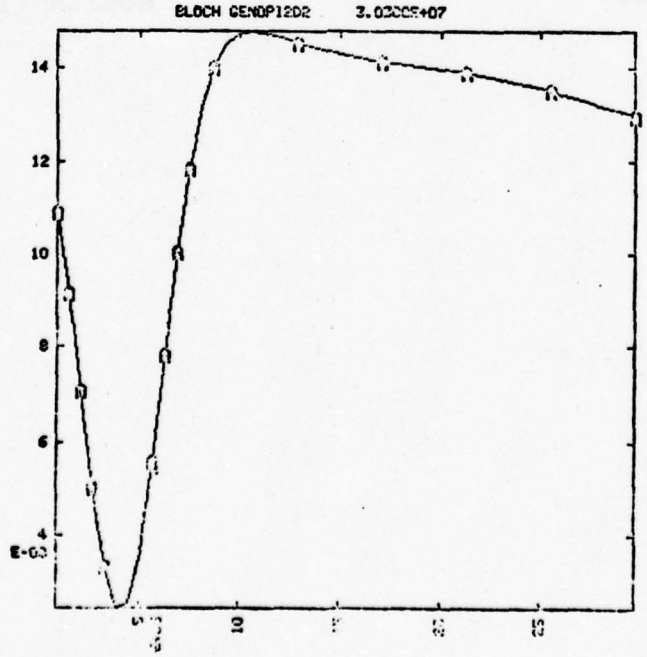

(c) (1 - v/c)

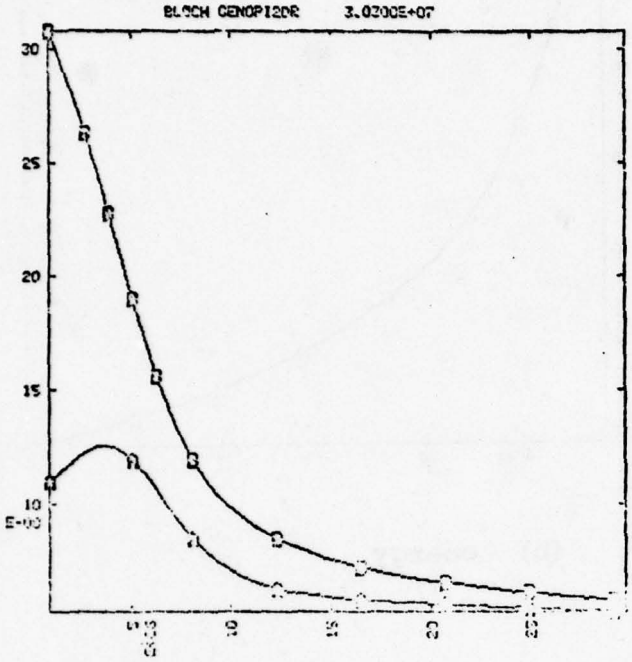

(d) K_{lin}, K_{nonlin}

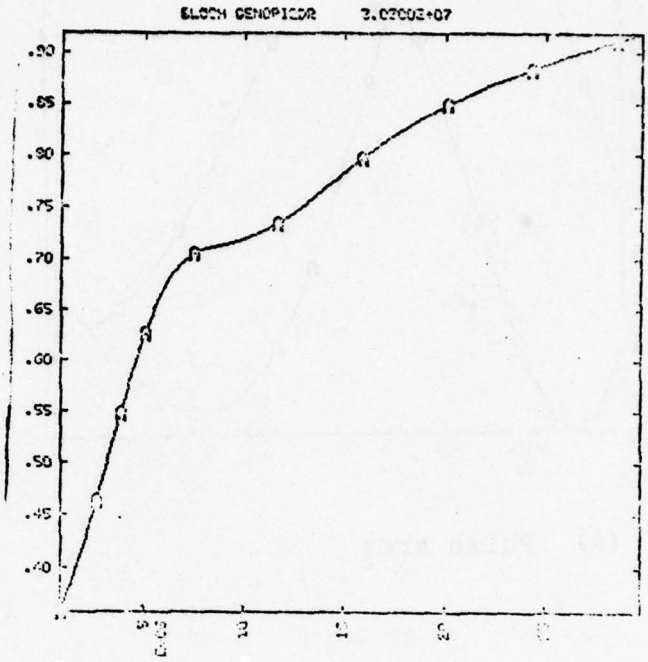

(e) K_{nonlin}/K_{lin}

Figure 18. Lossy propagation (0π); $t_e = t_f = 100$ psec; $\Delta\omega = 0.10$ cm^{-1}

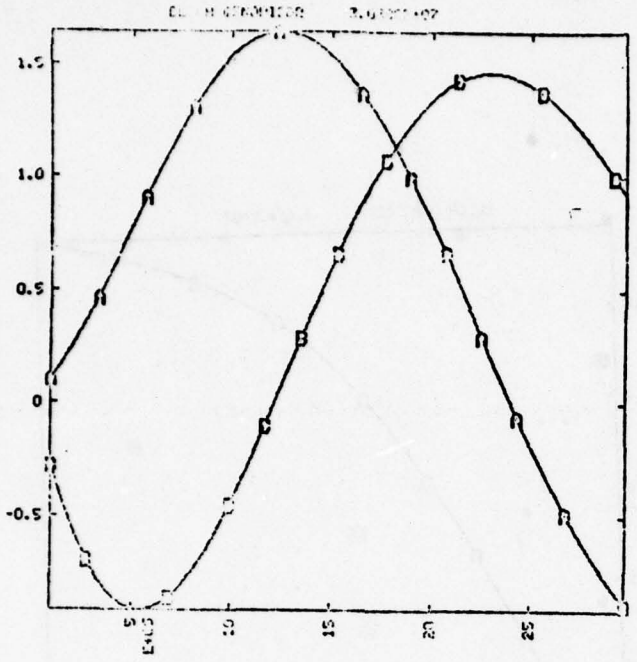

(a) Pulse area

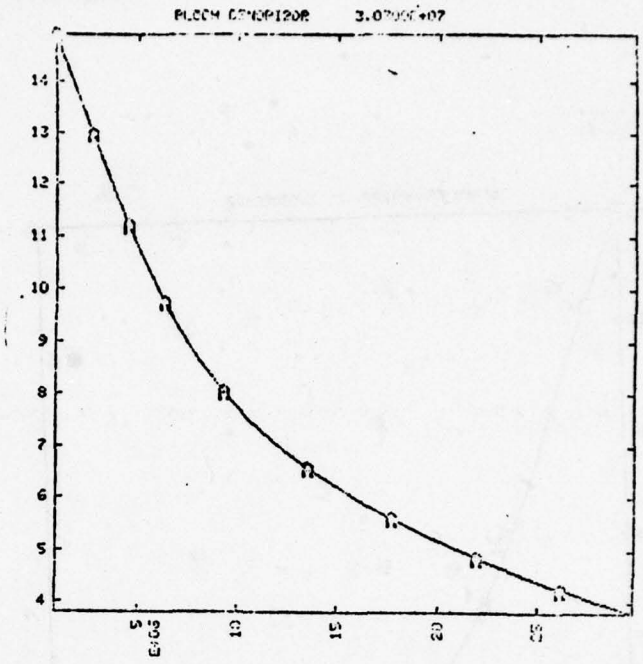

(b) energy

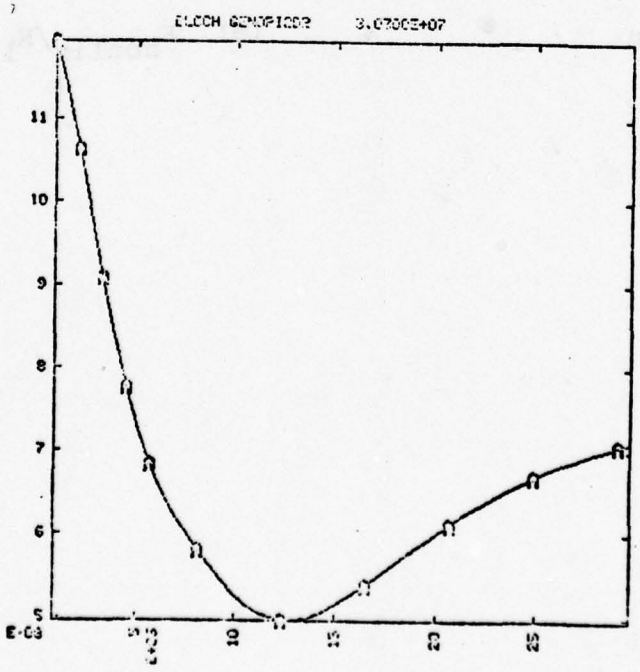

(c) (1 - v/c)

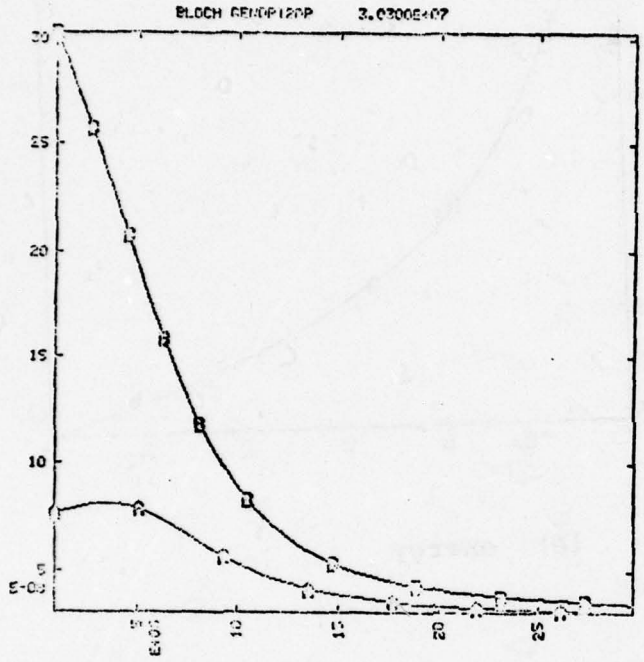

(d) K_{lin}, K_{nonlin}

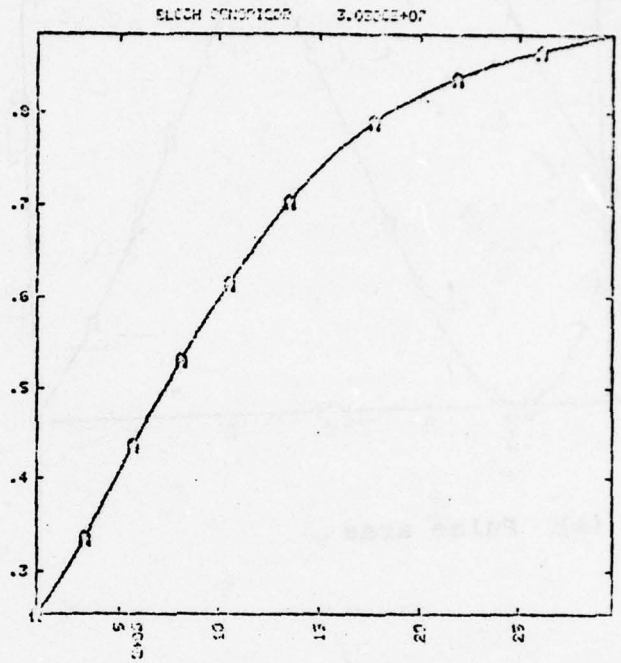

(e) K_{nonlin}/K_{lin}

Figure 12. Lossy propagation (0π pulse); $t_e = t_f = 100$ psec; $\Delta\omega = 0.15\ cm^{-1}$

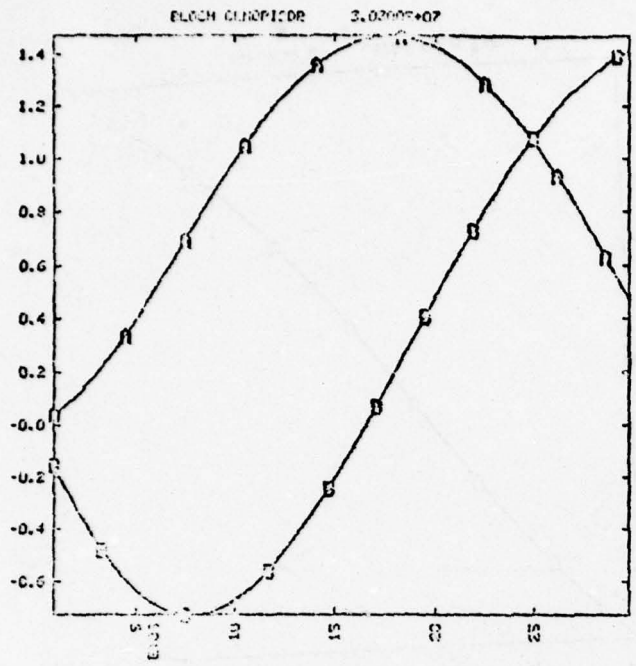

(a) Pulse area (real and imag.)

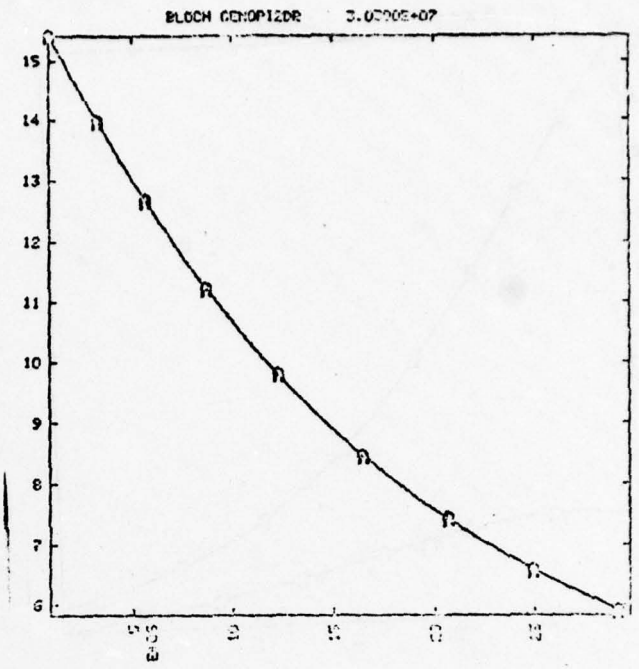

(b) energy

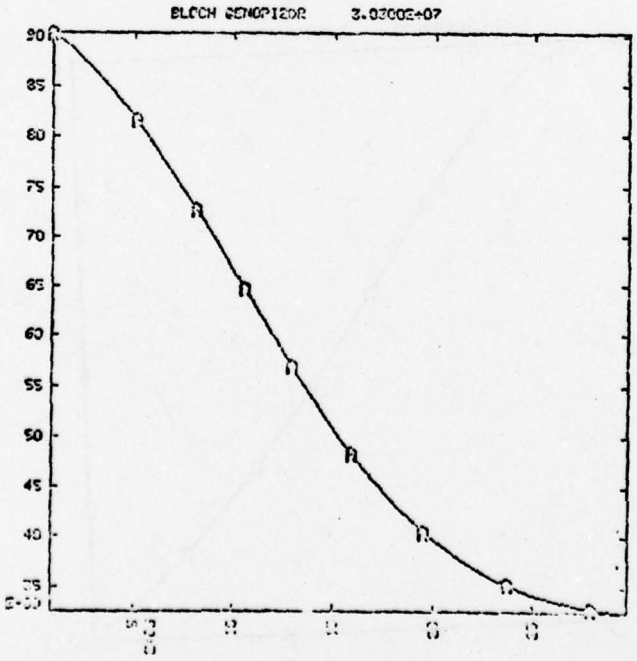

(c) (1 - u/c)

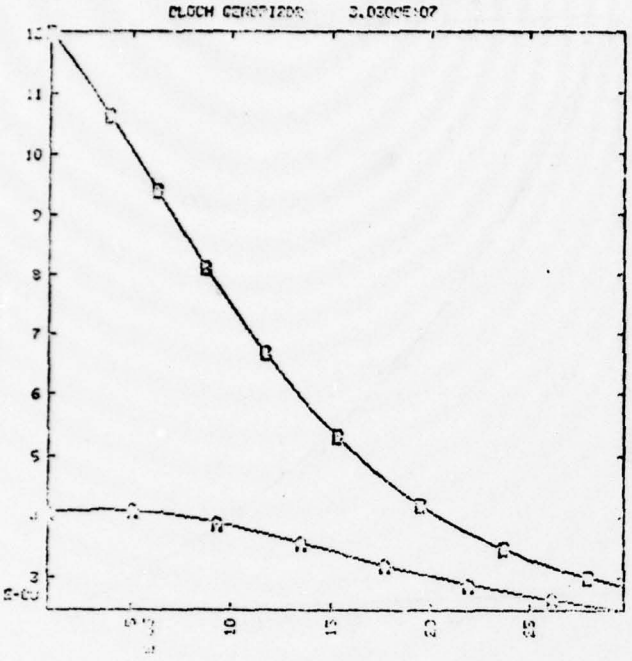

(d) K_{lin}, K_{nonlin} (cm^{-1})

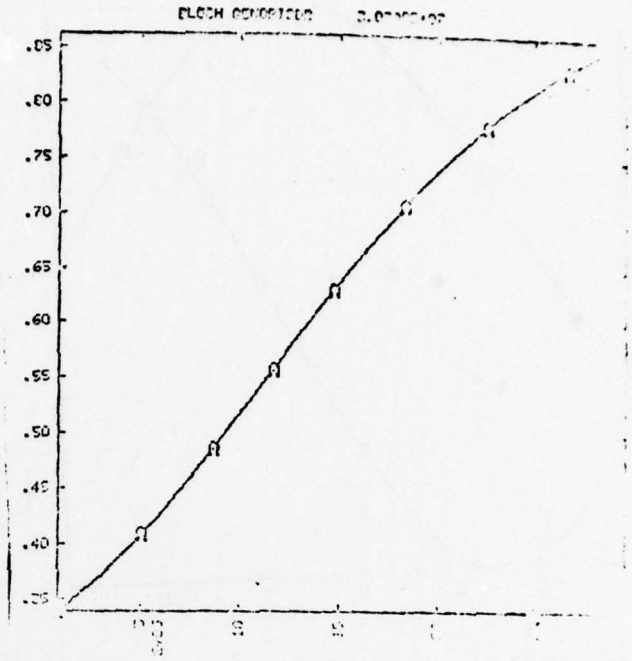

(e) K_{nonlin}/K_{lin}

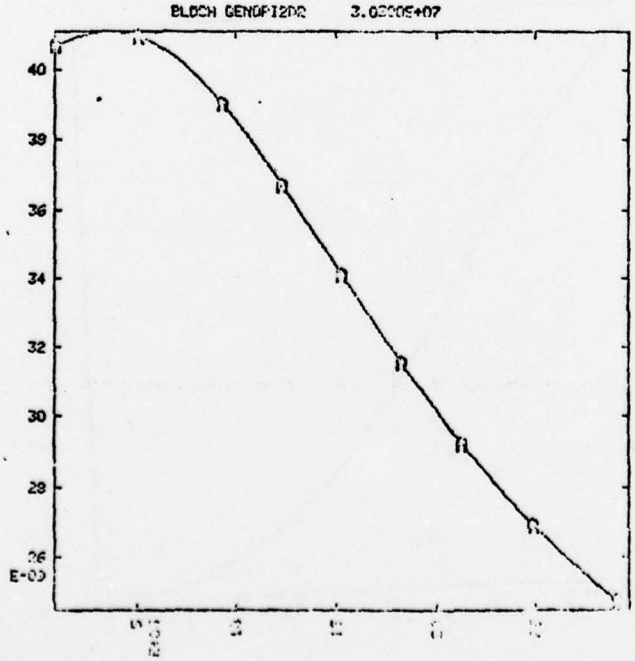

(f) $K(cm^{-1})$

Figure 20. Lossy propagation of zero-pi pulse versus distance; 18.577 cm [illegible] line; $t_e = t_f = 100$ psec.

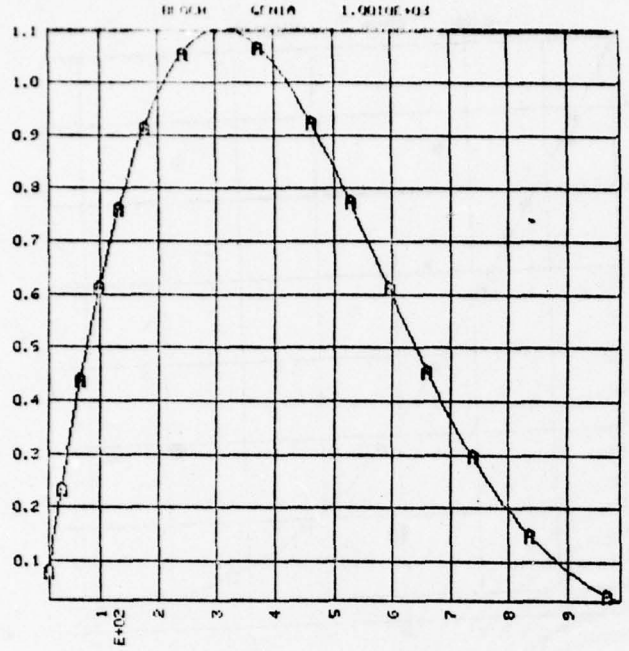

(a) pulse area

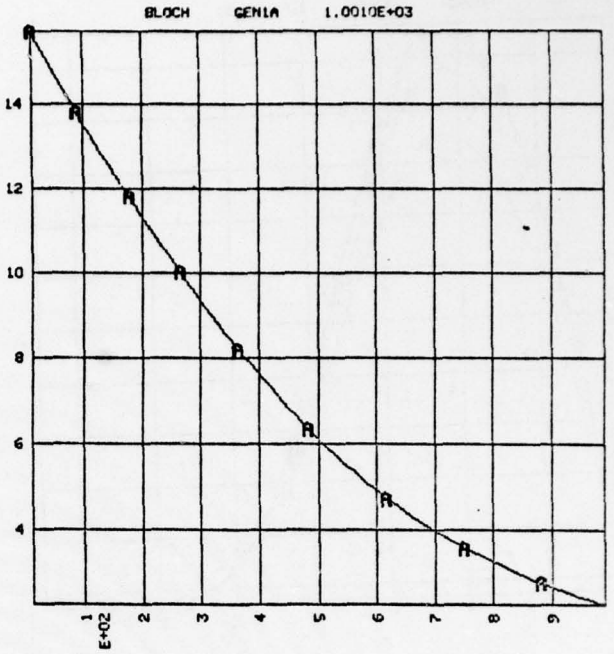

(b) normalized pulse energy

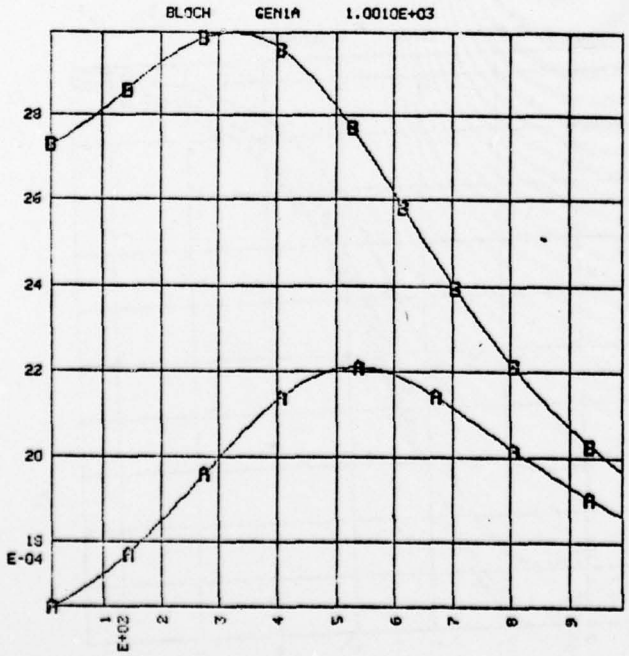

(c) linear and nonlinear absorption coefficients

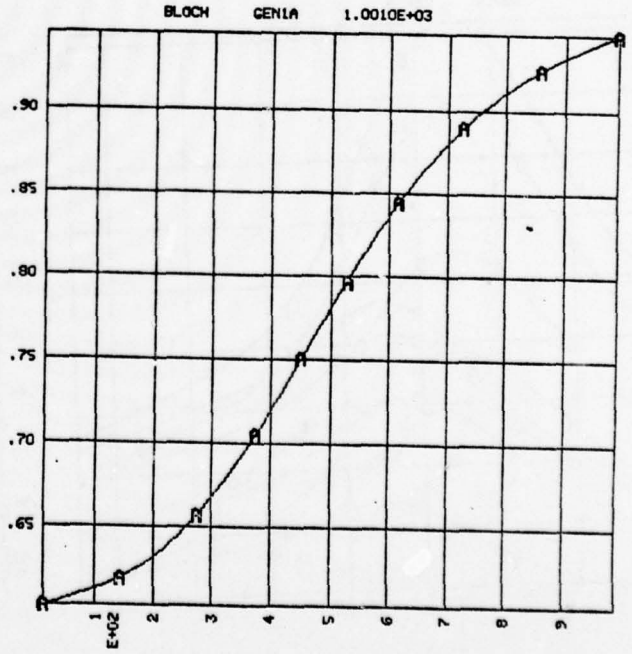

(d) ratio of nonlinear to linear absorption coefficient

Figure 21. Lossy propagation of zero-pi pulse versus distance; 20.204 cm^{-1} line; $t_e = t_f = 100$ psec.

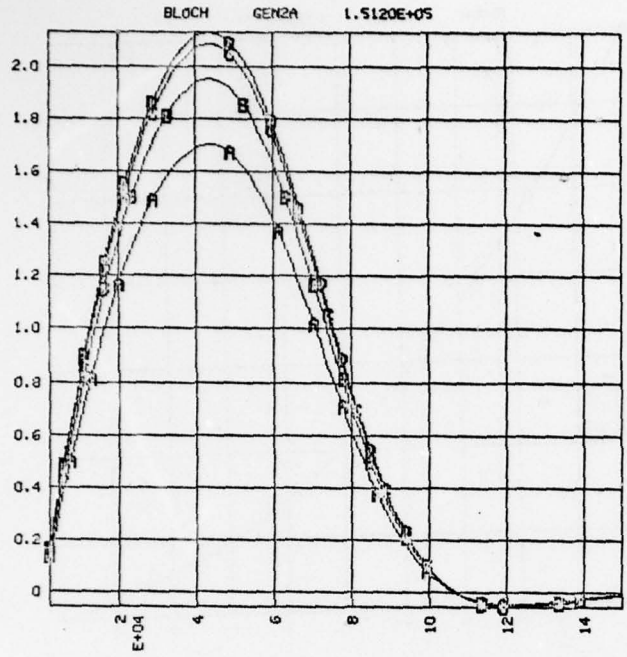

(a) pulse area; ABCD corresponds to $|M| = 3, 2, 1, 0$

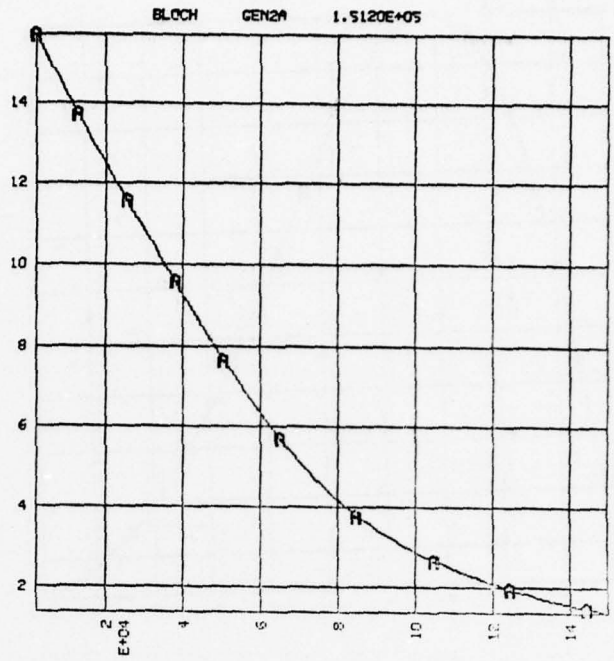

(b) normalized pulse energy

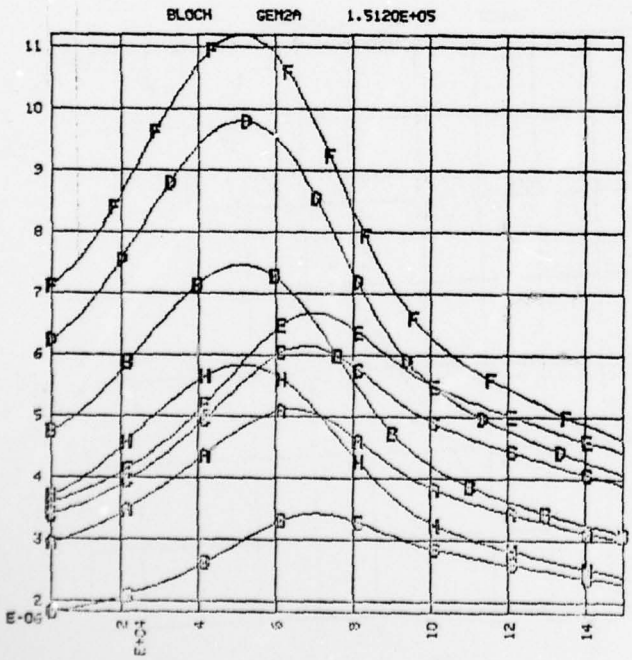

(c) linear and nonlinear absorption coefficients

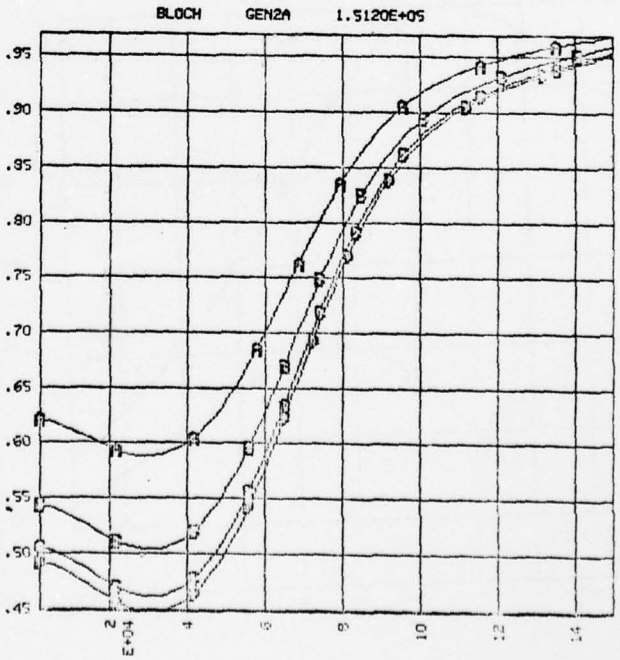

(d) ratio of nonlinear to linear absorption coefficients

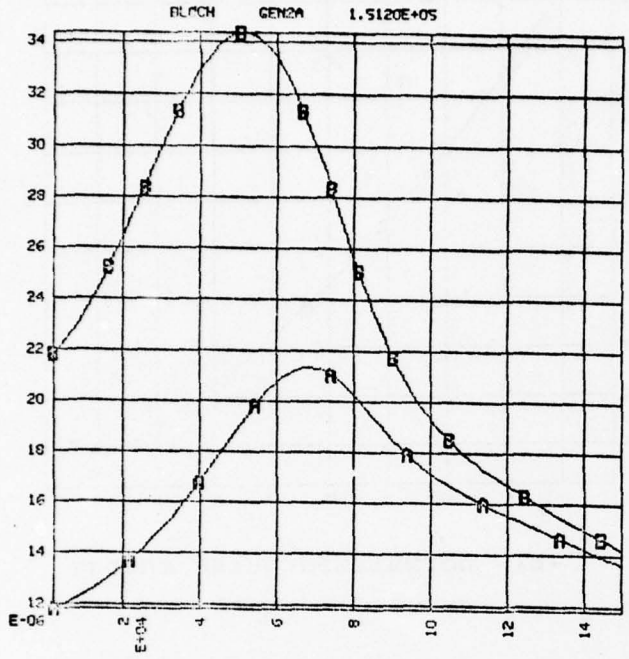

(e) linear and nonlinear absorption coefficients averaged over all M-levels

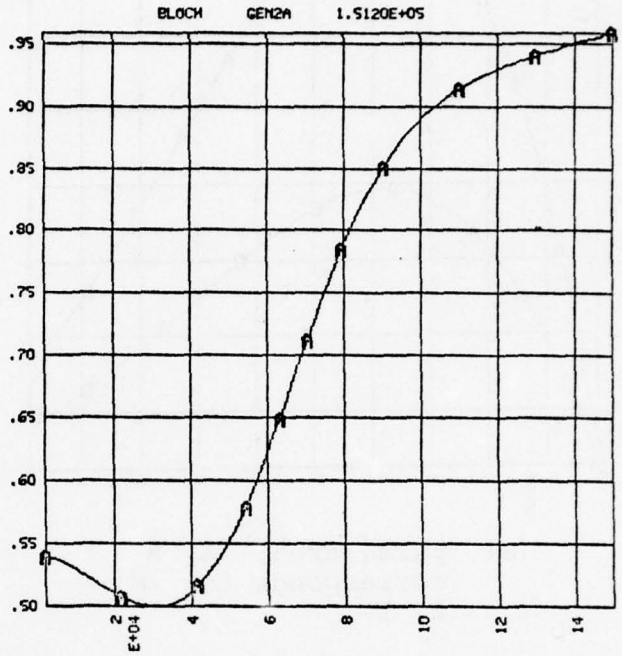

(f) ratio of averaged non-linear to linear absorption coefficients

Figure 22. Lossy propagation of zero-pi pulse versus distance; 25.080 cm $^{-1}$ line; $t_e = t_f = 100$ psec.

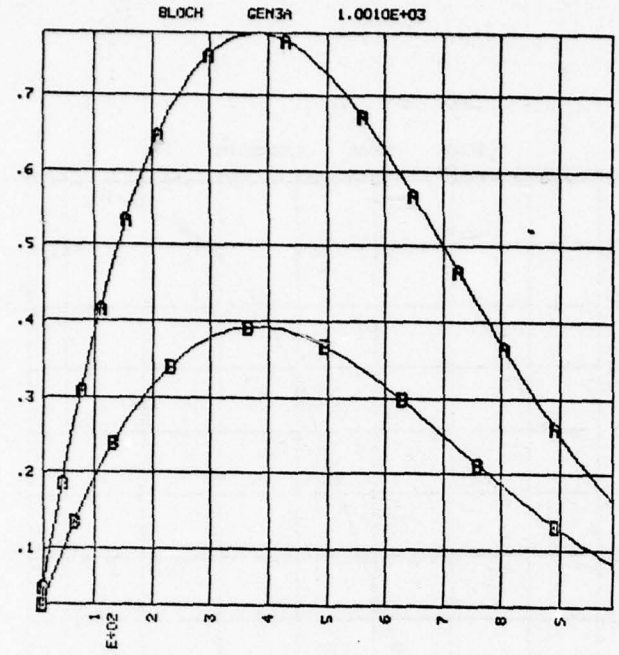

(a) pulse area; A, B corresponds to $|M| = 2, 1$

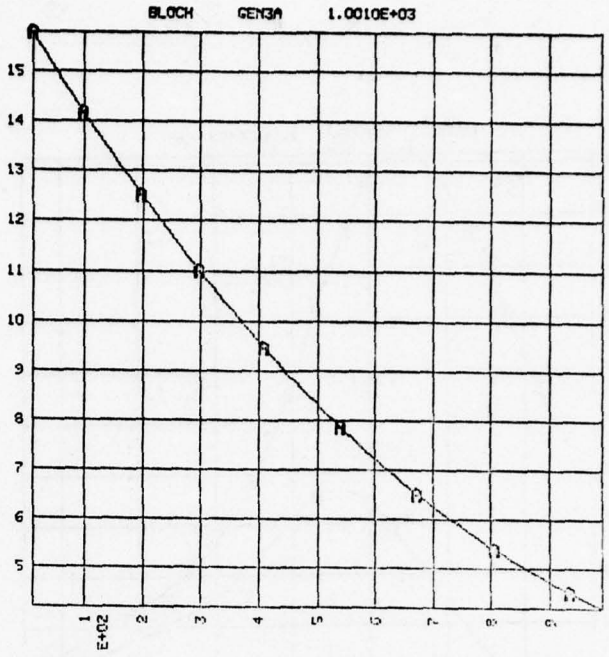

(b) normalized pulse energy

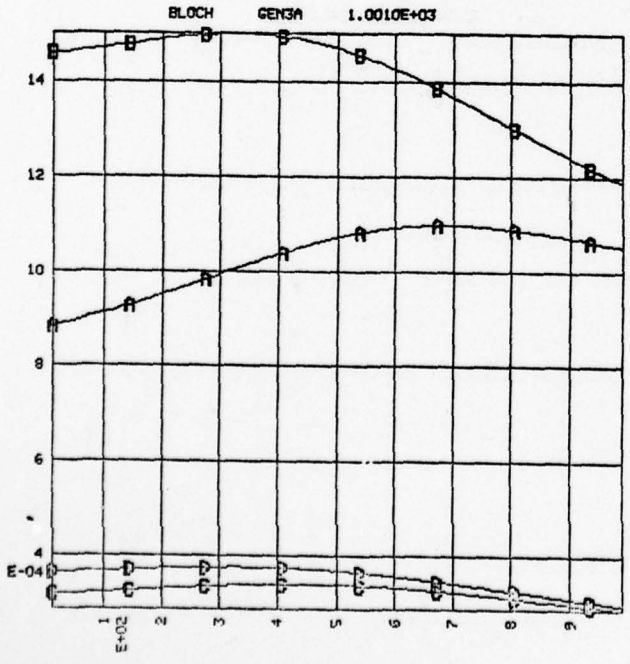

(c) linear (C, D) and nonlinear (A, B) absorption coefficients

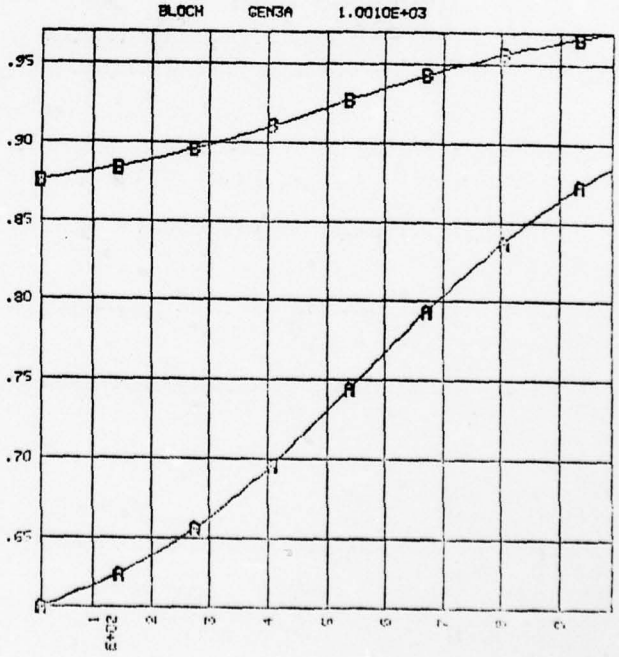

(d) ratio of nonlinear to linear absorption coefficients

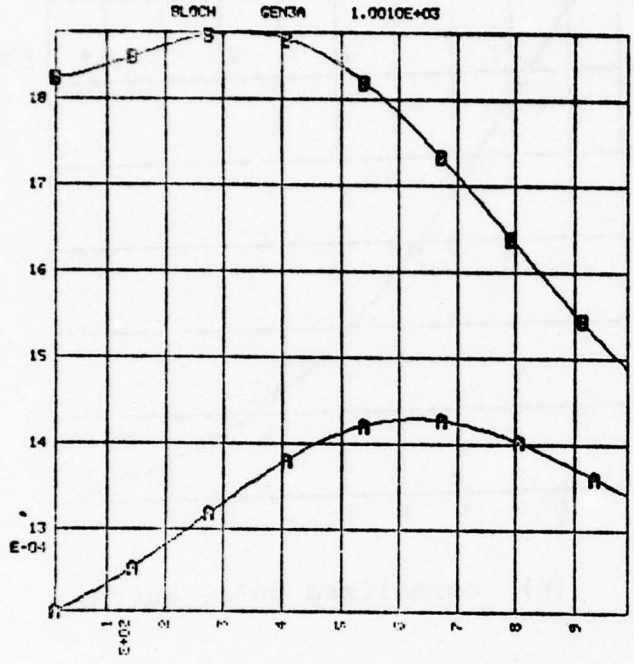

(e) linear (B) and nonlinear (A) absorption coefficients

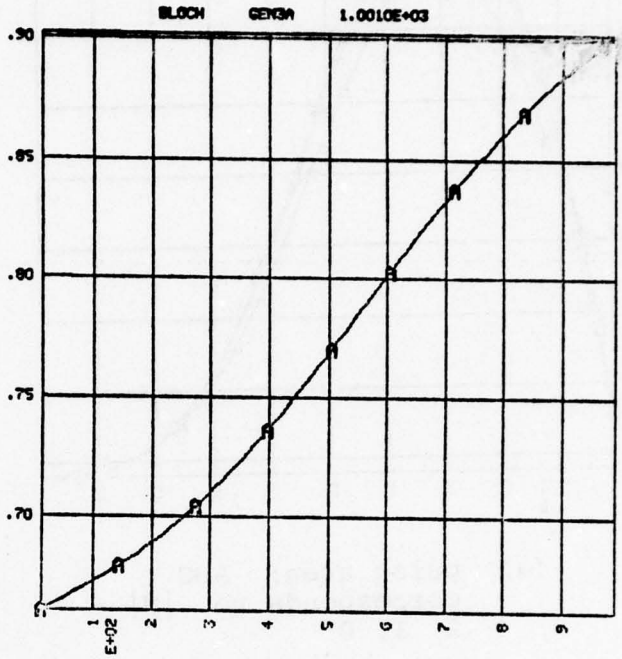

(f) ratio of averaged nonlinear absorption coefficients

Figure 23. Lossy propagation of zero-pi pulse versus distance; 30.560 cm $^{-1}$ line; $t_e = t_f = 100$ psec.

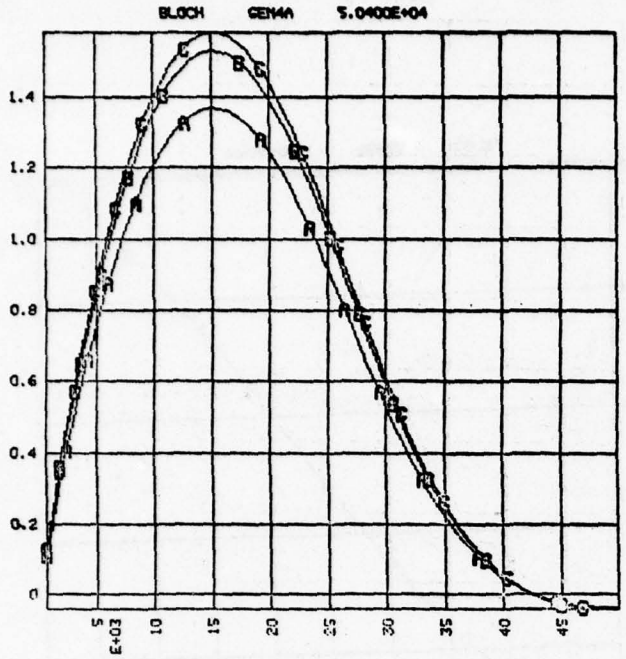

(a) pulse area; ABC corresponds to $|M| = 2, 1, 0$

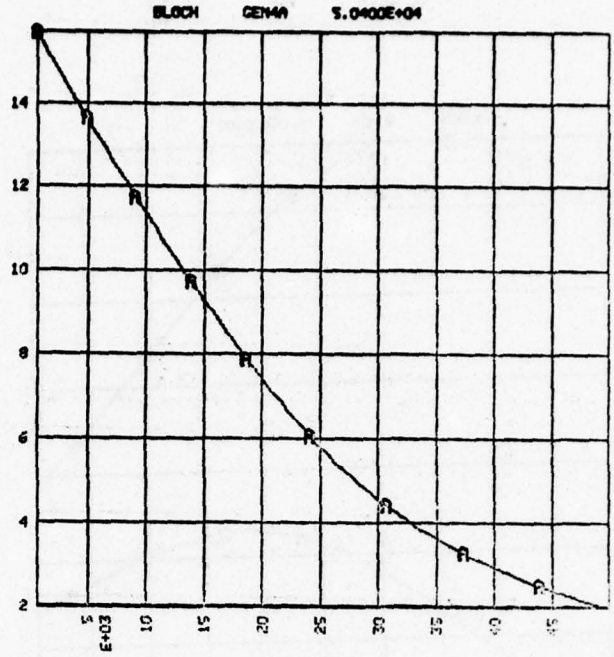

(b) normalized pulse energy

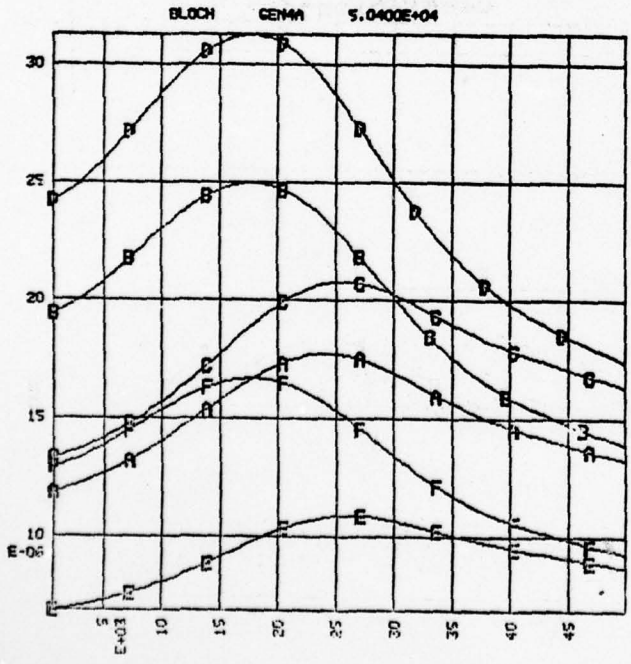

(c) linear (B, D, F) and nonlinear (A, C, E) absorption coefficients to $|M| = 2, 1, 0$

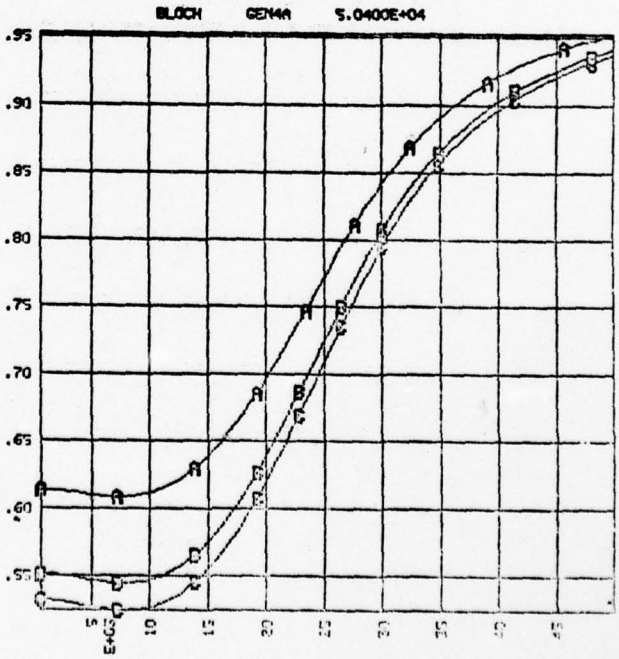

(d) ratio of nonlinear to linear absorption coefficients; ABC corresponds to $|M| = 2, 1, 0$

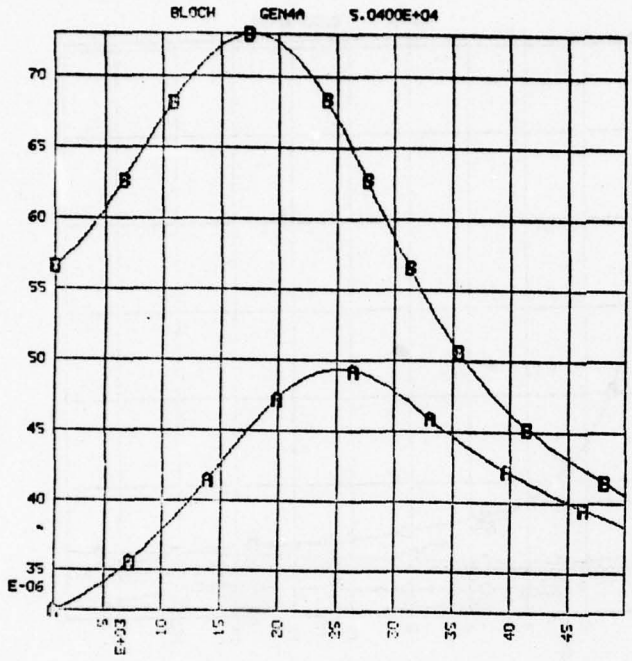

(e) linear and nonlinear absorption coefficients averaged over all levels

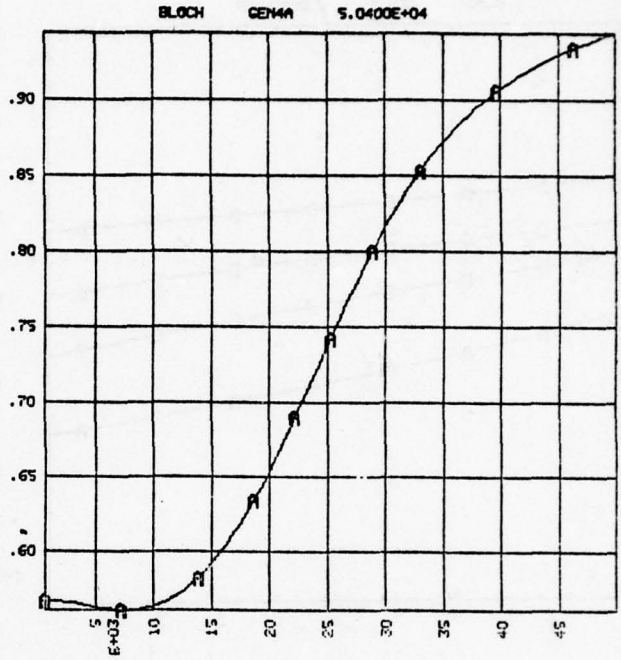

(f) ratio of averaged nonlinear to linear absorption coefficients

Figure 24. Propagation of CH_3F line in presence of absorption of 18.577 cm^{-1} H_2O line.

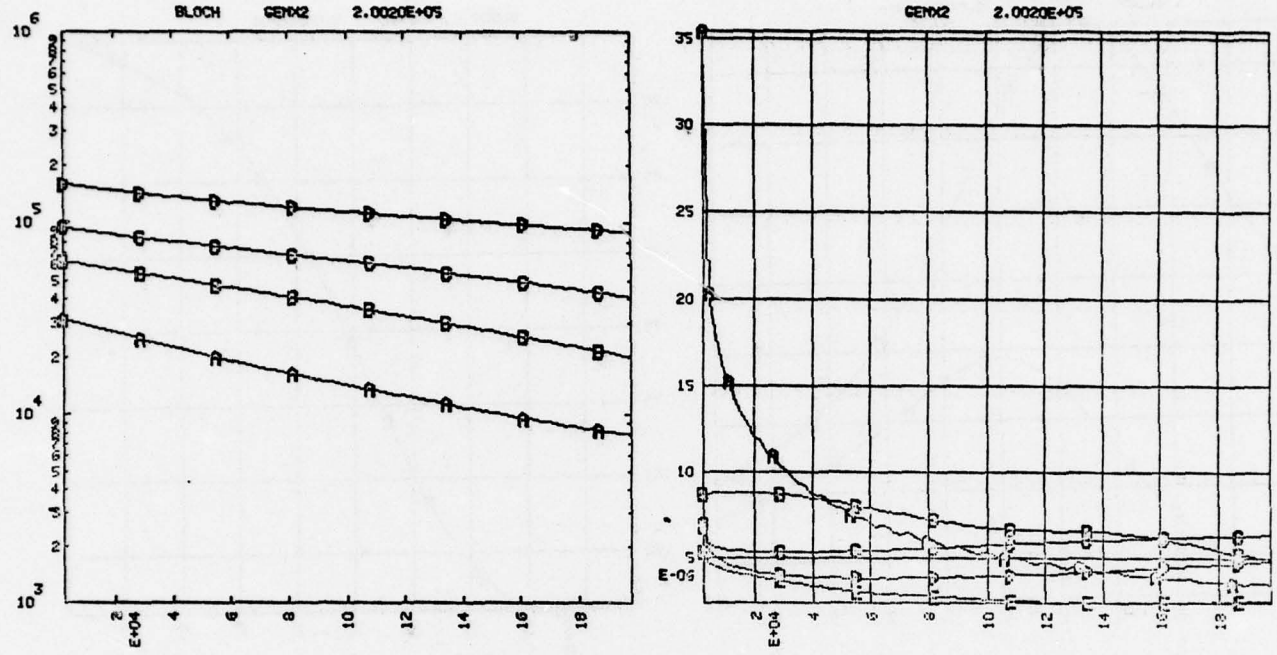

(a) energy as a function of distance

(b) the absorption coefficient

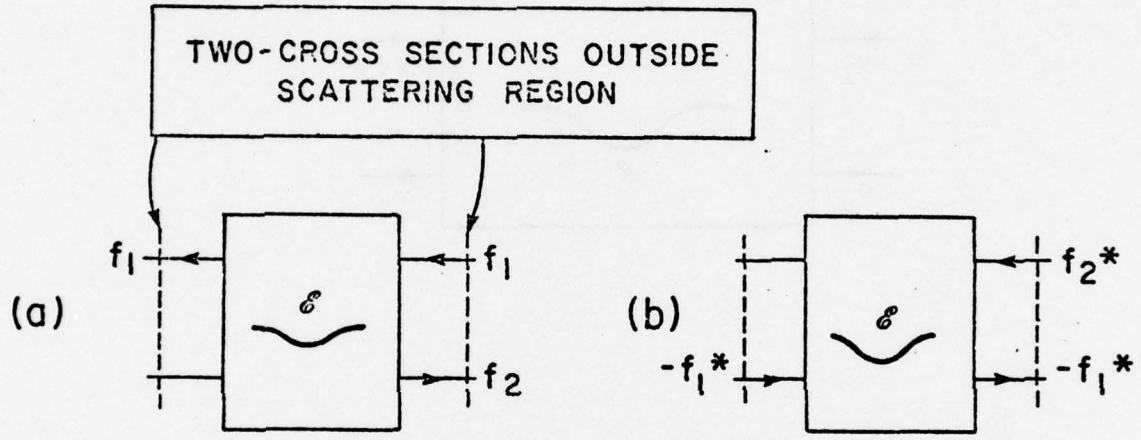

Figure 25. "Experiments" defining f and $\bar{f}$.

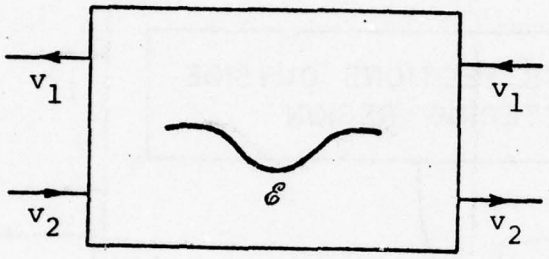

Figure 26. "Experiment" defining g.

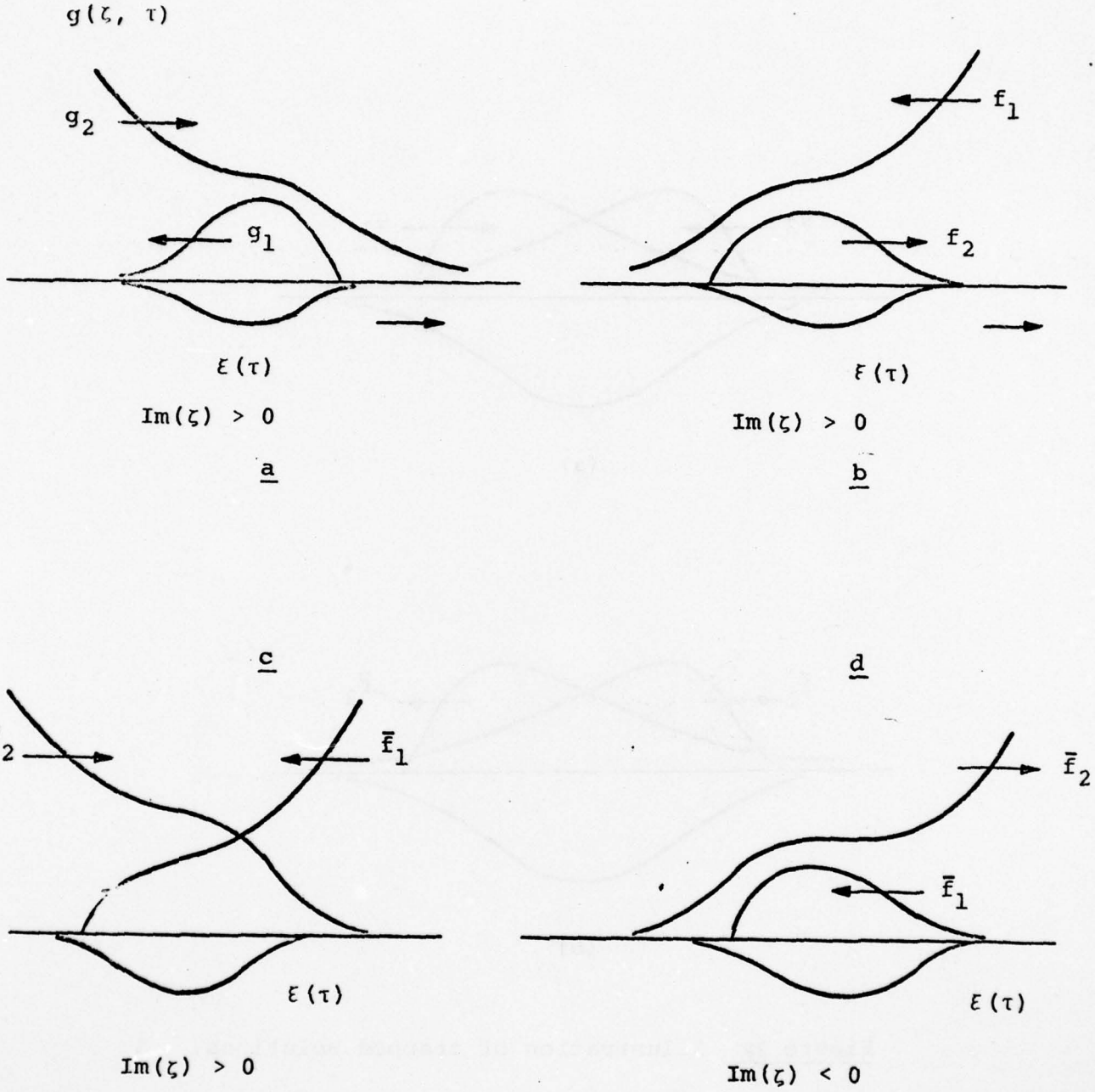

Figure 27 The functions g, f and $\bar{f}$ in complex ζ plane for assumed well ε(τ). Arrows indicate direction of group velocity. The reflected wave stops abruptly at end of well as indicated.

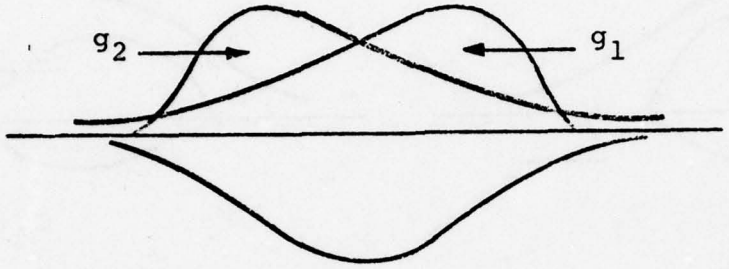

(a)

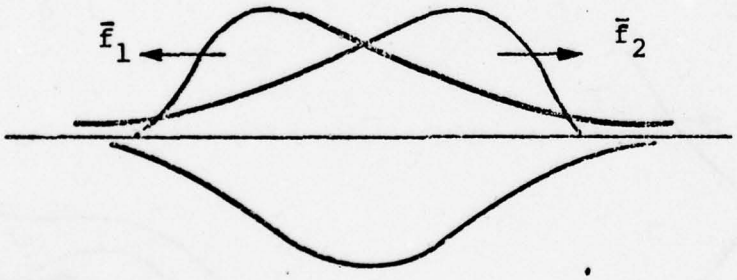

(b)

Figure 28 Illustration of trapped solutions.